Advanced Technologies for Energy Saving, Wireless Backhaul and Mobility Management in Heterogeneous Networks

A THESIS SUBMITTED IN FULFILMENT OF THE REQUIREMENTS FOR THE DEGREE OF DOCTOR OF PHILOSOPHY

Ran Tao
Supervisor: Jie Zhang

Department of Electronic and Electrical Engineering

University of Sheffield

October 2018

Acknowledgements

I'm grateful to my supervisors Professor Jie Zhang and Dr. Xiaoli Chu for their supports and encouragements throughout the four-year study. I want to especially thank Professor Jie Zhang, who taught me how to be an independent researcher, and also, Dr. Xiaoli chu, who provides me plenty of valuable suggestions about my research.

Also, I would like to thank my parents, Shengyin Lu and Zhiwen Tao, for their selfless help and love.

I would also like to thanks my colleagues: Yue Wu, Wuling Liu, Jiliang Zhang, Haonan Hu, Long Li, Jialai Weng, Baolin Zhang, Jiliang Zhang, Yao Huang, for their friendship and assistance during my four-year PhD time.

Abstract

In recent years, due to the increasing number of existing and new devices and applications, the wireless industry has experienced an explosion of data traffic usage. As a result, new wireless technologies have been developed to address the capacity crunch. Long-Term Evolution-Licensed Assisted Access (LTE-LAA) is developed to provide the tremendous capacity by extending LTE to 5 GHz unlicensed spectrum. Hyper-dense small cells deployment is another promising technique that can provide a ten to one hundred times capacity gain by bringing small cells closer to mobile user equipments [1]. In this thesis, I focus on three problems related to these two techniques.

In Chapter 3, I present a novel activation and sleep mechanism for energy efficient small cell heterogeneous networks (HetNets). In the cell-edge area of a macrocell, the coverage area of a sleeping small-cell will be covered by a range of expanded small-cells nearby. In contrast, in areas close to the macrocell, user equipment (UE) associated with a sleeping small cell will be distributed to the macrocell. Furthermore, the enhanced inter-cell interference coordination (eICIC) technique is used to support range-expanded small cells to avoid Quality of Service (QoS) degradation. Under both hexagonal and stochastic geometry based models, it is demonstrated that the proposed sleeping mechanism significantly reduces the energy consumption of the network compared with the conventional methods while guaranteeing the QoS requirements.

Small cells are currently connected to limited backhaul to reduce the deployment and operational costs. In Chapter 4, an optimisation scheme is proposed for small cells to utilise the bandwidth of macrocells as wireless backhaul. I provide the numerical analysis of the performance of both the targeted small cell and the whole network.

In Chapter 5, the mobility management (MM) of heterogeneous and LTE-LAA networks are investigated. To avoid Ping-Pong handover (PPHO) and reduce handover failure rate in HetNets, a self-optimisation algorithm is developed to change the handover parameters of a base station automagically. Furthermore, the MM of LTE-LAA networks is analysed. A new handover mechanism is proposed for LTE-LAA networks. Compared with the conventional LTE networks, LTE-LAA networks trigger the handover not only by using UE mobility, but also by the availability of the unlicensed band. A comprehensive analysis of

the handover triggering event and handover procedure is presented. Simulation results show that by introducing handover triggered by available unlicensed band, the ratio of handover to unlicensed spectrum has a significant improvement. Therefore, a noticeable enhanced throughput of UEs is achievable by LTE-LAA networks.

List of Publications

1. R. Tao, W.Liu, X. Chu, and J. Zhang, “A energy saving small cell sleeping mechanism in heterogeneous networks” , accepted by IEEE Transactions on Wireless Communications.

2. R. Tao, J. Zhang and X. Chu, "An energy saving small cell sleeping mechanism with cell expansion in heterogeneous networks," accepted by IEEE VTC2016-Spring, Nanjing, China, 15-18 May 2016.

3. Y. Wu, R. Tao, Y. Zhu, H. Zheng, X. Chu and J. Zhang, "Enhancing small cell capacity with in-band wireless backhaul," accepted by the 32nd URSI GASS, Montreal, Canada, 19-26 Aug 2017.

4. R. Tao, L. Li, X. Chu, and J. Zhang, “Handover mechanism and performance evaluation for lte-laa systems,” accepted by Signal Processing Advances in Wireless Communication (SPAWC), 2016 IEEE 17th International Workshop on. IEEE, 2016, pp. 1–5.

Table of contents

List of figures

List of tables

Abbreviations

3GPP 3rd Generation Partnership Project

ABSs Almost Blank Subframes

ACK Acknowledgement

AI Artificial Intelligence

BB Based Interface

BS Base Stations

CA Career Aggregation

CAC Call Admission Control

CAPEX Capital Expenditure

CDF Cumulative Density Function

CoMP Coordinated Multi-Point

CRE Cell Range Expansion

CRS Cell-specific Reference Signal

DSC Drone Small Cell

DTA Double Threshold Algorithm

EE Energy Efficiency

eICIC Enhanced Inter-cell Interference Coordination

eNB eNodeB

EPC Evolved Packet Core

ESF Even Subframe

FDD Frequency Division Duplex

FeICIC Further Enhanced Inter-cell Interference Coordination

FSO Free Space Optical

FTTC Fibre to the Cell

HetNets Heterogeneous Networks

HM Hysteresis Margin

i.i.d. Independent and Identically Distributed

IAB Integrated Access and Backhaul

IB-FD In-Band Full Duplex

ICIC Inter-cell Interference Coordination

ICT Information and Communication Technology

ISD Intersite Distance

KPI Key Performance Indicator

LAA Licensed-Assisted Access

LBT Listening Before Talk

LOS Line-of-Sight

LTE Long-Term Evolution

LTE-A Long-Term Evolution-Advanced

MIMO Multiple Input Multiple Output

MM Mobility Management

MME Mobility Management Entity

mmWave Millimetre Wave

MR Measurement Report

NLOS Non-Line-of-Sight

OPEX Operating Expense

OSF Odd Subframe

PA Power Amplifier

PCC Primary Component Carrier

PDF Probability Density Function

PPHO Ping-Pong Handover

QoS Quality of Service

RB Resource Block

RRC Radio Resource Control

RSRP Reference Signal Received Power

RSRQ Reference Signal Received Quality

S-GW Serving-Gateway

SCC Secondary Component Carrier

SDL Supplemental Downlink

SDN Software Defined Network

SINR Signal-to-Interference-Plus-Noise Ratio

SN Sequence Number

SON Self Organising Networks

SPPP Spatial Poisson Point Process

TDD Time Division Duplex

TTI Transmission Time Interval

TTT Time to Trigger

UAV Unmanned Aerial Vehicles

UE User Equipment

UNII Unlicensed National Information Infrastructure

WLAN Wireless Local Area Network

Table 1 List of Symbols

T, U	Date rate requirement
γ	SINR
P	BS transmitting power
σ^2	Noise power
h	Amplitude of a Rayleigh fading channel
α	Pathloss exponent
α_1, α_m	Pathloss exponent of macrocells
α_2, α_s	Pathloss exponent of small cells
K_m	Pathloss constant of macrocells
K_s	Pathloss constant of small cells
$\mathscr{L}$	Laplace transform
λ_1, λ_m	Density of macrocells
λ_2, λ_s	Density of small cells
N_A	Number of antennas
P_{0m}, P_{0w}	Static power consumption of macrocells/small cells
Δ_{pm}, Δ_{ps}	Slope of the power model of macrocells/small cells
P_{sm}, P_{ss}	Power consumption of macrocells/small cells in sleep mode
P_{tm}, P_{ts}	average transmit power of macrocells/small cells
P_{Mm}, P_{Ms}	Maximum average transmit power of macrocells/ small cells
ρ_s	Load of the small cell
ρ_m	Load of the macrocell
W	Bandwidth allocation
R	Size of the macrocell (Apothem of hexagon)
z	Switch off radius
θ	UE density
ε, η	Coverage probability threshold
β	Duty cycle
μ	Parameter of Exponential distribution
B_2	CRE bias factor for small cells
$\rho(t)$	Number of UEs come into the coverage of small cell A at time t
C_b	Bandwidth of wired backhaul
$\tau^{\dagger}$	Maximum portion of bandwidth can be utilised for wireless backhaul
Q_{out}	handover failure threshold
α_w	PPHO Weighting coefficient
$T_{attempt}$	Access opportunities
T_{cellTx}	Unlicensed channel occupied time period
$T_{sensing}$	LBT sensing time

Chapter 1

Introduction

1.1 Background

The wireless industry has an explosive growth in data demand in recent years and is now facing a much bigger challenge, an astounding 1000-fold data traffic increase in a decade [1]. Research in [2] shows that the number of mobile subscribers is estimated to reach 7.6 billion by 2020 from 4.5 billion in 2012, also the data requirement of each subscriber is expected to reach 82GB per year by 2020 from 10 GB in 2012.

To address the explosive growth in data demands, dense small cell deployment has been considered as a promising technique. In [1], the authors demonstrate that hyper dense HetNets can be a promising solution because it can provide a 10-100 times expected throughput gain, compared with the 5-20 times Massive Mutiple Input Mutiple Output (MIMO) gain.

HetNets, also named multi-tier mobile networks, are networks with various kinds of small cells or relays underlying traditional macrocells. Fig. 1.1 illustrates the architecture of HetNets. It can be seen that small cells provide the last mile wireless accesses to the mobile Internet UEs by core networks via backhauls. The researches of HetNets still face the following challenges:

- Interference Management: Interference management is a critical issue for the small cell deployment. As macrocells and small cells share the same frequency spectrum, for the downlink transmission, UEs associated to macrocells will suffer additional interference from small cells and vice versa for the UEs connected to small cells, for the uplink transmission, macrocells will suffer interference from small cell UEs and vice versa for small cell. These two kind cross-tier interference can be coordinated by Inter-Cell Interference Coordination (ICIC), enhanced Inter-Cell Interference Coordination (eICIC), Further enhanced Inter-Cell Interference Coordination (FeICIC)

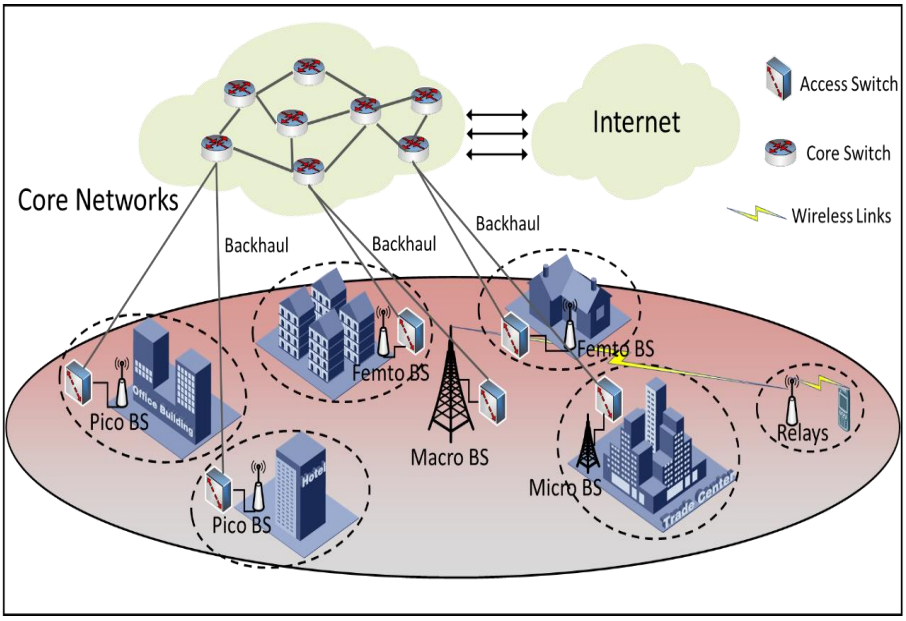

Fig. 1.1 The architecture of HetNets

techniques. The eICIC technique is used in the thesis to guarantee the QoS of UEs in the cell edge area. The detail of eICIC technique will be explained in details in the Sect. 2.1. FeICIC [3]was proposed in Release 11 of 3rd Generation Partnership Project (3GPP) standard, compared with eICIC technique, FeICIC technique is more complex and can reduce the capacity loss of macrocells. Moreover, due to the dense deployment of the base stations (BSs), especially small cells, the interference received from BSs of the same tier, which is defined as co-tier interference, should also be mitigated. It is noted that Millimetre Wave (mmWave) has the characteristics of highly attenuated pathloss and low penetration. In that case, the co-tier interference can be effectively retained.

- Mobility Management: Mobility management (MM) aims to guarantee the service continuation and the quality of UEs when the current attached BS for a mobile UE cannot provide acceptable performance. Due to the dense deployment of small cells in the HetNets, the number of cell selections and handovers in the networks will in-

crease on a large scale, and thus signalling overhead. To overcome the problem, a network architecture with split control (C)-plane and user (U)-plane has been proposed. In this new network architecture, small cells can be activated to provide data to UEs only, while macrocells take care of controlling the UEs' connectivity. Hence, the control signalling caused by frequent handovers between small cells can be significantly reduced. It is noted that this kind of network architecture has also been used in my work in Sect. 5.2.

In recent years, lots of researches target on MM in software defined network (SDN). The key concept of SDN is the decoupling of data as well as control planes, and the centralisation of control planes [4]. In the handover procedure, the SDN controller handles the necessary handover signalling and manages the handover decisions in HetNets.

- Backhaul: Backhaul is defined as the links between the radio access networks and the core networks. Wireless based backhaul for small cells has been considered in lots of researches due to its low cost and flexibility. The frequency division duplex (FDD) and in-band full duplex (IB-FD) approaches used in wireless backhaul will be explained in chapter 4. In Release 15 of 3GPP standard, integrated access and backhaul (IAB) has been proposed [5]. The bandwidth allocation between backhaul links and access links in each small cell is flexible with IAB to meet the dynamic traffic demand. All backhaul and access links are expected to transmit in mmWave spectrum band due to the abundant bandwidth mmWave spectrum has. Moreover, by using the directional beamforming technique, all backhaul and access links can share the same wireless channel without interference.

To further improve the deployment efficiency of HetNets, the evolution of small cells is still under research. In this part, the introduction of the two promising techniques for the future small cells: caching on the edge and drone small cells, will be provided.

- Caching on the edge: In recent years, there is a growing interest to improve the storage capacity (i.e., cache) of small cells, as this can help to reduce the cost of small cell backhaul deployment. The cache of small cells can alleviate the burden of the network backhaul by proactively storing the content that the serving UEs might be highly interested in small cells at the off-peak time period. With the development of artificial intelligence (AI), the UEs' profiles can be built through big data analysis on the available data.

- Drone small cells: Drone small cells (DSCs) are defined as the wireless BSs, e.g., small cells, equipped in low-attitude flying devices, such as unmanned aerial vehicles

(UAVs), to provide wireless service especially for unexpected event [6]. The main advantage of DSCs is that the DSCs can provide wireless connection whenever and wherever needed because of their flexibility. For example, DSCs are effective for seasonal rural traffic, e.g., ski resorts in winter and hiking routes in summer.

The large scale increase of the small cell density will generate both economic and environmental problems due to the increasing power consumption and CO_2 emissions. Research in [7] shows that the Information and Communication Technology (ICT) 's share of global carbon emissions already reached 2% in 2010, moreover, the share is expected to grow every year, and will likely double to 4% by the year 2020. The increase of BSs also signifies the growth of overall energy consumption. Although energy consumption of small cells is much less than that of macrocells, due to the dense deployment in the foreseeable future, the small cells will consume about 4.4 TWh of power by 2020. In this situation, switching off BSs selectively can be a desirable technique to achieve energy saving in mobile networks [8]. There are two main reasons why BS sleeping techniques are favoured by operators: (1) the BS consume the highest proportion ($60\% - 80\%$) of energy in mobile networks [9]. Furthermore, the fixed parts of BS power consumption, e.g., power supply, accounts for about 25% of the total energy consumption [10]. (2) BS sleeping techniques can be implemented directly on the current network architecture since there are no hardware replacement requirements, cost saving is achieved.

In hyper-dense heterogeneous and small cell networks, many UEs are transferred from macrocells to small cells. Therefore, providing fast and reliable backhaul connection between the core network and small cells becomes a critical issue for such HetNets [11, 12]. Wired backhaul, which uses copper or fibre cables, can provide high data rate links between macrocells and small cells [13]. However, the expense to provide wired backhaul is extremely high, especially when the small cells are deployed in a large scale. The work in [13] shows that the availability of high speed wired backhaul is not satisfied. Moreover, certain locations which have difficulty with being accessed by wired backhaul may restrict the universal deployment of small cells. Sometimes the small cells connect to the core network via low capacity wired backhaul (e.g., DSL links), in this situation, the QoS of UE cannot be guaranteed. On the contrary, wireless backhaul, which is cost effective and flexible [14, 15], can be treated as a promising technique to offer high speed data links for small cells. Compared to wired backhaul, the management of wireless backhaul resources, e.g., power and spectrum, is more complicated due to the finite power and radio spectrum constraints.

Small cells have short coverage and are usually deployed in a dense and unplanned manner. For these reasons, MM in such dense heterogeneous and small cell networks has become one of the most challenge issues. The ping-pong Handover (PPHO) in HetNets is

one of the most crucial problems that can cause UEs' QoS degradation. PPHO easily occurs due to the frequent movement of UEs in dense small cell networks. Because it wastes the network resources and decreases the QoS of UEs, network operators must reduce the adverse effects introduced by PPHO.

Furthermore, to meet the challenges of the explosive data, the wireless industry is on the hunt for solutions to boost network capacity. Excavating more capacity on the licensed spectrum is the first choice as its security and reliability. However, due to the limited bandwidth of the licensed spectrum, the cost of utilising more licensed spectrum is extremely high. Improving spectrum efficiency is another choice. However, in a dense small cell scenario, the licensed spectrum is easily congested so that complex inter-cell interference management needs to be involved. Given all the challenges, operators are motivated to extend LTE spectrum to unlicensed spectrum to add more available spectrum to meet the increasing demand [16]. The unlicensed 2.4 GHz and 5 GHz bands that Wi-Fi systems operate in have been considered as essential candidates to provide extra spectrum resources for mobile networks. Furthermore, the initially targeted unlicensed band has up to 500 MHz of the potentially available spectrum[17]. In 3GPP, Licensed -Assisted Access (LAA) technology was initiated as part of Release 13 to allow both licensed and unlicensed spectrum to be assessed by LTE systems. LAA extends LTE to unlicensed spectrum in a unified LTE network architecture and aggregates the licensed and unlicensed spectrum via carrier aggregation [16], which provides a more efficient resource utilisation and offers high speed, seamless continuity, as well as improved reliability in broadband multimedia services for small cell UEs [18].

1.2 Motivation

1.2.1 Energy Saving through Small Cell Sleeping Mechanism

BS sleeping is one of the most effective techniques to achieve network energy savings. Many studies on cell sleeping strategies in HetNets have been accomplished, e.g., [19–26]. In [19], the UEs from sleeping cells were offloaded to the neighbouring cells without considering their cell types. In [20, 21], although a stochastic geometry based HetNet model was used, the authors maximised energy efficiency (EE) based on a non-convex optimisation approach, no BS sleeping strategies are provided. The authors in [22] proposed an algorithm to calculate the upper and lower bounds of the active small cells' optimal density, which was based on the ratio between the small cell cost and the macrocell cost, but the distance between the sleeping small cells and macrocells was not considered. In [23],

the authors switched off the small cells with fewer UEs, but the impact of macrocells was not considered. The authors in [24, 25] presented an energy model, which considered the energy savings of the whole network when the small cell was in switched off and the UEs were transferred to the macrocell, but no numerical analysis of the mechanism was given. In [26], the authors provided a sleeping mechanism, which turned off the small cells close to macrocells but was based on a split control/user plane network.

Switching off small cells by considering their distance to the macrocells is a promising mechanism, but the research targets on this in HetNets is insufficient. In this situation, a small cell sleeping algorithm considering the impact of the distance between the sleeping small cells and macrocells on network power consumption is proposed.

1.2.2 Optimise Wireless Backhaul

It is necessary to propose a brief introduction of wireless backhaul in the beginning of the part. The term backhaul network refers to the intermediate network that includes the links between the radio access network and the core network. In HetNets, providing a high quality connectivity between the small cell and the core network is a challenge and the wireless backhaul is becoming a attractive solution due to the rapidly developing point-to-point microwave technologies. The detailed explanation of wireless backhaul will be introduced in Sect. 2.3.

The performance evaluation of the wireless backhaul links and UE capacity in HetNets is a less researched topic. In [27], the authors numerically analysed the network throughput performance of a single tier IB-FD network. In [28], a framework was designed to model the downlink rate coverage probability of a user in a given HetNet with wireless backhaul, but the whole network throughput has not been considered. The works in [29] considered the case of HetNets with IB-FD enabled small cells, the analytical expressions for coverage and average downlink rate were presented using tools from the field of stochastic geometry. However, the whole network throughput performance was not analysed.

It's obvious that the research targeting on the performance evaluation of wireless backhaul in HetNets is not enough. In this situation, I propose numerical analysis of the capacity of a target small cell and throughput of the entire networks. Moreover, I present a scenario where the small cells are connected to the limited wired backhaul to reduce the capital expenditure (CAPEX) and operating expense (OPEX) , the limited backhaul may become the bottleneck with the network traffic increase. DD and IB-FD approaches are implemented in the analysis and a comparison between both approaches is presented.

1.2.3 Mobility Management in HetNets and LTE-LAA

Self-organizing network (SON) functions have been introduced in the LTE and LTE-A standards by the 3GPP as an excellent solution that promises enormous improvements in network performance [30, 31]. One of the critical objectives of the SON architecture is to automatically optimise the LTE handover parameters e.g, PPHO ratio, handover failure rate, to improve the overall system performance and reduce the network operational' expenditure.

In [32], the authors proposed a handover optimisation algorithm to get optimum values of the handover key performance indicators (KPI) from the initial suboptimal parameter settings, but the KPI was not weighted during the optimisation. Thus the results are not accurate enough. In [33, 34], the authors provide self-optimising algorithms that adjust the handover parameters time to trigger (TTT), hysteresis margin (HM) to reduce the negative impact caused by call dropping, handover failure and PPHO. However, their performance may be not good enough and some parts of their designed algorithms have potential be improved. The authors in [35] proposed a comprehensive algorithm for handover among macrocells and small cells in LTE-A by using self-organising instructions. However, the optimisation procedure is not introduced in detail. Therefore, it's still worth making more contribution to this area.

Despite having many advantages, LTE-LAA still has handover challenges. MM in LTE-LAA networks is different from that in conventional networks. In [36, 37], the handover procedure and the signalling flowing in conventional LTE networks were presented. In [38–40], the network architecture with split control and user plane was proposed. This dual connectivity network can significantly reduce handover delays and is also used in the proposed handover mechanism.

It's worth noting that quite a few papers target on the analysis of MM in LTE-LAA networks. The handover procedures and handover trigger event are more challenging than that in conventional LTE networks due to the coexistence with Wi-Fi systems.

1.3 Contribution

In this section, the contributions of my work are presented.

In Chapter 3, I propose an energy saving small cell sleeping mechanism in heterogeneous mobile networks. It is regularly to switch off the small cell when it has an energy saving and transfer all its traffic to the macrocell [24, 25] . However, when the small cell sleeping is far away from the macrocell, the energy saving of the network will not be significant. Therefore, I use the small cell to cover the sleeping cells for this scenario, to achieve more energy saving. Furthermore, I use eICIC technique[41] to ensure their QoS require-

ments. Using stochastic geometry based HetNets model, numerical expressions of the UEs' coverage probability and cell association probability of the proposed sleeping strategy is derived. Compared with conventional approaches, the proposed one achieves a better performance.

In Chapter 4, I propose an optimal scheme for the small cells to utilise the macrocell links as their in-band wireless backhaul. Compared with [42, 43], I consider the situation where the small cells are connected to the limited backhaul. Furthermore, using stochastic geometry based HetNets model, numerical analysis of the network throughput and the capacity of a target small cell is presented. In addition, I compare the IB-FD and FDD approaches in details. The results show that, when only a few small cells need to utilise the wireless backhaul of the macrocell, the FDD performs better than the IB-FD in terms of the small cell capacity. On the contrary, when the macrocell needs to communicate with a large number of small cells, the IB-FD performs better than the FDD.

In Section 5.1 of Chapter 5, the contributions are highlighted as follows. Firstly, the optimisation objects use exponentially weighted history in case of sudden fluctuations of system output. Secondly, the UEs' speed is considered in the optimisation. Thirdly, the adjustment of HM and TTT is independent, because the handover ratio is quite sensitive to the TTT settings, adjusting the TTT only after UEs' outage probability performance maintaining bad for a certain period is a better choice. In conclusion, by adjusting the TTT and HM, the PPHO can be optimised and a balance between PPHO rate and handover failure rate can be obtained.

In Section 5.2 of Chapter 5, I give a detailed analysis of the proposed handover scheme in LTE-LAA networks. Compared with handover in traditional LTE networks, which would only be triggered by UE's mobility in licensed bands, in LTE-LAA networks, handover can also be triggered by the availability of unlicensed bands in the serving cells. In such a case, the UEs' capacity can be improved in a large scale. The handover trigger events and novel handover procedures are explained in details. Simulations are performed to evaluate the performance of the proposed handover scheme with availability triggered handover considered.

1.4 Thesis Plan

The thesis is organised as follows:

- Chapter 2: State of the Art and Research Challenges

  In Chapter 2, the reviews of HetNets research will be provided first in Sect. 2.1, including the introduction of BS categories, the network topology, current techniques

applied in HetNets, as well as interference modelling in a stochastic geometry based network. Then, the reviews of energy efficient BS sleep techniques in HetNets will be given in Sect. 2.2, mainly about the analysis of BS power consumption and the analysis of traffic in mobile networks, a discussion of related works about BS sleeping techniques is also presented in this section. In Sect. 2.3, a description of wired and wireless backhaul for small cells as well as a discussion of the related works are presented. In Sect. 2.4, an overview of handover process in LTE system and an introduction of LTE-LAA networks are provided, followed by the discussion of handover research.

- Chapter 3: An Energy Saving Small Cell Sleeping Mechanism with Cell Expansion in HetNets

  In Chapter 3, a novel small cell sleeping mechanism is provided to decrease the energy consumption in HetNets. The main idea of the proposed method is explained as follows: in the cell-edge area of a macrocell, the service area of a sleeping small cell will be covered by a range-expanded small cell nearby; in areas close to the macrocell, UEs associated with a sleeping small cell will all be handed over to the macrocell. Furthermore, the eICIC technique is applied to support the range expanded small cells to avoid QoS degradation.

  The analysis of small cell sleeping mechanism in hexagonal HetNets and in stochastic geometry based HetNets is presented in Sect. 3.1 and Sect.3.2 respectively. Furthermore, a comparison of the results in both sections is provided at the end of the chapter.

- Chapter 4: Enhancing Small Cell and Network Capacity using Wireless Backhaul

  In Chapter 4, an optimal scheme for the small cells to utilise the macrocell links as their wireless backhaul is proposed. In Sect. 4.3, the capacity of a target small cell with a certain distance to the macrocell is discussed. In Sect. 4.4, the numerical analysis of the whole network throughput is presented.

- Chapter 5: Mobility Management Analysis in HetNets and in LTE-LAA Network

  In Chapter 5, the MM in ultra-dense small cell networks and in LTE-LAA networks is analysed. Specifically, in Sect. 5.1, the handover optimisation mechanism that changes the network performance by adjusting the values of HM and TTT in an automatic way is proposed. In Sect. 5.2, the handover scheme which combines mobility triggered handover and availability triggered handover, is designed for LTE-LAA networks. A detailed analysis of the trigger event, channel selection and handover procedures are also presented for the proposed handover scheme.

- Chapter 6: Conclusion and Future Work

  In Chapter 6, the conclusion is presented with the directions for the future work.

Chapter 2

State of the Art and Research Challenges

In this chapter, the topics related to HetNets are reviewed. Specifically, a brief introduction of HetNets is provided first, followed by the analysis of energy efficient BS sleeping techniques, wireless backhaul techniques for small cells, MM in LTE networks, and MM in LTE-LAA networks. Related works and the remaining research gaps are also provided.

2.1 Reviews of HetNets Research

To address the explosive growth in data demands, deploying heterogeneous small cells in a traditional macro mobile network is considered as a quite promising technique. In such a HetNet, various classes of low power nodes (LPNs), including microcells, picocells, femtocells and relays are distributed throughout the macrocell network. According to the definition of the base station classes in [44], base stations can be categorized by Macro Cell (Wide Area Base Station), Micro Cell (Medium Range Base Station) , Pico Cell (Local Area Base Station) and Femto Cell (characterized by Home Base Station), where Wide Area Base Stations are characterised by requirements derived from Macro Cell scenarios with a BS to UE minimum coupling loss equal to 70 dB, Medium Range Base Stations are characterised by requirements derived from Micro Cell scenarios with a BS to UE minimum coupling loss equal to 53 dB, and Local Area Base Stations are characterised by requirements derived from Pico Cell scenarios with a BS to UE minimum coupling loss equal to 45 dB [44]. Small cells, which are defined as low-powered radio access nodes, encompass femtocells, picocells, and microcells.

In HetNets, macrocells provide a wide range of coverage umbrella and small cells are usually deployed in a more targeted manner in traffic hot zones [45]. The small cells and macrocells can be deployed in the same frequency range, or in a separate frequency range. It is noted that when small cells and macrocells share the same frequency, cell range expansion

(CRE) technique will normally be used to increase the number of UEs associated to the small cells[45]. Furthermore, in order to protect the QoS of UEs in the CRE area, the eICIC technique has been proposed [41, 45, 46]. The eICIC technique can eliminate the higher interference suffered by UEs in CRE region and the theory is explained as follows: The Almost Blank Subframes (ABSs) transmitted by macrocells are allocated to UEs in the CRE area. Since macrocells transmit only Cell-specific Reference Signal (CRS) in ABSs, the interference from macrocells can be mitigated significantly, hence, QoS of UEs in CRE area can be guaranteed.

As for the network topology, the macrocells are normally assumed to be regularly deployed as hexagonal cells because macrocells are expected to guarantee the network coverage and their locations should be carefully designed [26]. Small cells require an evolution of the traditional mobile model. The deployment of small cells can keep the familiar grid model, or in a deterministic way [47, 48]. In most recent works, the small cells are randomly placed, e.g., [49–51]. In these papers, the small cells are all assumed to follow Spatial Poisson Point Process (SPPP) distribution. An appealing aspect of this distribution mode is that the randomness actually allows significantly improved tractability and the signal-to-interference-plus-noise ratio (SINR) distribution can be found explicitly [52]. Fig. 2.1 is an illustration of SPPP distributed small cells with density $5*10^{-4}/m^2$ in a $1\times 1\text{km}^2$ area.

Using Fig. 2.1 as an illustration, a derivation of the SINR based coverage probability of UEs will be provided in this part.

Assume that the distance between the UE u and its associated small cell t is r_{tu}, the expression of the SINR of UE u is $SINR=\frac{P_2 hl(r_{tu})}{I_r+\sigma^2}$, where h is the Rayleigh fading of the link from small cell t to the UE u, $l(r_{tu})$ is the pathloss between small cell t and UE u, I_r is the interference from other small cells, and σ^2 is the noise power.

The SINR based coverage probability can be expressed as:

$$\begin{aligned}\mathrm{P_c}(T) &= \Pr[\mathrm{SINR} > T] \\ &= \Pr[\frac{P_2 hl(r_{tu})}{\mathrm{I_r}+\sigma^2} > T] \\ &= \mathrm{E_{I_r}}[\Pr(h > \frac{T}{P_2 l(r_{tu})}(\mathrm{I_r}+\sigma^2))].\end{aligned} \tag{2.1}$$

Due to the Rayleigh fading, where the power $h \sim exp(1)$, the coverage probability can be derived as:

$$\mathrm{P_c}(T) = \exp(\frac{T}{P_2 l(r_{tu})}\sigma^2)\cdot \mathrm{E_{I_r}}[\exp(\frac{T}{P_2 l(r_{tu})}\mathrm{I_r})]. \tag{2.2}$$

Substitute $(\frac{T}{P_2 l(r_{tu})})$ with s, according to [53, Theorem 2.27], $\mathrm{E_{I_r}}[\exp(sI_r)]$ can be expressed as:

$$\begin{aligned}\mathrm{E_{I_r}}[\exp(sI_r)] &= \mathrm{E_{I_r}}[e^{-sI_r}] \\ &= \int e^{-sI_r} f_{I_r}(I_r) dI_r \\ &= \mathscr{L}_{I_r}(s). \end{aligned} \tag{2.3}$$

Hence, in the remaining parts of this thesis, $\mathscr{L}_{I_r}(s)$ is used as the expression of $\mathrm{E_{I_r}}[\exp(sI_r)]$ for simplicity. Here, I give a derivation of $\mathscr{L}_{I_r}(s)$:

$$\begin{aligned}&\mathscr{L}_{I_r}(s) \\ &= \mathrm{E}[\exp(-s\sum_{x\in\phi_2} P_2 h_x ||x||^{-\alpha_2})] \\ &= \mathrm{E}[\prod_{x\in\phi_2} exp(-sP_2 h_x ||x||^{-\alpha_2})] \\ &\overset{(a)}{=} \exp(-\lambda_2 \int_{R^2} 1 - E_{h_x}[exp(-sP_2 h_x ||x||^{-\alpha_2})] dx) \\ &\overset{(b)}{=} \exp\left(-\lambda_2 \int_{R^2} \frac{1}{1+\frac{||x||^{\alpha_2}}{sP_2}} dx\right) \\ &\overset{(c)}{=} \exp\left(-\pi\lambda_2 \frac{(sP_2)^{\alpha_2/2}}{\mathrm{sinc}(2/\alpha_2)}\right), \end{aligned} \tag{2.4}$$

where (a) uses the expression of the probability generating function (PGFL) for a PPP [54], (b) used $h_x \sim exp(1)$, and (c) uses standard machinery, where the integral is converted form Cartesian to polar coordinates.

Substitute s with $\frac{T}{Pl(r_{tu})}$, according to (2.2), $\mathrm{P_c}(T)$ can be written as:

$$\mathrm{P_c}(T) = \exp(\frac{T}{P_2 l(r_{tu})}\sigma^2) \cdot \exp\left(-\pi\lambda_2 \frac{(\frac{T}{P_2 l(r_{tu})}P)^{\alpha_2/2}}{\mathrm{sinc}(2/\alpha_2)}\right), \tag{2.5}$$

where T is the coverage probability threshold, P_2 is the small cell transmission power, λ_2 is the small cell density, α_2 is the pathloss exponent for small cells. σ^2 is the noise power.

In dense small cells HetNets, Energy efficiency, Mobility Management, wireless backhaul have become quite popular research topics [15].

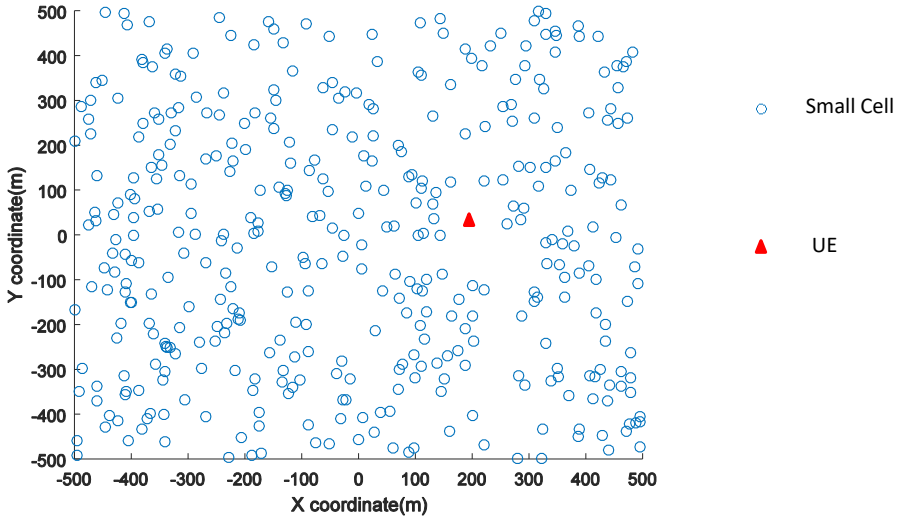

Fig. 2.1 A 1×1 km^2 view of Poisson distributed small cells

2.2 Reviews of Energy Efficient BS Sleep Techniques in HetNets

Mobile networks have experienced immense growth in traffic data, which leads to much more greenhouse gas emission and energy consumption[55].

According to previous researches, five approaches can be summarized to reduce the energy consumption in mobile networks[8].

- Energy efficiency improvement on hardware components.
- Utilizing green and renewable energy resources.
- Turning off selected components.
- Transmission process optimisation.
- Deploying and planning heterogeneous networks.

The approaches of the first category are to design the hardware components (e.g., power amplifier) in a more energy efficient way [56, 57]. From an EE perspective, the performance of most components in a mobile network is unsatisfactory. For instance, the power amplifier, which consumes the largest amount of power in a macrocell, translating only less than 20% of its input power to the output power, more than 80% of the input energy is dissipated as heat [58]. Researches show that the ratio of the output power to input power of the power amplifier can be optimised to reach 70% [58]. However, the implementation cost for these approaches is high. Hence, for network operators, a careful consideration for both operational and economical costs is needed before decisions on hardware selection.

The second category covers approaches that utilize renewable and green resources. It is noted that as green energy technologies develop, the green and renewable energy such as wind and solar energy can be utilized to power BSs [59]. For the developing countries without mature network infrastructures, planning green power supplied BSs can be a long-term environmental solution for the wireless communication industry. However, for developed countries, the high replacement cost will be a serious problem.

The third category includes the approaches that switch off some BSs in the mobile network during the off-peak hours [60–63]. The approaches in this category save the network energy by monitoring the traffic load, then switching some BSs into sleep mode, or reactive the certain BSs in the network. Unnecessary energy consumption can be avoided with these BSs sleeping mechanisms. These approaches turn off certain elements, including but not limited to BSs, power amplifiers, cooling equipments [64]. As shown in Fig. 2.2, BSs consume the largest amount of energy in mobile networks. In addition, dense BSs deployment has been more and more popular in recent years, which leads to smaller coverage area and more random traffic patterns, making sleep mode operations more desirable. Considering that some elements must be kept on to support the basic operations of the network, the energy savings are not as high as the approaches in category 1. In addition, BS sleeping mechanisms have negative impacts on the QoS of the networks, unless some specific remedial algorithms are adopted concurrently [19, 65, 66]. Furthermore, it's worth noting that because the sleep techniques are based on the current network architecture, they have the advantage of being easier to test and implement.

The approaches in the fourth category optimise the radio transmission process. The techniques including the MIMO technique, cognitive radio transmission, channel coding, resource allocation for signalling, and cooperation relaying have been researched to improve the EE [67, 68].

The approaches of the fifth category are to deploy lower power-consuming small cells in the network. Compared with conventional homogeneous macrocell deployment, the Het-

Nets deployment reduces energy consumption by shortening the propagation distance between nodes in the network. The number of small cells, as well as their locations, needs to be carefully planned because when too many small cells are deployed, the trend of energy saving may even be reversed.

2.2.1 Energy Consumption of Mobile Networks

From Fig. 2.2 [8], it's easy to see that BSs are the main contributor of the network energy consumption, consuming nearly 60% of the whole energy of a typical mobile network, and the increase in the number of BSs also impacts the overall network energy consumption significantly [67].

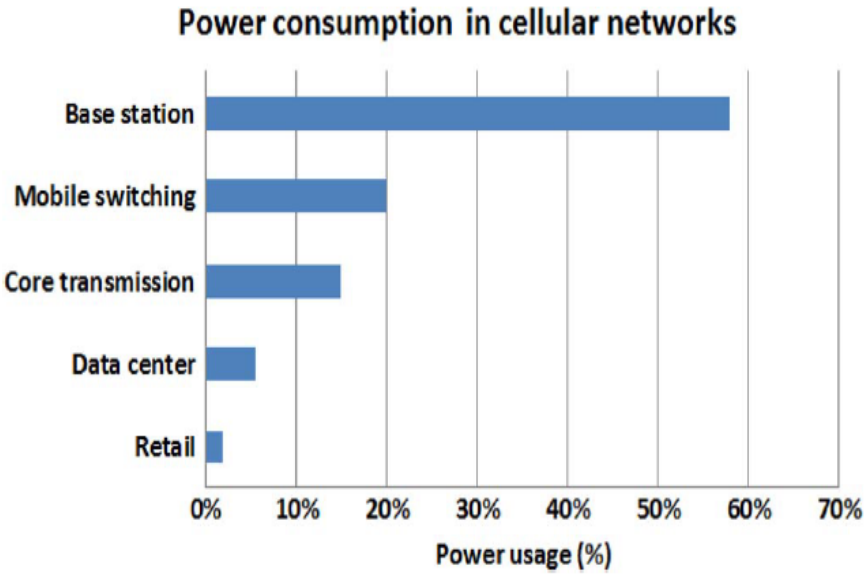

Fig. 2.2 Energy consumption in mobile networks

Due to the ultra dense deployment of small cells in recent years, the energy consumption of small cells has already become a critical problem . The small cells consume much less energy compared to macrocells. However, due to the large scale deployment of the small

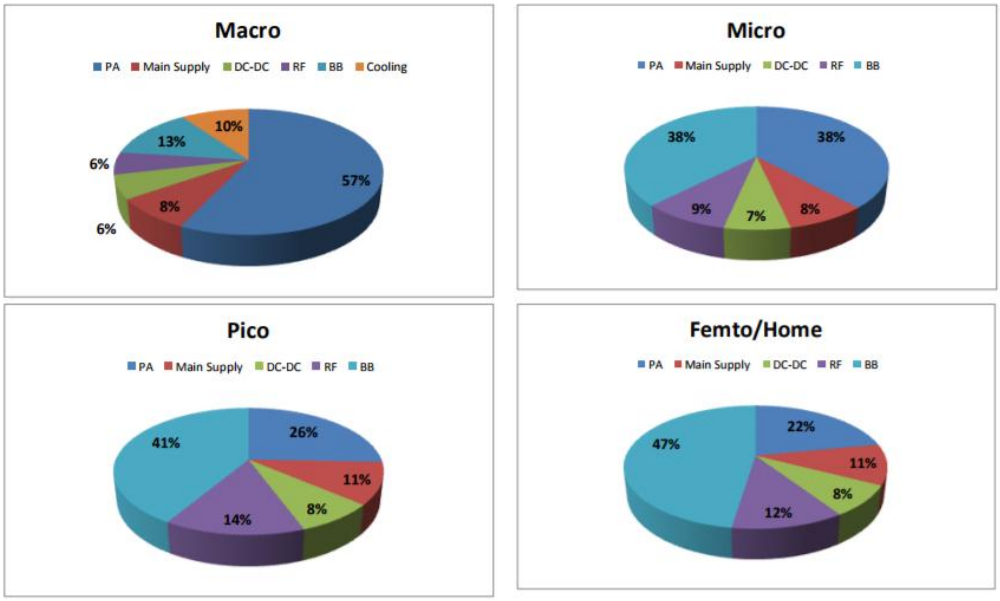

Fig. 2.3 Breakdown of power consumption in BSs

cells in the near future, it is estimated that they will consume around 4.4 TWh of power by the year 2020 [69].

In this part, an explanation of the BS power consumption with variable load will be given. In fact, it is mainly the power amplifier (PA) power consumption that varies with traffic load. From Fig. 2.3 [70] it can be seen that this scaling over the load largely depends on the BS type: for macrocells the PA accounts for 55- 60% of the overall power consumption at full load, whereas for low power nodes such as pico cells and femtocells the PA power consumption accounts to less than 30% of the total, it is mainly the baseband interface (BB) part that dominates the power consumption. For microcells, the BS power consumption is more balanced.

Fig. 2.4 [70] explains BS power consumption curves for the LTE system with 10 MHz bandwidth and 2x2 MIMO configuration. Three sectors are used for macrocells, whereas omni-directional antennas are considered for the smaller BS types. From Fig. 2.4, it can be seen that the BS power consumption is load dependent for macrocells and microcells, however, for picocells and femtocells, the load dependency is negligible. The reason is that for low power small cells, the impact of the PA is diminishing, and the power consumption of other components hardly scales with the load.

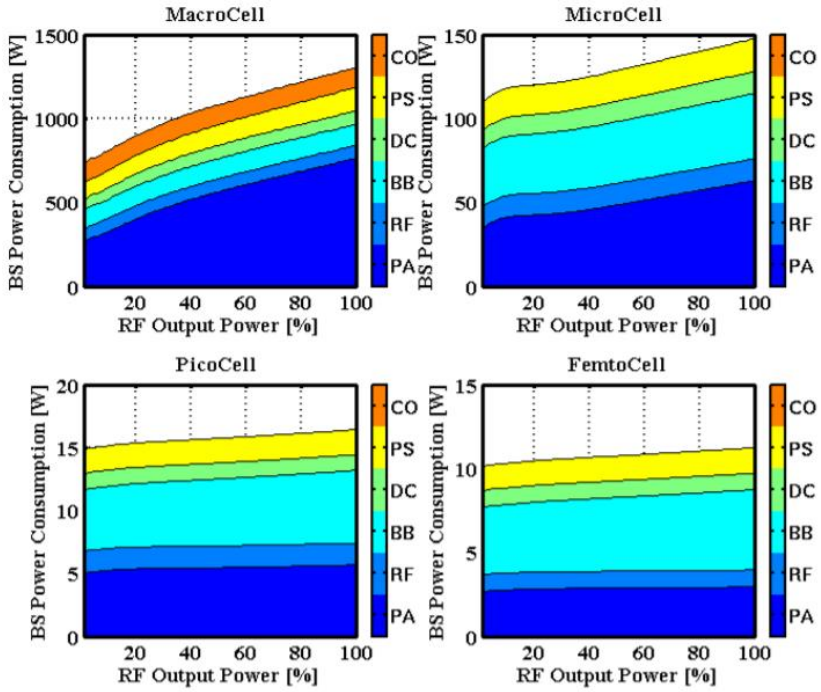

Fig. 2.4 Power consumption dependency on relative linear output power in all BS types for a 10MHz bandwidth, 2x2 MIMO configurations and 3 sectors (only Macro) scenario based on the 2010 State-of-the-Art estimation.

As shown in Fig. 2.4 [70], it can be seen that the relationships between RF output power (P_t) and BS power consumption (P_c) are almost linear. In that case, the power consumption model can be written as:

$$Pc = \begin{cases} N_A(P_0 + \Delta_p P_t) & 0 < P_t \leq P_M \\ N_A P_s & P_t = 0, \end{cases} \tag{2.6}$$

where N_A is number of antennas, P_0 is the static power consumption, Δ_p is the slope of the power model, P_s is the power consumption for the BS in sleep model, $P_t = \rho P_M$ is the average transmit power, ρ is the load of the corresponding BS, and P_M is the maximum average transmit power of the BS.

As mentioned before, (2.6) is an easy way to approximate the BS power consumption based on Fig. 2.4. A more accurate power consumption model at maximum load is provided

in [70]. The breakdown of the BS power consumption when $P_t = P_M$, can be expressed as:

$$P_c = N_{TRX} \frac{\frac{P_t}{\eta_{PA}} * (1 - \sigma_{feed}) + P_{RF} + P_{BB}}{(1 - \sigma_{DC})(1 - \sigma_{MS})(1 - \sigma_{cool})}, \tag{2.7}$$

where N_{TRX} is the number of transceiver chains, P_{BB}, P_{RF}, σ_{DC}, σ_{MS}, σ_{cool}, η_{PA} can be referred to Tab. 6 from [70].

2.2.2 Traffic Variation and Prediction in Mobile Networks

The authors in [71, 72] provided the prediction of daily and weekly traffic. Simply stated, the day or week traffic profile can be modelled as a periodic sinusoidal profile. Fig. 2.5 [73] illustrates the aggregated network load in each hour and hourly load of three top loaded base stations in a network. Most of the researches evaluate the performance of BS sleep mechanisms according to the periodic sinusoidal traffic model, but it's worth noting that the real data traffic has also been used in BS sleeping techniques to evaluate the energy saving [74, 75].

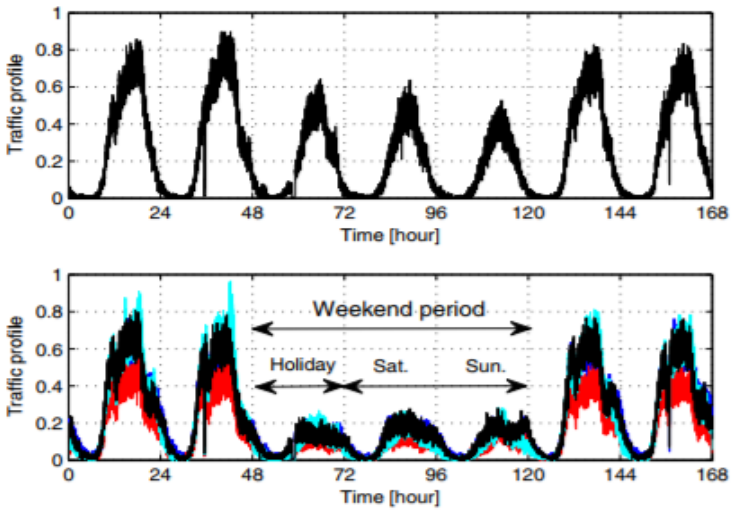

Fig. 2.5 Normalized weekly traffic profile. The top figure shows the centre BS and the bottom figure shows the four neighbouring BSs (The four colour represents four neighbouring BSs).

2.2.3 Related Works and Discussions

The authors in [9, 61] presented macrocell range expansion mechanisms based on adaptive cell zooming with varying traffic loads. In [73], the authors proposed a network-impact switching-on/off algorithm that can be operated in a distributed manner with low computational complexity. In [76], the authors proposed a cell sleeping algorithm to switch off low load cells and compensating for the coverage loss by expanding the neighbouring cells through antenna beam tilting. In [66], the authors proposed several switch-off patterns in homogeneous networks with different service arrival rates, where the coordinated multiple point (CoMP) transmission technology was used to extend cell coverage. In [77], the authors proposed an energy saving mechanism for LTE networks to decide whether or not to switch off an eNodeB (eNB) based on the average distance of its associated UEs. In [78], the authors made a conclusion that the cell sleeping mode operation was effective in energy saving when the traffic is light and cell size is small. In [79], an energy saving mechanism was used to reduce the number of active BSs while guaranteeing the coverage probability.

Recent efforts related to cell sleeping modes have been made in small cell networks. In [80], the authors provided fixed time sleeping scheme to save the energy of femtocells. In [74, 81], the authors proposed a sleep mode mechanism in dense small cell networks, which switched off idle small cells or cells with few UEs.

All the existing works mentioned above focused on homogeneous networks. More recently, BS sleeping mode has also been studied for HetNets energy saving. In [82], an optimal sleep/wake-up mechanism was provided to maxmise the energy saving of the HetNets. In [83], the authors provided a repulsive cell activation scheme in terms of the minimum separation distance between the small cells to achieve improved EE. In [19], the authors derived the EE in homogeneous and heterogeneous networks with various sleeping strategies. In [21], a numerical analysis of a random sleeping strategy and a simulation based sleeping mechanism were presented. In [22], the authors analysed the optimal BS density that minimises the network energy consumption for both homogeneous and heterogeneous networks. In [84], the authors proposed a sleeping control scheme by switching off small cells with low traffic load and offloading the traffic to their nearest macrocells. In [85], the authors only demonstrated that switching off small cells close to macrocells achieves higher EE, but no small cell sleeping mechanism was proposed. In [24], a small cell activation mechanism for HetNets was proposed. The authors maximised the network energy saving by considering the traffic load transferred from macrocells to the active small cells.

To conclude, many efforts have been made to provide the BS sleeping techniques. However, it is obvious to see that the sleeping algorithms considering the influence of macrocells in HetNets energy saving is insufficient. In [25, 26], the authors studied the energy saving

of HetNets by turning off small cells close to macrocells. However, when the sleeping small cell is far away from the macrocell, the energy saving of the network will not be significant. Hence, more researches are needed to provide more advanced small cell sleeping algorithms.

2.3 Reviews of Wireless Backhaul Technologies

In the past few decades, significant development of information and communications technology (ICT) has been realized, especially the wireless communication systems have been playing a crucial role because of the increasing requirement from the wireless service. As the number of wireless UEs and resource requirements keep increasing, it is generally agreed that the dense small cells deployment can be a promising technique to meet the challenges. In such a situation, the problems of how to forward hundreds of gigabits backhaul traffic in ultra dense small cell networks with satisfied QoS need to be solved.

The backhaul evolution for 5G includes wired and wireless backhaul technology. In [14, 86], the analysis and comparison of wired and wireless backhaul technique have been provided.

Deploying wired backhaul for small cells can be an approach as it is reliable in high data rate transmission, in fact, fibre optic backhaul is the most preferable solution in terms of both bandwidth and latency. However, it's not an economically viable option. In some locations, highly reliable wired backhaul may not be necessary for small cells because small cells serve quite limited traffic compared to macrocells.

The alternative is to deploy wireless backhaul. Compared with wired backhaul, wireless backhaul is more flexible and cost-efficient. With line- of-sight (LOS) communication path, up to several gigabits per second highly directional wireless links are supported by point-to-point microwave or free space optical (FSO) communications. Non-line-of-sight(NLOS) wireless backhaul solutions mainly occupy sub-6 GHz licensed/unlicensed bands, and can provide up to several hundreds of megabits per second link capacity [86].

Fig. 2.6 [15] illustrates the wireless backhaul architecture. In Fig. 2.6 [15], the wireless backhaul traffic of small cells is transmitted to the macrocell and then the aggregated backhaul traffic at the macrocell is forwarded to the core network by fibre to the cell (FTTC) links.

Recently, in-band full duplex (IB-FD) based wireless backhaul has been investigated in many researches. In-band wireless backhaul link uses the same frequency bands where the mobile system operates. In [87–89], IB-FD has been demonstrated to be a promising technique to improve the spectral efficiency. IB-FD technique can be applied to enable

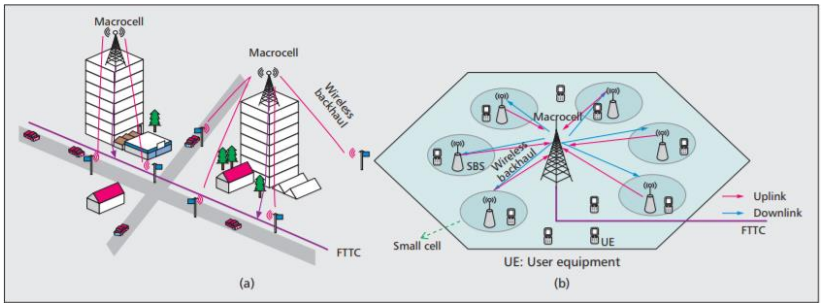

Fig. 2.6 The central solution of 5G wireless backhaul networks: a) the central scenario; b) the central scenario logic architecture.

simultaneous transmission of access and backhaul information in the same frequency. Compared with out-band wireless backhaul , in-band wireless backhaul can improve spectrum reuse, but both the backhaul and access link will suffer the additional interference.

More advanced techniques have been applied together with wireless backhaul to enhance the network throughput. Massive MIMO systems can achieve capacity increase and EE improvement simultaneously. Using massive MIMO technique to provide wireless backhaul allows a high degree of spatial multiplexing, enabling backhaul BSs to provide sufficient bandwidth to support small cells using the same frequency resource [42, 90, 91]. Millimeter-wave (mmWave) has been recently considered for wireless backhaul because of its rich and low cost spectrum [92, 93]. However, it is worth noting that mmWave backhaul link significantly depends on the LOS transmission, and the distance between the macorcells and small cells are long with several obstacles. Moreover, mmWave backhaul link is vulnerable to atmospheric attenuation, e.g., the water molecules in the air. Therefore, it can be seen that CAPEX of mmWave backhaul is high, as more complex design for radio transmitter and receiver is need to ensure they are precisely aligned for LOS transmission, furthermore, higher antenna gain is required to overcome penetration losses. Due to these limitations of mmWave backhaul, the traditional radio frequency wireless backhaul is still attractive to network operators.

It's noted that the wired backhaul cannot be fully overlooked due to its reliability and huge capacity [94], the backhaul transmission will certainly combine both wired and wireless backhaul, e.g., sometimes the small cells connect to the core network by low capacity backhaul (e.g., [95]), in this situation, wireless backhaul is needed to enhance the small cell throughput.

2.3.1 Related Works and Discussions

Most of the related works target on developing optimisation algorithm to improve UEs' QoS or reducing network energy consumption with wireless backhaul [86, 96–100]. In [96], the authors investigated the problem of joint optimisation of downlink cell association and wireless backhaul bandwidth allocation in HetNets. In [97, 99], the authors optimised the resource used as wireless backhaul to enhance the network throughput. In [98], an optimal transmit power allocation algorithm was derived in a closed form under QoS requirements in an IB-FD wireless backhaul based system. In [100], the authors investigated the problem of minimising the network energy consumption in mm-wave wireless backhaul based dense small cell HetNets.

The are also some researches which focus on the performance evaluation of the wireless backhaul based networks. In [27], the authors analysed the network throughput performance of an IB-FD network using stochastic geometry model, but it was only for a single tier network. In [28], the authors developed a framework to model the downlink rate coverage probability of UEs in a given HetNet with wireless backhaul, but the whole network throughput has not been considered. In [101], the authors proposed a general and tractable mobile model with wireless mm-wave backhaul together with wired backhaul, the rate coverage probability of UEs was also analysed. In [102], the authors numerically analysed delay performance of wired and wireless backhaul in HetNets. A comparison of wireless and wired backhaul for static and mobile UEs was provided. The work in [29] considered the case of HetNets with IB-FD enabled small cells, the authors provided analytical expressions for coverage and average downlink rate using tools from the field of stochastic geometry. However, the authors didn't consider the whole network throughput performance. The authors in [14] investigated the flexible high-capacity hybrid wireless and optical mobile backhauling for small cells. In [15], the authors discussed and compared the EE of wireless backhaul networks for different system architectures and frequency bands.

To conclude, lots of efforts have been made in the research area of wireless backhaul. However, most of the papers targeted on the wireless backhaul resource optimisation to enhance UEs' QoS. In [28, 29, 101], the authors theoretically analysed the coverage probability of UEs. It is noted that the work related to the numerical analysis of whole network throughput is insufficient. Hence, more investigation needs to be implemented in this area.

2.4 Reviews of Mobility Management in Heterogeneous Networks

As mentioned before, one of the most promising techniques in wireless communication to meet the data explosion is the integration of small cells into macrocell mobile networks[52]. Small cells are considered as promising solutions to enhance network capacity and support the emerging home and enterprise applications.

Mobility Management (MM), in the presence of small cells , is one of the most challenging issues, owing to the dense network layout, the short cell radii and the potentially unplanned deployment [52].

2.4.1 Overview of Handover Process in LTE

In this part, a brief introduction of handover process in LTE will be given. In mobile networks, the handover is the process through which a mobile UE communicates with one BS is switched to another BS during a call or a data service. The handover process is typically divided into four stages: measurements, processing, decision, execution.

A. Measurements and Processing Stages

Handover measurements are based on the the primary and secondary synchronisation signals in the downlink direction, which are transmitted on the central 72 sub carriers of the first and sixth subframe in each frame [103]. Reference Signal Received Power (RSRP) and Reference Signal Received Quality (RSRQ) are the two basic measurements supported on the UE side [104]. Fig. 2.7 [105] depicts the measurement procedure for small cells in Long-Term Evolution-advanced (LTE-A).

B. Handover Decision

The handover decision phase is performed at the source cell based on the signal quality measurements offered by the UE.

To trigger the handover procedure, the UE need to send an measurement report (MR) to the source cell if the layer 3 filtered measurements meets an event entry condition. In LTE-A, there are eight types of entry condition, which can be found in Section 9.2 in [106].

In LTE systems, UEs exchanged among eNBs operating in the same frequency band are triggered by event A3: neighbour becomes offset better than server, which is illustrated in Fig.2.8. The M_s and M_t are the filtered RSRP of the serving cell and target cell respectively.

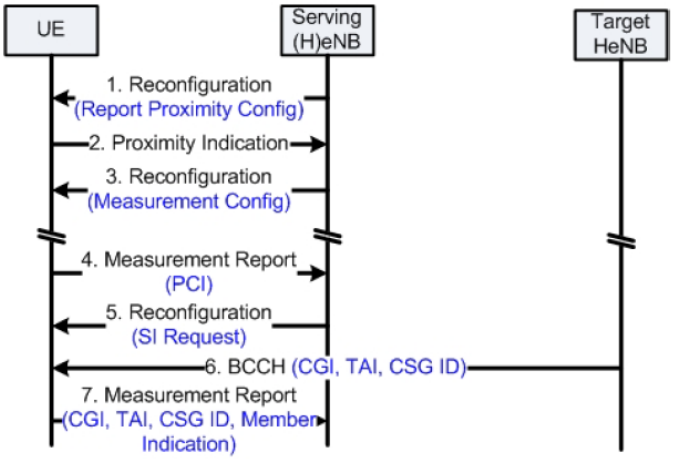

Fig. 2.7 Measurement signalling in LTE-A

Hyst is the hysteresis parameter and $CIO_{s,t}$ is the cell-specific offset. Once the event A3 condition is met, the UE starts the time trigger. Only when event A3 entry condition is satisfied through the whole TTT time window, the UE will report the event A3 to the source cell via measurement reports, that may trigger the handover.

C. Handover Execution

With the presence of small cells, the signalling and delay overheads are increased and more sophisticated signalling procedures are needed to integrate the femtocell specific processes into the handover execution phase. An overview of the signalling flow in handover execution phase is illustrated in Fig. 2.9 [105]. The detailed procedure can be found in [105].

2.4.2 Analysis and Definition of Ping-Pong Handover and Handover Failure

PPHO can be seen as an unnecessary handover. In fact, the occurrence of a PPHO is determined by the time duration that a UE connects to a cell directly after a handover, which named time-of-stay. The time-of-stay starts when the UE sends a handover complete message to a BS, and ends when the UE sends another handover complete message to another BS. When the time-of-stay is less than a threshold (e.g., 1 s), and the new target BS is the same BS as the source BS in the previous handover process, this handover is treated as a PPHO. Simply say, a handover from cell B to cell A then handover back to cell B is defined as a PPHO if the time-of stay is less than a threshold [107].

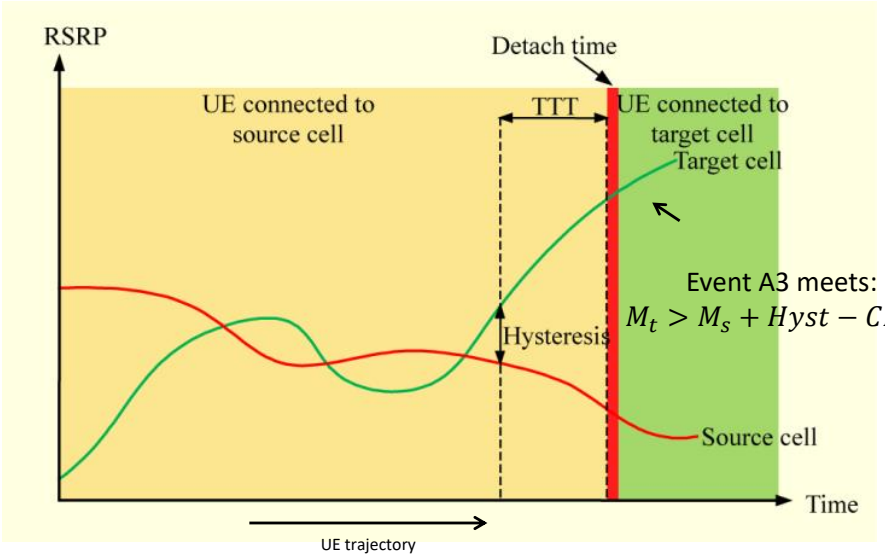

Fig. 2.8 A3 event entry condition

A detailed definition of handover failure is provided in [106]. However, in order to reduce the complexity of the handover algorithm, a simple explanation from [108] is used in the these, that is a handover failure is observed if the UE's wideband SINR is lower than a threshold (e.g., Q_{out}=-8 dB) during the handover.

2.4.3 Related Works and Discussions

In [109–113], the authors provided the numerical analysis of handover, but did not target on handover performance optimisation. Specifically, in [109, 112], the authors derived the numerical expressions of handover failure rate and PPHO rate. In [110], the authors provided the numerical analysis of average handover rate. In [111], a numerical analysis for the handover delay effect was given. In [113], the authors analysed handover delay based on Markov Chain.

In [114], a novel cost-based adaptive hysteresis scheme was proposed to optimise the

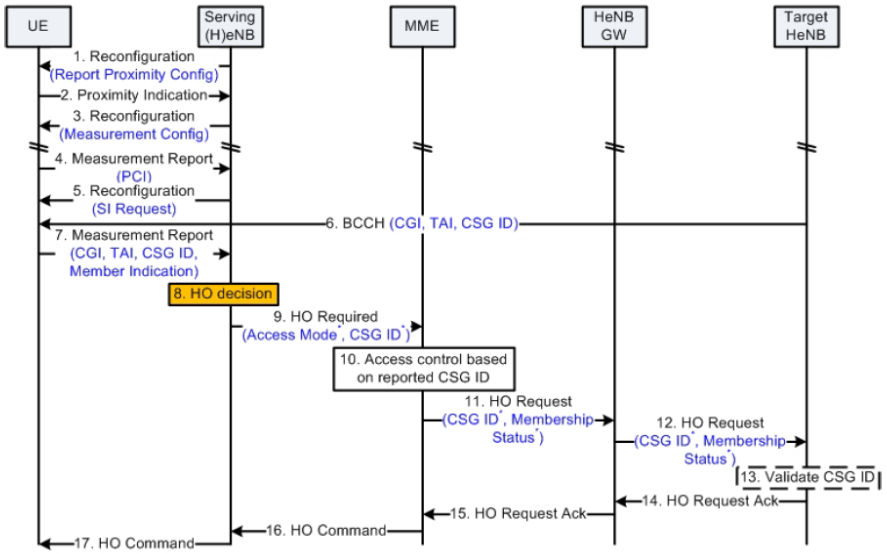

Fig. 2.9 Handover execution signalling procedure

handover failure rate. In [115], the authors reduced the handover failure rate and unnecessary handovers by adjusting the handover parameters adaptively and automatically. In [116, 117], the authors analysed the relationship between handover probability with UEs' speed and distance from the macrocell to small cells. In [118–120], the authors provided schemes to reduce unnecessary handovers, to be more specific, Double Threshold Algorithm (DTA) and Call Admission Control (CAC) mechanisms were used to optimise the unnecessary handovers. In [33, 121–123], the authors optimised the PPHO rate by adjusting handover parameters such as TTT or HM, however, the negative effect on UE's QoS had not been considered. In [124], the authors analysed handover between macrocells to small cells and macrocell to macrocells, providing optimisation of PPHO rate and handover failure rate. In [33], the authors proposed a self-optimising algorithm which tuned the handover parameters to diminish negative effects (call dropping , handover failures, PPHO). In [34, 124, 125], the authors optimised PPHO in LTE networks by adjusting handover parameters while guaranteeing UEs' QoS.

To conclude, a lot of researches have been done in MM in LTE networks. However, the works related to the self-optimisation of PPHO is insufficient. Actually, the adjusting of handover parameters during the PPHO optimisation will cause negative effect on UEs' QoS, e.g., the handover failure rate and UE's outage probability will increase. It is necessary to keep the negative impact within a tolerable range.

2.5 Handover Mechanism for LTE-LAA Networks

To meet the challenges of the explosive data increase, the wireless industry is on the hunt for solutions to boost the capacity. Due to the lack of licensed of the spectrum for mobile networks, finding more capacity in unlicensed spectrum has been proposed in recent years [126]. The unlicensed 2.4 GHz and 5 GHz bands that Wi-Fi systems operate in have been considered as important candidates to provide extra spectrum resources for mobile networks.

2.5.1 LTE Carrier Aggregation with Unlicensed Band

In 3GPP, the most attractive unlicensed band is the 5GHz Unlicensed National Information Infrastructure (UNII) band which are mainly used by IEEE 802.11-based Wireless Local Area Network (WLAN), or Wi-Fi [18]. Different countries have their own demands on 5 GHz UNII band. Fig.2.10 [127] shows the 5 GHz band that is currently in consideration.

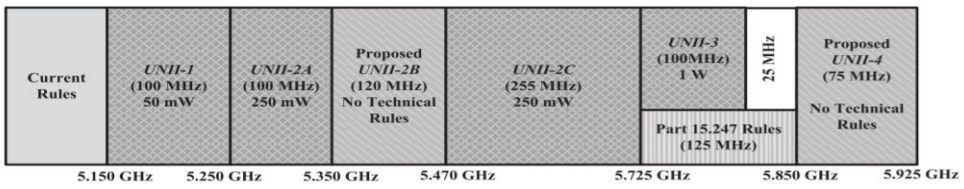

Fig. 2.10 5 GHz unlicensed band in consideration

The transmission relying only on unlicensed spectrum is unstable because the nature of being unlicensed makes it difficult to provide guaranteed QoS. Hence, the utilisation of licensed spectrum cannot be ignored during the spectrum access extension. Because UEs require to access to both licensed and unlicensed spectrum under a unified LTE network. LTE-LAA in unlicensed spectrum is designed as an extension of the LTE career aggregation (CA) protocol [127]. If there is additional capacity demand, to manage the different components carriers, CA may be employed with one carrier serving as Primary Cell, and others serving as secondary cells (SCCs) [128], both primary cell and secondary cell are accessible to one user simultaneously. To enable LTE and Wi-Fi coexist peacefully, LAA supports the listening before talk (LBT) technology, which is set to be a global standard as it enables to meet regulatory requirements worldwide.

LTE-LAA extends LTE to unlicensed spectrum and aggregates the unlicensed spectrum to licensed spectrum with the same CA technology in LTE. Compared with LTE or Wi-Fi networks, LTE-LAA can provide better capacity and large coverage area while allowing seamless data flow between licensed and unlicensed spectrum through a single evolved packet core(EPC). Meanwhile, within LTE-LAA, all UEs are operated in a unified network because of the same access technology for both licensed and unlicensed spectrum. Significant signal overhead in the unlicensed spectrum can be saved by the unification because the control plane signals always transmit over the licensed bands. Based on the user traffic requirement, configuration information can be conveyed from Primary Component Carrier (PCC) to dynamically remove/add SCCs. There are two operation modes for LTE-U/LTE-LAA: supplemental downlink (SDL) and time-division duplex (TDD). In the SDL mode, the unlicensed band is used to carry data traffic of the licensed spectrum, while the UL and control channel remain in the licensed spectrum. On the other hand, in the TDD carrier aggregation mode, the unlicensed spectrum is able to transmit both uplink and downlink data traffic, and the control signal remains in the licensed spectrum.

2.5.2 Listening Before Talk in LTE-LAA

In this part, the main challenge for the coexistence of LTE-LAA and Wi-Fi system will be analysed first. When LTE-LAA operates in the frequency band occupied by Wi-Fi systems, the performance of Wi-Fi systems will be affected significantly, but the performance of LTE is almost unchanged. This is because Wi-Fi systems move to silent mode due to the Carrier Sense Multiple Access/Collision Avoidance mechanism. However, the LTE systems will continuously transmit with minimum time gap even in the absence of traffic.

To enable the peaceful coexistence of LTE-LAA and Wi-Fi systems, the LBT technique has been introduced [18, 129]. LBT requires LTE-LAA device to periodically stop the signal transmitting and detect the activities of other channel occupants on a scale of milliseconds. Fig. 2.11 shows the LBT channel access mechanism in unlicensed band [129]. The LTE-LAA BSs need to listen to the target channel to detect the interference level at preassigned periodic time instants, which are called 'access opportunities' and denoted as '$T_{attempt}$' in Fig. 2.11. At each access opportunity, the BSs sense the unlicensed band, which takes $T_{sensing}$ seconds. Only if the energy level is below a pre-assigned threshold, the UEs or BSs are able to occupy the channel for a fixed time period, named as T_{cellTx} in Fig. 2.11 [129]. Otherwise, the BSs will wait for the next access opportunity.

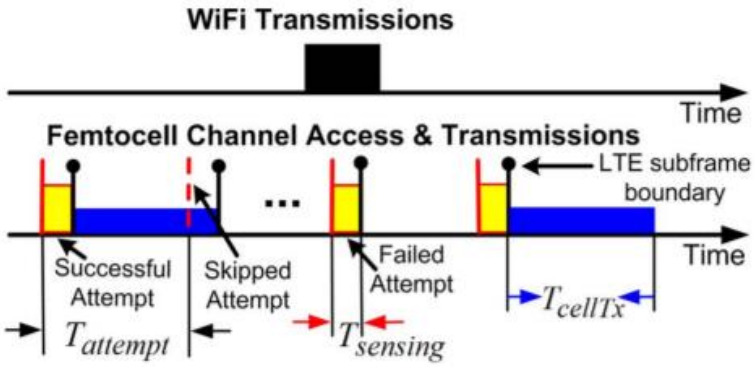

Fig. 2.11 LBT in unlicensed band

2.5.3 Related Works and Discussions

Handover in LTE- WiFi networks is a less researched topic. In [17], a handover procedure was provided between Wi-Fi APs and LTE systems. In [130], [131], [132], handover decision algorithms between Wi-Fi and LTE systems were proposed to optimise UEs' battery lifetime, load balancing and network throughput. In [133], an optimal RAT selection algorithm was provided to maximise the whole system throughput in an LTE-WiFi network with offload capability. In [134], the offloading method was proposed to optimise network throughput and energy consumption. In [135], the authors investigated UE offloading schemes. A win-win situation of Wi-Fi and LTE systems can be obtained by transferring Wi-Fi UEs to LTE systems and allocating unlicensed spectrum to these offloaded UEs. In [136], a Wi-Fi offloading framework was presented to maximise the aggregate UE satisfaction in HetNets.

To conclude, the works targeting on handover and UE offloading in LTE-WiFi networks are insufficient. Furthermore, most of the works in this area only consider handover between LTE and Wi-Fi systems. In [137], the authors analysed handover between LTE BSs in LTE unlicensed networks. However, the detailed handover procedure and handover trigger event were not provided.

2.5.4 Summary

Energy efficient BS sleeping, wireless backhaul techniques and Mobility Management are discussed in this section. To be more specific, in Sect. 2.1, a brief introduction of HetNets is provided, including the discussion of various types of BSs, the eICIC and CRE techniques, as well as a detailed derivation of Laplace transformation used in stochastic geometry based network model. In Sect. 2.2, an introduction of energy efficient BS sleep techniques is provided, mainly about the description of BS power consumption breakdown and the load dependent BS power consumption formula . In Sect. 2.3, the description of wireless backhaul architectures is presented, followed by the explanation of the techniques normally used together with wireless backhaul, such as IB-FD. In Sect. 2.4, an introduction of MM in HetNets is given, including handover process and the definitions of PPHO and handover failure. In Sect. 2.5, an explanation of LTE-LAA networks is given. The CA and LBT techniques are described in this section. Furthermore, for each topic, the related works are summarised and the remaining gaps are identified.

Chapter 3

An Energy Saving Small Cell Sleeping Mechanism with Cell Expansion in HetNets

For densely deployed small cells, energy efficiency (EE) is a critical figure of merit. Due to the dynamics of wireless traffic load, some BSs are lighted loaded in off-peak time but are still active. The active BS with low traffic load waste energy in a large scale. Recently, the adaptive BS density control technology, which adjusts the BS density based on switching of selected BSs, is widely investigated to save energy. However, when BSs are switched off, radio link coverage and QoS have to be guaranteed.

In this chapter, a novel activation and sleeping mechanism is proposed for small cells to decrease the energy consumption in HetNets. The main idea of the proposed method is explained as follows: in the cell-edge area of a macrocell, the service area of a sleeping small cell will be covered by a range-expanded small cell nearby; in areas close to the macrocell, UEs associated with a sleeping small cell will be handed over to the macrocell. Furthermore, the eICIC technique is applied to support range expanded small cells to avoid QoS degradation. Numerical results indicate that the proposed sleeping mechanism significantly reduces the energy consumption of the network while guaranteeing the UEs' QoS requirement.

3.1 Small Cell Sleeping Mechanism in Hexagonal HetNets

3.1.1 System Model

A: Network Model

A two tier network with macrocells (tier 1) and small cells (tier 2) is considered in this section. In the model, both two tiers are considered as mobile network model consisting of hexagonal cells with radius r for small cells and R for macrocells. The network consists of multiple macrocells and the UEs of small cells receive the interference from all these macrocells, but for simplicity, I analyse the sleeping mechanism for the small cells in one macrocell coverage area. In this section, as UEs are deployed uniformly, the small cells are assumed to follow homogeneous and continuous distribution, as shown in Fig. 3.4. Moreover, this assumption is made to enable closed form expressions to be determined. Actually, this assumption has already been made in [47, 138, 139]. A comparison between the proposed homogeneous and continuous small cell network model as well as the more realistic deployment model has been given in Appendix A.

The active user equipments (UEs) are assumed to be uniformly distributed in the network coverage area and the UE density is expressed as $\theta(t)$ at time t.

Both macrocells and small cells are assumed to share the same frequency band and each BS has a limited bandwidth denoted as W Hz here. In addition, all BSs in the same tier transmit an equal fixed power, P_m for the first tier and P_s for the second tier.

In this section, the noise power is assumed to be negligible compared with the interference and only SIR is considered here. The justification is provided here: Assume that the inter-cell interference is constant over the whole area [140], in that case, the inter-cell interference can be approximated at a reference point within the considered small cell. Using Fig. 3.1 as an illustration, the reference point is chosen at the centre of small cell A, and the interference received P_{I_t} at the reference point can be approximated as:

$$\begin{aligned} P_{I_t} &\geq P_{I_B} + P_{I_C} + P_{I_D} + P_{I_E} + P_{I_F} + P_{I_G} \\ &\geq 6P_s(2r)^{-\alpha_s}, \end{aligned} \tag{3.1}$$

where P_{I_B} represents the interference received from small cell B, values of $P_s, \alpha_s, (2r)$ are all listed in Tab. 3.1, where $P_s = 1W$ is the transmitting power of small cells, $\alpha_s = 3.67$ is the pathloss exponent of small cells. Although two values of small cell intersite distance (ISD) (2r) are provided in this section, in (3.1), the larger value (2r=80m) is selected to approximate the lower bound of the interference from small cells.

From (3.1), the minimum value of P_{I_t} is computed as $6.22 * 10^{-7}W$, while the noise

Table 3.1 System parameters of Sect .3.1

Parameter	Value
Macrocell ISD (2R)	800 m
small cell ISD (2r)	[40,80]m
Spectrum Allocation (W)	20 MHz
Pathloss Exponent (α_m, α_s)	3.76, 3.67
Pathloss Constant (K_m, K_s)	$3*10^{-2}$, $8.71*10^{-4}$
P_m [dBm]	46
P_s [dBm]	30
Number of Antennas(N_A)	1,1
P_{0M}, P_{0s} [W]	130, 6.8
Δ_{pm}, Δ_{ps}	4.7 ,4.0
P_{mM}, P_{mS} [W]	20.0, 0.5
UE Density (θ) [m^{-2}]	[3000:200:200]*10^{-4}
Date Rate Requirement (T) [Mbps]	[0.8,0.6,0.4]
Coverage Probability Threshold (ε)	0.8

power is normally assumed to be -104 dbm$(3.98*10^{-12}W)$[26], which is negligible compared with that of interference. Hence, SIR is considered instead of SINR in this section.

The SIR received by a typical user in the downlink can be written as:

$$\gamma_d = \frac{P_i K_i d_{lu}^{-\alpha_i}}{\sum_{j\in\phi_B, j\neq l} P_i k_i d_{ju}^{-\alpha_i}}, \tag{3.2}$$

where P_i is the BS transmission power, K_i the pathloss constant, α_i is the pathloss component, ϕ_B is the set of all interfering base stations and d_{lu} is the distance between the BS_u and UE_l. $\sum_{j\in\phi_B, j\neq l} P_i k_i d_{ju}^{-\alpha_i}$ is the set of the interference received of the typical UE.

The achievable data rate is

$$r_d = \frac{w}{N_u}\log_2(1+\gamma_d), \tag{3.3}$$

where w is the bandwidth available to a cell, N_u is the number of active users served by the BS.

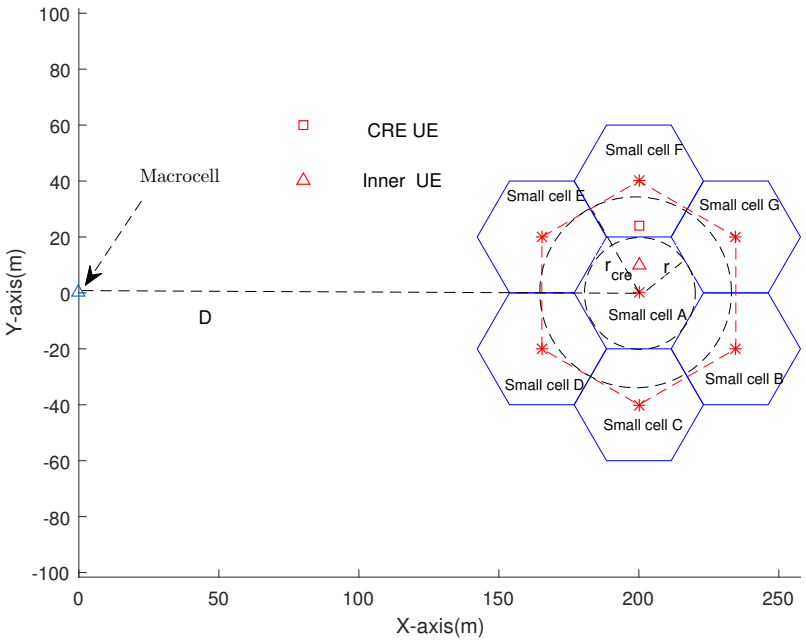

Fig. 3.1 Cell range expansion scenario

B: Power Consumption Model

In Sect. 2.2, the construction of a BS transceiver and the energy consumption mode is provided in details. The power consumption model can be expressed as:

$$Pc = \begin{cases} N_A(P_{0(i)} + \Delta_{p(i)}P_{t(i)}) & 0 < P_{t(i)} \leq P_{M(i)} \\ N_A P_{s(i)} & P_{t(i)} = 0 \end{cases} \tag{3.4}$$

where N_A is number of antennas, $P_{0(i)}$ is the static power consumption, $\Delta_{p(i)}$ is the slope of the power model, $P_{s(i)}$ is the power consumption for the BS in sleep model, $P_{t(i)} = \rho_i P_{M(i)}$ is the average transmit power, ρ_i is the load of the corresponding BS, and $P_{M(i)}$ is the maximum average transmit power of the BS. Values of the parameters are assigned in Table 3.1 .

When a small cell is switched off, the load of the sleeping small cell is transferred to the macrocell, the variation of energy consumption of the whole network can be expressed as:

$$P_{reward} = P_{0s} + P_{Ms}\Delta_{ps}\rho_s - P_{Mm}\Delta_{pm}\rho_m, \tag{3.5}$$

where ρ_s is the load of the sleeping small cell and ρ_m is the load transferred to the macrocell.

$P_{0s} + P_{Ms} \cdot \Delta_{ps} \rho_s$ is the power consumption of the sleeping small cell, and $P_{Mm} \Delta_{pm} \rho_m$ is the increase of the power consumption of the macrocell.

3.1.2 Analysis of the Proposed Method

In this section, an analysis of the proposed approach is provided. The impact of the distance from the sleeping small cell to the macrocell on the power consumption is investigated.

The coverage probability is defined by:

$$\begin{aligned} &\Pr(r_d > T) \\ &= \Pr\left[\frac{w}{N_u}\log_2(1+\gamma_d) > T\right] \\ &= \Pr\left[\frac{w}{N_u}\log_2\left(1+\frac{P_i K_i d_{lu}^{-\alpha_i}}{\sum_{j\in\phi_B, j\neq l} P_i K_i d_{ju}^{-\alpha_i}}\right) > T\right], \end{aligned} \tag{3.6}$$

where r_d is expressed in (3.3), T is the minimum data rate requirement of the UEs, w is the bandwidth allocated to the BS, and N_u is the number of UEs of the BS. In the derivation, the power of interference in coverage area of the considered small cell is assumed to be equal to that at the BS [140].

An example of the considered scenario is shown in Fig. 3.1. The network power consumption of two approaches is compared: (1) The UEs in dashed line hexagon are served by small cell A. (2) The UEs in dashed line hexagon are all handed over to the macrocell. Assume that the distance between the two neighbouring small cell is $2r$ and the distance between the small cell A and the macrocell is D.

For the first approach, small cell A is active and its association area is expanded to the dashed hexagon to serve part of the traffic load from small cells (B,C,D,E,F,G). For the sake of simplicity, both small cell A and the dashed hexagon are modelled as circles during computation of the cumulative density function (CDF) of UEs' locations. Denoting the distance between a random UE in CRE area to small cell A as d, the CDF of d is written as:

$$F_d(d_0) = \frac{d_0^2 - r^2}{r_{cre}^2 - r^2}. \tag{3.7}$$

Proof. Using Fig. 3.1 as a illustration,

$$\begin{aligned} F_d(d_0) &= \Pr(d < d_0) \\ &= \frac{\pi(d_0^2 - r^2)}{\pi(r_{cre}^2 - r^2)} \\ &= \frac{d_0^2 - r^2}{r_{cre}^2 - r^2}. \end{aligned} \tag{3.8}$$

□

Based on (3.6), the coverage probability of UEs in the annulus G_{CRE} can be written as:

$$\begin{aligned} G_{\mathrm{CRE}} &= \Pr\left[\frac{W_{\mathrm{CRE}}}{(S_{\mathrm{CRE}} - S_{\mathrm{inner}})\theta(t)} \log_2(1 + \frac{P_{\mathrm{s}} K_{\mathrm{s}} d^{-a_{\mathrm{s}}}}{I_{\mathrm{s}}}) > T\right] \\ &= \Pr\left[\log_2(1 + \frac{P_{\mathrm{s}} K_{\mathrm{s}} d^{-a_{\mathrm{s}}}}{I_{\mathrm{s}}}) > \frac{T(S_{\mathrm{CRE}} - S_{\mathrm{inner}})\theta(t)}{W_{\mathrm{CRE}}}\right] \\ &= \Pr\left(1 + \frac{P_{\mathrm{s}} K_{\mathrm{s}} d^{-a_{\mathrm{s}}}}{I_{\mathrm{s}}} > 2^{\frac{T(S_{\mathrm{CRE}} - S_{\mathrm{inner}})\theta(t)}{W_{\mathrm{CRE}}}}\right) \\ &= \Pr\left[d^{-\alpha_{\mathrm{s}}} > \left(2^{\frac{T(S_{\mathrm{CRE}} - S_{\mathrm{inner}})\theta(t)}{W_{\mathrm{CRE}}}} - 1\right) \frac{I_{\mathrm{s}}}{P_{\mathrm{s}} K_{\mathrm{s}}}\right] \\ &= \Pr\left\{d < \left[\left(2^{\frac{T(S_{\mathrm{CRE}} - S_{\mathrm{inner}})\theta(t)}{W_{\mathrm{CRE}}}} - 1\right) \frac{I_{\mathrm{s}}}{P_{\mathrm{s}} K_{\mathrm{s}}}\right]^{-\frac{1}{\alpha_{\mathrm{s}}}}\right\}, \end{aligned} \tag{3.9}$$

where $\frac{W_{cre}}{(S_{cre} - S_{inner})\theta(t)}$ is the average bandwidth allocated to each UE in the CRE area, $\log_2(1 + \frac{P_s K_s d^{-a_s}}{I_s})$ is the spectrum efficiency based on Shannon's Formula, $\theta(t)$ is the UE density at time t, I_s is the interference from other small cells, which approximates (3.1), S_{CRE} is the area of the dashed hexagon, and S_{inner} is the area of small cell A shown in Fig. 3.1. Since the coverage area are assumed to be hexagons, $S_{cell} = 6\sqrt{3}r_{CRE}^2$, and $S_{inner} = 6\sqrt{3}r^2$. The values of T, P_s, K_s are assigned in Tab. 3.1.

Combining (3.7) and (3.9), G_{CRE} can be expressed as:

$$G_{CRE} = \frac{\left\{\frac{\left[2^{\frac{T(S_{cre} - S_{inner})\theta(t)}{W_{cre}}} - 1\right] I_s}{P_s K_s}\right\}^{-\frac{2}{a_s}} - r^2}{r_{cre}^2 - r^2}. \tag{3.10}$$

The QoS of UEs in the annulus has to be guaranteed, i.e., $G_{CRE} \geq \varepsilon$, where ε is the

coverage probability threshold. From (3.10), the minimum value of W_{cre} is given by

$$W_{cre} = \frac{T(S_{cell} - S_{inner})\theta(t)}{\log_2\left\{\frac{\left[\varepsilon(r_{cre}^2 - r_{inner}^2) + r_{inner}^2\right]^{-\frac{a_s}{2}} P_s K_s}{I_s} + 1\right\}}. \tag{3.11}$$

The total bandwidth requirement is

$$W_s = W_{inner} + W_{cre} = W\beta + W_{cre}, \tag{3.12}$$

where W is the network bandwidth, $0 \leq \beta \leq 1$ is the duty cycle for macrocell. In the simulation of this part, $\beta = 0.5$, and therefore the macrocell schedules transmissions only in the odd subframes (OSFs), and leaves the even subframes (ESFs) blank, as assumed in [141]. Definitely, with a decreasing β, the coverage area of the small cell increasingly expands. However, β must be chosen under the constraints to guarantee the QoS of the UEs in the small cell coverage area.

For the second approach, the resource needed when the UEs in the small cells are served by the macrocell is analysed. The CDF of the distances between the macrocell and UEs in a small cell is derived first. The distance between the macrocell and the small cell is D and the radius of the small cell is r. When treating the small cell coverage area as a circle, the CDF of D is expressed as [142]

$$\begin{aligned} F_d(d_0) = \frac{1}{\pi r^2}[\frac{\pi}{2}(d_0^2 + r^2) - d_0^2 \text{asin}\frac{D^2 + d_0^2 - r^2}{2d_0 D} \\ + r^2 \text{asin}\frac{d_0^2 - D^2 - r^2}{2Dr} \\ - \frac{1}{2}\sqrt{(d_0^2 - (D-r)^2)((D+r)^2 - d_0^2)}]. \end{aligned} \tag{3.13}$$

Proof. The Proof can be referred to the Appendix of [142].

Then, the required resource W_m is the solution of the equation

$$Pr(\frac{W_m}{(S_{cell})\theta(t)}\log_2(1 + \frac{P_m K_m d^{-a_m}}{I_m + I_s}) > T) > \varepsilon, \tag{3.14}$$

where I_m is the interference from macrocells except the serving macrocell, I_s is the interference from all the small cells. ε is the coverage probability threshold. $S_{cell} = 6\sqrt{3}r_{cre}^2$ is the area of the dashed hexagon shown as Fig. 3.1.

Following some trivial derivation, (3.14) is rewritten as

$$\Pr(d \leq (\frac{(2^{TS_{cell}\theta(t)/W_m}-1)(I_m+I_s)}{P_m K_m})^{-\frac{1}{a_m}}) > \varepsilon. \tag{3.15}$$

Substituting (3.13) into (3.15), I obtain simultaneous equations

$$\begin{cases} \frac{1}{\pi r^2}[\frac{\pi}{2}(d_0^2+r^2) - d_0^2 asin\frac{D^2+d_0^2-r^2}{2Dd_0} \\ +r^2 asin\frac{d_0^2-D^2-r^2}{2Dr} \\ -\frac{1}{2}\sqrt{(d_0^2-(D-r)^2)((D+r)^2-d_0^2)}] = \varepsilon, \\ d_0 = (\frac{(2^{TS_{cell}\theta(t)/B_m}-1)(I_m+I_s)}{P_m K_m})^{-\frac{1}{a_m}}, \end{cases} \tag{3.16}$$

and W_m is solved numerically from (3.16).

After solving W_s and W_m, the power consumption of the two approaches can be derived as follows.

For the first approach, using Fig. 3.1 as an illustration, suppose that UEs in the dashed hexagon are served by the macrocell, the power consumption increase of the macrocell P_1 is expressed as:

$$P_1 = P_{Mm}\Delta_{pm}W_m, \tag{3.17}$$

where W_m can be find according to (3.13) and (3.15).

For the second approach, using Fig. 3.1 as an illustration, assume that UEs in the dashed hexagon are all served by small cell A, the power consumption of small cell AP_2 can be written as:

$$P_2 = P_{0s} + P_{Ms}\Delta_{ps}W_s, \tag{3.18}$$

where W_s is expressed in (3.12).

Comparing the two approaches, the difference of the power consumption of the two approaches P_{dif} can be written as:

$$P_{dif} = P_2 - P_1. \tag{3.19}$$

It can be seen that, $P_{dif} < 0$ means that leaving one small cell switching on to serve UEs in this area saves more energy than handing off all traffic to the macrocell, and vice versa. Hence, in the proposed approach, I use D which makes $P_{dif} = 0$ as the critical point to decide whether I need to switch off all the small cells or use small cell to cover the area of

sleeping small cells. Fig. 3.2 compares the two methods with different UE density θ based on (3.19). The turquoise dashed line represents $P_{dif} = 0$.

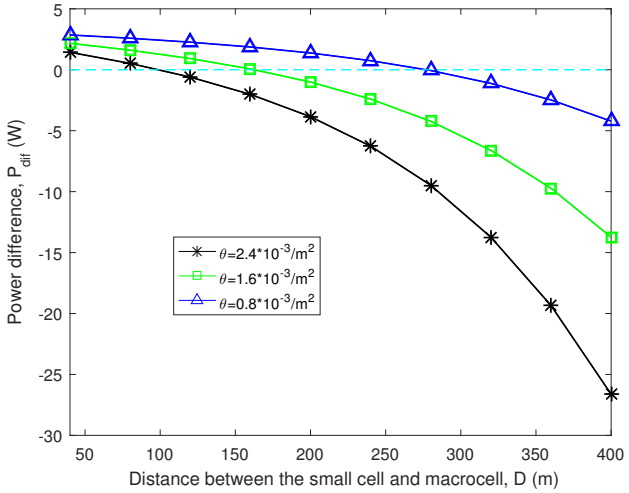

Fig. 3.2 Difference of the power saving of the two methods

3.1.3 Analysis of Day Traffic Profile

The traffic profile in mobile networks has already been analysed in Sec. 2.2.2. The day and week traffic profile can be modelled as a periodic sinusoidal profile [73], just as Fig. 2.5 shows. Here, for simplicity, the day traffic load is treated as a trapezoidal function [9, 25], which is illustrated in Fig. 3.3. In this section, only the decreasing traffic profile ($\theta(t)$) from 24:00 to 12:00 is considered because of its symmetry.

3.1.4 BS Switch Off Patterns

In this chapter, UEs are supposed to be uniformly distributed in the area, so that the small cells are switching off uniformly according to the distance to the macrocell. Figure 3.4 illustrates some basic cell range expansion patterns.

3.1.5 The Proposed Strategy

In this part, an analysis of the energy consumption of the proposed strategy is provided. As mentioned before, the duty cycle for macrocell is denoted as β, and the range of β is defined as $0 \leq \beta \leq 1$. Then, the resource required for UEs in the cell expansion area can be calculated similarly with (3.9). It is necessary to ensure that the resource required from

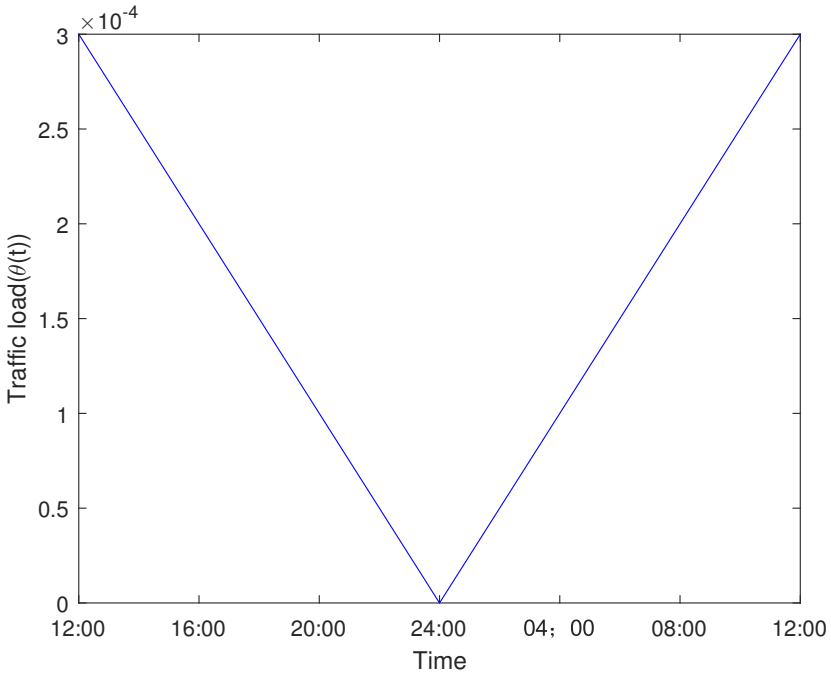

Fig. 3.3 Day Traffic Load

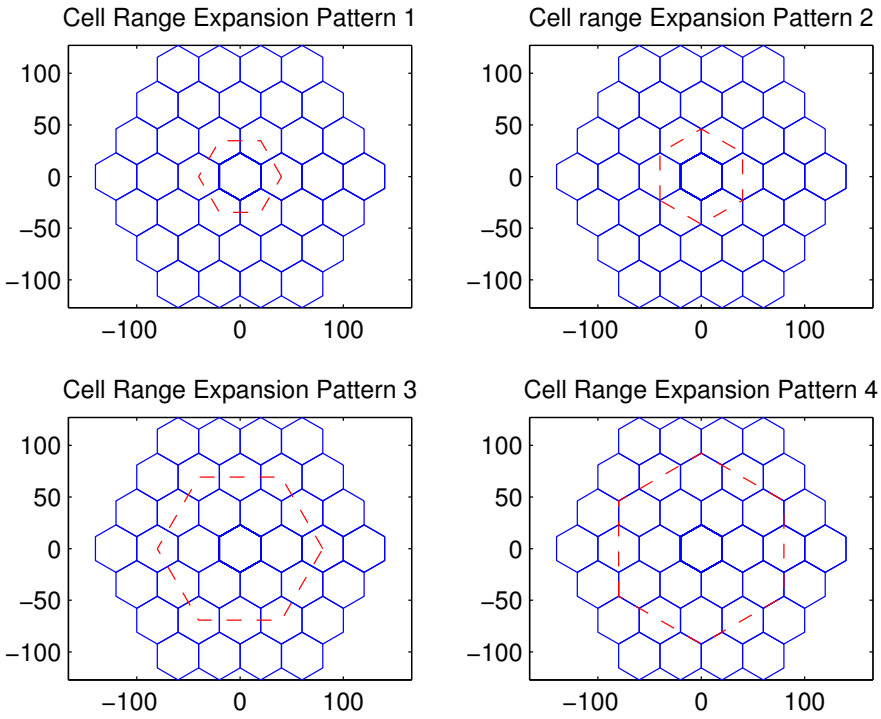

Fig. 3.4 Cell range expansion patterns

these UEs should not exceed the capacity limitation, which can be expressed as:

$$W_{cre} \leq W(1-\beta), \tag{3.20}$$

where W is the network bandwidth. β is the duty cycle. Based on the (3.9) and (3.20), the accurate value of W_{cre} can be solved numerically with a given β. It's noted that in reality, r_{cre} must meet the small cell switching off pattern given in Fig. 3.4, which is denoted as r^*_{cre} in real situations. Furthermore, it is noted that the power saving will reach the maximum with the largest r_{cre}, so that β here should be chosen as small as possible under the limits. The minimum value of β will be explained further. In addition, the QoS of UEs in the inner area must be guaranteed to meet the requirement. From Fig. 3.1, it can be seen that a user in small cell A will experience the interference from the macrocell covered by (macrocell at the original point) , other macrocells (I_m) and other small cells (I_s). Suppose that the minimum distance between the macrocell at the original point and small cell A is D_{min}, the interference can be approximated as:

$$I_{total} = P_m K_m D_{min}^{-\alpha_m} + I_m + I_s, \tag{3.21}$$

where $P_m K_m D_{min}^{-\alpha_m}$ is the interfering power from the macrocell covered by. I_m is the interference from other macrocells and I_s is the interference from all the small cells except A. Suppose that the distance between a random inner UE to its associated small cell is d, here, the inner UE is defined as the UE in the coverage area of an un-expanded small cell. Using Fig. 3.1 as an illustration, the distance between the inner UE and small cell A is d. The CDF of the d can be expressed as:

$$\begin{aligned} F_d(d_0) &= \mathrm{P_r}(d \leq d_0) \\ &= (\frac{d_0}{r})^2. \end{aligned} \tag{3.22}$$

Based on (3.6), the coverage probability of UEs in the inner area G_{inner} can be written as:

$$\begin{aligned} G_{inner} =& \Pr\left[\frac{W\cdot\beta}{S_{inner}\cdot\theta(t)}\log_2(1+\frac{P_sK_sd^{-\alpha_s}}{I_{total}})>T\right] \\ =& \Pr\left[\log_2(1+\frac{P_sK_sd^{-a_s}}{I_{total}})>\frac{TS_{inner}\theta(t)}{W\beta}\right] \\ =& \Pr\left(1+\frac{P_sK_sd^{-a_s}}{I_{total}}>2^{\frac{TS_{inner}\theta(t)}{W\beta}}\right) \\ =& \Pr\left[d^{-\alpha_s}>\left(2^{\frac{TS_{inner}\theta(t)}{W\beta}}-1\right)\frac{\mathrm{I_{total}}}{P_sK_s}\right] \\ =& \Pr\left\{d<\left[\left(2^{\frac{TS_{inner}\theta(t)}{W\beta}}-1\right)\frac{\mathrm{I_{total}}}{P_sK_s}\right]^{-\frac{1}{\alpha_s}}\right\}, \end{aligned} \tag{3.23}$$

where $\frac{W\cdot\beta}{S_{inner}}$ is the average bandwidth allocated to the UE in inner area, $\log_2(1+\frac{P_sK_sd^{-\alpha_s}}{I_{total}})$ is the spectrum efficiency based on Shannon Formula. S_{inner} is the area of small cell A, shown as the dashed line in Fig. 3.1, which can be expressed as: $S_{inner}=6\sqrt{3}r^2$. $\theta(t)$ is the UE density at time t. The values of W, P_s, K_s can be found in Tab. 3.1.

Combine (3.22) and (3.23), G_{inner} can be expressed as:

$$G_{inner}=\frac{\left[\frac{\left(2^{\frac{TS_{inner}\theta(t)}{W\beta}}-1\right)I_{total}}{P_sK_s}\right]^{-\frac{2}{a_s}}}{r^2}. \tag{3.24}$$

Recalling that the QoS of UEs in the inner area must be guaranteed, which can be expressed as: $G_{inner}\geq\varepsilon$, where ε is the coverage probability threshold. From (3.24), the maximum value of I_{total} can be derived as:

$$I_{total}\geq\frac{(\varepsilon r^2)^{\frac{\alpha_s}{2}}P_sK_s}{2^{\frac{TS_{inner}\theta(t)}{W\beta}}-1}. \tag{3.25}$$

Combine (3.25) and (3.21), the minimum distance D_{min} can be derived as:

$$D_{min}=\left[\frac{\frac{(2^{\frac{T\cdot\theta(t)\cdot\pi\cdot r_{inner}^2}{W\cdot\beta}}-1)}{(\varepsilon r_{inner}^2)^{-\frac{\alpha_s}{2}}P_sK_s}-I_m-I_s}{P_mK_m}\right]^{-\frac{1}{\alpha_m}}. \tag{3.26}$$

Moreover, when the small cells in the range of D_{min} are all pushed into sleeping mode, the total bandwidth should be guaranteed within the capacity limitation ($W \cdot \beta$), which can be expressed as:

$$\sum_{n=0}^{D_{min}} W_m(D) < W \cdot \beta, \tag{3.27}$$

where W_m can be easily found according to the (3.13) and (3.15) before. Then, the minimum value of duty cycle β_{min} with corresponding $\theta(t)$ under the constraints can be found to maximise the cell coverage.

According to the (3.6) to (3.19) before, D can be calculated similarly, except the minimum distance between the two neighbouring small cell is r^*_{cre} here. Meanwhile, the total traffic to macrocell should not exceed the capacity. The actual distance of D can be expressed as:

$$D^* = max\{D, D_{min}\}. \tag{3.28}$$

3.1.6 The Conventional Method

For the conventional method [25, 26], the small cell will be sent into sleep mode as long as the power reward is positive.

Here, D can be solved similarly according to (3.5), meanwhile, D must have a maximum value D_{max} in case of overloading of the macrocell. The actual distance D is:

$$D^* = min\{D, D_{max}\}. \tag{3.29}$$

3.1.7 Network Power and Energy Consumption

The power consumption P_{net} is defined as the total power consumption of the macrocell and all the active small cells within the coverage area of the macrocell. The expression of P_{net} with UE density θ can be expressed as:

$$\begin{aligned} P_{net} &= P_M + P_s \\ &= P_{0(M)} + \Delta_{p(M)} \rho_M P_{m(M)} + N_s \left(P_{0(s)} + \Delta_{p(s)} \rho_s P_{m(s)} \right) \\ &= P_{0(M)} + \Delta_{p(M)} \left(\frac{\sum_{n=0}^{D_*} W_m(n)}{W} \right) P_{m(M)} + N_s \left(P_{0(s)} + \Delta_{p(s)} \left(\frac{W_s}{W} \right) P_{m(s)} \right), \end{aligned} \tag{3.30}$$

where $\sum_{n=0}^{D_*} W_m(D)$ is the total bandwidth needed of the macrocell to serve the UEs form the small cells within the distance D^*, and W_m can be derived according to (3.13) and (3.15). N_s is the number of active small cells and can be approximated as: $N_s = round(\frac{\pi(R^2-D^2)}{(6\sqrt{(3)}r_{CRE}^{*\,2})})$. W_s is expressed in (3.12). $P_{0(M)}, \Delta_{p(M)}, P_{m(M)}, P_{0(s)}, \Delta_{p(s)}, P_{m(s)}$ can be found in Tab. 3.1.

The energy consumption in time period T is:

$$\begin{aligned} E_{Net} &= E_M + E_s \\ &= \int_0^T \sum_{d<D^*} P_{Cm}(d,\theta(t))\,dt + \int_0^T \sum_{d>D^*} P_{Cs}(d,\theta(t))\,dt \\ &= \sum_{i=0}^{N} \{ (\int_{\tau_i}^{\tau_{i+1}} \sum_{d<D^*} \Delta_{pm} \cdot P_{Mm} \cdot \frac{W_m(d,\theta(t))}{W} + P_{0(M)})\,dt \\ &+ (\int_{\tau_i}^{\tau_{i+1}} \sum_{d>D^*} \Delta_{ps} \cdot P_{Ms} \cdot \frac{W_s(d,\theta(t))}{W} + P_{0(s)})\}\,dt, \end{aligned} \tag{3.31}$$

where E_M and E_s is the energy consumption of the macrocell and all active small cells. P_{Cm} represents the power consumption of sleeping small cell covered by the macrocell and P_{Cs} is the energy consumption of a small cell. $W_m(d,\theta(t))$ and $W_s(d,\theta(t))$ can be derived according to (3.13) to (3.15), and (3.7) to (3.12), d means the distance between the target small cell and macrocell. D^* is expressed in (3.28). τ_i and τ_{i+1} are the time slots and N is number of time slots. In this section, the UE density is assumed to be $[200:200:3000]*10^{-4}/\mathrm{m}^2$ from 24:00 to 12:00, hence the number of time slots is 14 (N=14). The values of Δ_{ps}, Δ_{pm}, P_{Ms}, P_{Mm} can be found in Tab. 3.1.

3.1.8 Results Analysis

Now the results provided by the proposed and conventional methods will be analysed and simulated.

Simulation Set-up

Fig. 3.5 and Fig. 3.6 are generated according to (3.30). Fig. 3.7 is generated based on (3.31). Matlab is used to implement the formulas to generate the figures. The parameters such as the pathloss exponents (α_m , α_s), pathloss constant (K_m, K_s), data rate requirements (T), outage probability threshold (ε), BS transmission power (P_m,P_s) and ISD of BSs (2R,2r) are all provided in Tab. 3.1. The macrocell is deployed at the origin and small cells are deployed as continuous and homogeneous hexagonal model. The pathloss of the macrocell is defined as: $128.1+37.6*log_{10}(d)$ and the pathloss of small cells is defined as:$140.7+36.7*log_{10}(d)$.

Network Power Consumption

Fig. 3.5 and Fig. 3.6 illustrate that the relationship between the network power consumption from (3.30) and UE density for the two approaches with different UE data rate threshold (T).

Fig. 3.5 illustrates the relationship when the initial distance between the two neighbouring small cells is 40m. It's obvious that the network power rises significantly with the increase of UE density. Moreover, as expected, the proposed method performs much better than the existing method most of the time. It's noted that all the curves have rapid descending on some points, which represents the cell range expansion patterns change, resulting in significant power decrease. Another remarkable phenomenon is that the curves representing the conventional methods fluctuate at some points. The reason is that in conventional methods, with UE density increasing, a small cell will cover the nearby sleeping small cells which were covered by the macrocell before, which results in a low power consumption. Hence, it can be seen that the power even decrease even when the UE density increases, which verified the idea from another side.

Fig. 3.6 depicts the relationship when the initial distance between the two neighbouring small cells is 40m, 2 times of Fig. 3.5, so that the cell range pattern cannot vary frequently during the decrease of UE density, which is also reflected in the Fig. 3.6, the curves descends smoothly most of the time.

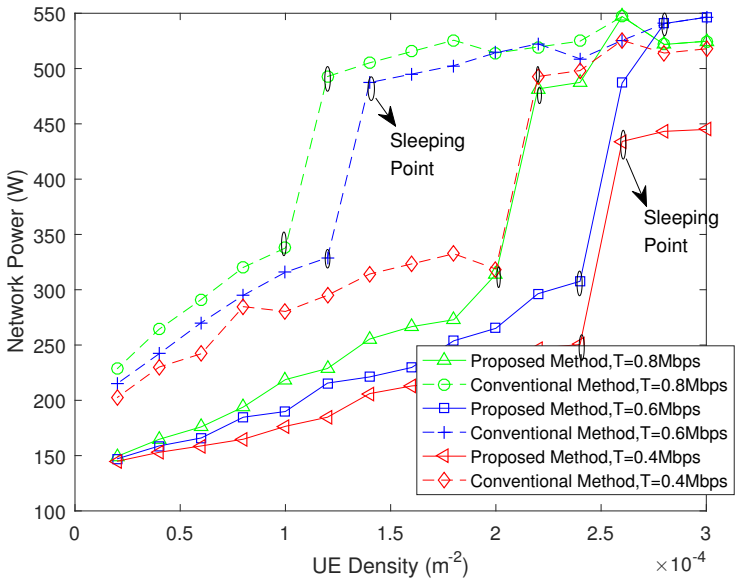

Fig. 3.5 Power with different UE density with initial small cell radius 20m

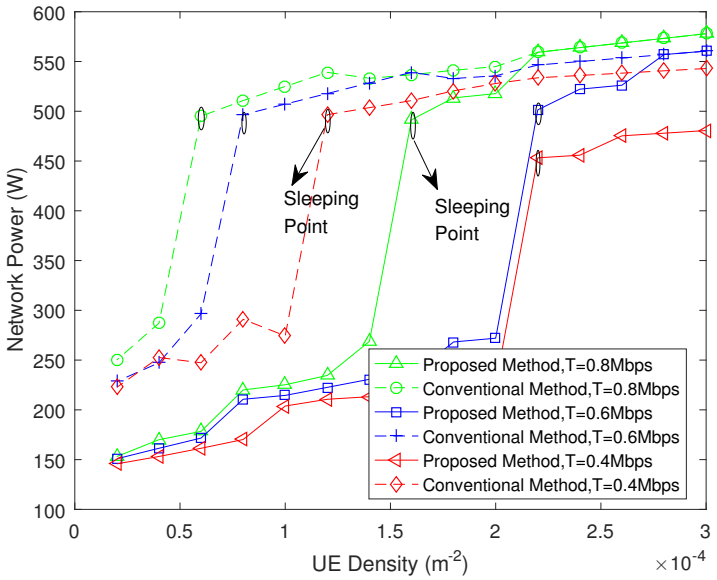

Fig. 3.6 Power with different UE density with initial small cell radius 40m

Network Energy Consumption

Fig. 3.7 describes the energy consumption from 18:00 to 06:00. Here, the network energy consumption (E_{Net}) is derived according to (3.31), including the energy consumption of the macrocell and all small cells. For the scenario r=20m, the energy saving of the proposed method compared with the conventional method is 4000KJ (26.3%), 6100KJ (32.5%), 5100KJ (26.2%) respectively when the data rate requirement is 0.4,0.6 and 0.8 Mbps. For the second scenario r=40m, the energy saving is 6400KJ (32.7%), 6200KJ (29.3%), 4900KJ (21.8%) respectively. Moreover, compared with the second scenario, it can be found that the energy consumption of the network with r=40m is much higher than that of r=20m, the reason is that the cell range pattern for the second scenario cannot be changed often with the UEs density decrease, so that the small cells are unable to be pushed into sleeping mode in most of the time, which results in higher energy consumption.

3.2 Stochastic Geometry based Small Cell Sleeping Mechanism

In this section, a stochastic geometry based analysis of the proposed small cell sleeping mechanism is provided. Instead of assuming the small cells are placed deterministically on a regular grid, in this section their distribution is assumed to follow a homogeneous Poisson point process. The main advantage of this assumption is that the small cell positions are all

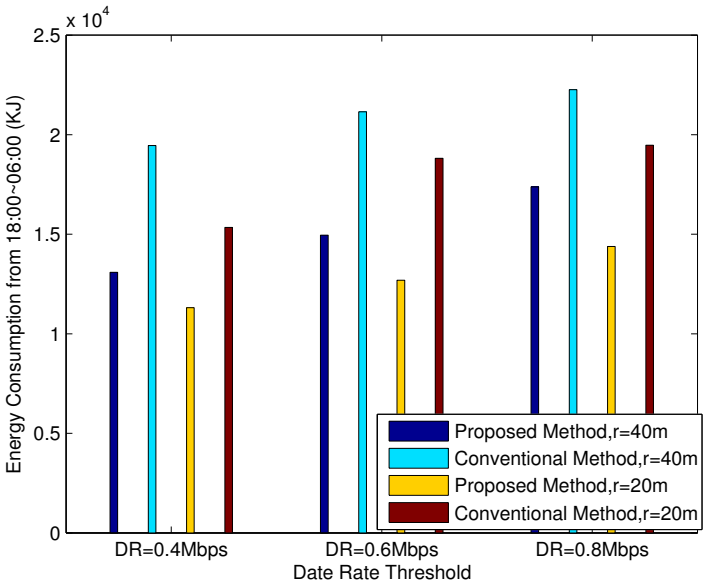

Fig. 3.7 Network energy consumption

independent which allows substantial tools to be brought to bear from stochastic geometry. To be more specific, the stochastic geometry based method can provide a more accurate derivation of the coverage probability and the interference. Furthermore, with Poisson point process based position model, the small cell density varies with different locations. Hence, it is more realistic since in a real environment some parts of the small cell intensity is higher (e. g. block of flats), than that of others (e. g. public parks).

For the proposed method, in the cell-edge area of a macrocell, small cells will be put into sleep where possible and their service areas will be covered by range-expanded small cells nearby and the macrocell; in areas close to the macrocell, UEs associated with a sleeping small cell will be handed over to the macrocell. A comparison of the proposed method and conventional methods will be given, the results show that the proposed approach outperforms the conventional ones significantly and using eICIC technology can effectively improve the QoS of the UEs.

3.2.1 Contribution

In this section, the energy consumption of the HetNets is minimised, meanwhile the QoS of the UEs is guaranteed. Using stochastic geometry based HetNets model, the expressions for (1) UE associate probability to macrocell/small cells. (2) Probability density function of the distance between the UEs and associated macrocell/ small cells. (3) Coverage Probability are derived. Moreover, just as explained in Sect. 3.1, an optimisation strategy which combines adaptive small cell zooming and small cell sleeping approaches is proposed to

minimise the network power consumption. The results show that the proposed method has a significant improvement in terms of network power saving compared with that of conventional methods.

Unique aspects of my work in this section can be summarized as follows:

- An accurate system model is provided. The following problem is considered and solved: after switching off small cells close to the macrocells , there will exist holes around the macrocells. I solve the problem and provide a specific and accurate interference calculation.
- Expressions for association probability and coverage probability in a two-tier HetNet under the proposed sleeping scheme is proposed.

3.2.2 Small Cell Sleeping Strategy

- Proposed Sleeping Strategy: an energy-saving small cell sleeping mechanism in a HetNet is proposed in this section. Just as Fig. 3.8 shows, the small cells whose distance to the macrocell smaller than z are all pushed into sleeping model. Furthermore, the density of the remaining small cells is controlled by using cell range expansion (CRE) technique. It is noted that as the UEs inside the dashed circle are close to the macrocell, the assumption is made that all the UEs from the sleeping cells within the dashed circle can only be offloaded to the macrocell.

  The eICIC technique is applied to improve the QoS of UEs in the edge of small cells. The macrocell can mute its downlink transmissions in certain subframes called almost blank subframes (ABSs). In this section, that ABSs are assumed to be allocated only to the UEs in the small cell range expansion area to avoid the interference from the macrocell. The UEs located close to the small cells and in the coverage are of the macrocell are scheduled with normal subframes.

  In existing works [25, 26], the authors only switched off small cells close to the macrocell and handed over the associated UEs to the macrocell. However, I notice that the network power saving of this kind of approach is not significant, because a number of small cells in the area far from the macrocell are still active.

- Conventional Sleeping Strategy: the repulsive sleeping scheme in [26] is selected as the conventional method in this section. The small cells inside the circle around the macrocell are turned off and the associated UEs are all handed over to the macrocell.
- Random Sleeping: Each small cell has an equal probability to be put into sleep mode.

3.2.3 Downlink System Model

A two tier HetNet with macrocells (tier 1) and small cells (tier 2) is considered in the system model. Due to the fact that the the macrocells' location should be carefully designed to maintain their coverage, in my model, the macrocells are considered to be regularly deployed as hexagonal cells[26]. On the contrary, small cells are densely deployed to boost the network capacity, hence the small cells are assumed to form a homogeneous Poisson Point Process (HPPP) with intensity λ_2 as shown Fig. 3.8.

Both macrocells and small cells are assumed to share the same frequency band and each BS has a limited bandwidth denoted as W Hz here. All BSs in the same tier are assumed to transmit an equal fixed power P_k, $k = 1$ for the first tier and $k = 2$ for the second tier. The downlink desired and interference signals experience path loss, and for each tier different path loss exponents α_k are allowed. The received power of a UE from a BS of k^{th} tier at a distance x can be expressed as $P_k h_x x^{-\alpha_k}$, where h_x is the small scale fading gain. Under Rayleigh fading assumption, $\{h_x\}$ is a sequence of independent and identically distributed (i.i.d.) exponential random variables with $h_x \sim exp(1)$.

Let d_k denote the distance of the typical user from the nearest AP of k^{th} tier. It's assumed that each user will associate to the base station based on the rule:

$$j = \arg \max_{k \in \{1,2\}} \{P_k B_k d_k^{-\alpha_k}\}, \tag{3.32}$$

where B_k is the cell association bias factor for the k^{th} tier. In this section, only the association bias for tier 2 (small cell tier) is considered, which is denoted as B_2 here. Fig.3.8 illustrates the system model. The area inside the dashed circle with radius z is named as area A and the area outside the dashed circle is named as area B. Assume that all small cells within area A are switched off and the associated UEs will be handed over to the macrocell. In area B, small cells are partially turned off.

In the given setup, a user u can be in the area A connected to the macrocell, named set A here, and the following three disjoint sets, where j is expressed in (3.33):

$$u \in \begin{cases} U_1 \; if \; j = 1, \; P_1 R_1^{-\alpha_1} \geq P_2 R_2^{-\alpha_2} B_2 \\ U_2 \; if \; j = 2, \; P_2 R_2^{-\alpha_2} \geq P_1 R_1^{-\alpha_1} \\ U_3 \; if \; j = 2, \; P_2 R_2^{-\alpha_2} \leq P_1 R_1^{-\alpha_1} < P_2 R_2^{-\alpha_2} B_2, \end{cases} \tag{3.33}$$

where the set U_1 is the set of UEs in the area outside the dashed circle connected to the macrocell, the set U_2 is the set of unbiased small cell UEs in the area outside the dashed line circle. The set U_3 is the set of biased UEs in the area outside the dashed circle. Fig. 3.9 is

displayed to illustrate the UE association model.

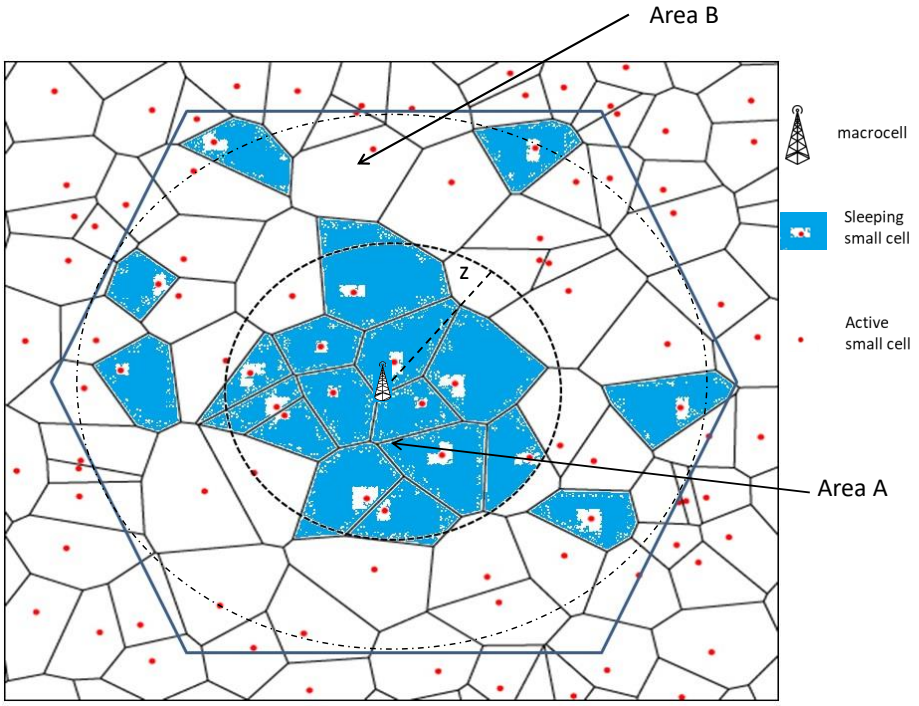

Fig. 3.8 Illustration of the system model

For a typical UE_u in set A or set U_1, the received SINR is given as :

$$\gamma_u = \frac{P_1 h_{m,u} d_{m,u}^{-\alpha_1}}{\sum_{i \in \mathscr{C}_2} h_{i,u} d_{i,u}^{-\alpha_2} P_2 + \sigma^2}, \tag{3.34}$$

where P_1 is the transmit power of macrocell, $h_{m,u}$ is the Rayleigh fading of the link from the macro BS to the UE_u, and $h_{i,u}$ are the Rayleigh fading of interfering links from small cells to the UE_u. $d_{m,u}$ is the distance between the macro BS to the UE_u, and $d_{i,u}$ are the distance from interfering small cells to the UE_u. $\mathscr{C}_2$ is the set of interfering small cells.

For a typical UE_u in set U_2, the received SINR can be expressed as follows:

$$\gamma_u = \frac{P_2 h_{l,u} d_{l,u}^{-\alpha_2}}{\sum_{i \in \mathscr{C}_2 \setminus l} h_{i,u} d_{i,u}^{-\alpha_2} P_2 + I_m + \sigma^2}, \tag{3.35}$$

where P_2 is the transmit power of cells, $h_{l,u}$ is the Rayleigh fading of the link from the serving small cell l to the UE_u, and $h_{i,u}$ are the Rayleigh fading of interfering links from other small cells

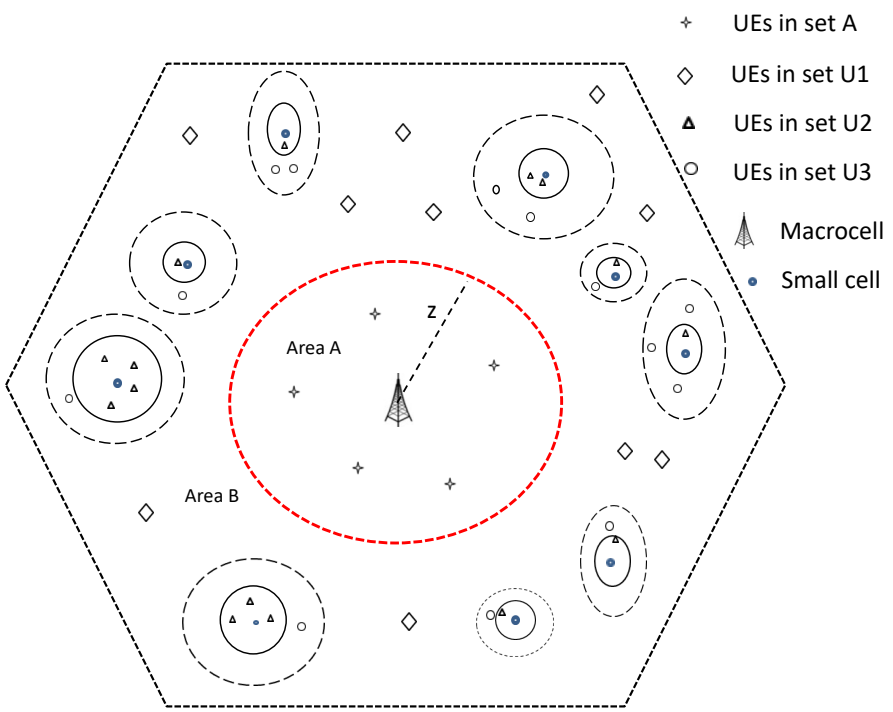

Fig. 3.9 Illustration of the UE association model

to the UE_u. $d_{l,u}$ is the distance between the serving small cell l to the UE_u, and $d_{i,u}$ are the distance from interfering small cells to the UE_u. $\mathscr{C}_2$ is the set of interfering small cells. I_m is the interference from the macrocell.

For a typical UE_u in set U_3, the received SINR can be expressed as follows:

$$\gamma_u = \frac{P_2 h_{l,u} d_{l,u}^{-\alpha_2}}{\sum_{i \in \mathscr{C}_2 \setminus l} h_{i,u} d_{i,u}^{-\alpha_2} P_2 + \sigma^2}. \tag{3.36}$$

The description of the parameters can be found in (3.35). It is noted that I_m is omitted here due to the reason that the ABSs, where the macrocell mute its downlink transmissions, are allocated only to the UEs in set U_3 to avoid the interference from the macrocell.

Assuming each BS allocates resource equally to its active UEs, the achievable data rate of UE_u can be written as:

$$r_u = \frac{W}{N} log_2(1+\gamma_u), \tag{3.37}$$

where N is the number of the active UEs associated to the serving BS, w is the bandwidth allocated to

UEs of the serving BS, U is the data rate requirement of UEs, η is the coverage probability threshold. γ_u is the SINR for UE_u which can be found in (3.34), (3.35) and (3.36). The coverage probability here is defined as the probability that the data rate of UE_u is above the threshold U, which can be expressed as $\mathbb{P}\{r_u > U\}$.

The service coverage constraint of UE_u can be expressed as:

$$\mathbb{E}\{\mathbb{P}\left(\frac{w}{N} log_2(1+\gamma_u)\right) > U\} > \eta. \tag{3.38}$$

The power consumption model used in this part is from (3.4).

3.2.4 Coverage Probability Analysis

In this section, the BS coverage probability will be derived and verified by the simulation in Sect. 3.2.5. For convenience, $\alpha_1 = \alpha_2 = 4$ is assumed in this section. Furthermore, for simplicity, the interference from the macrocell to the UEs in set U_2 is averaged, which can be written as:

$$\mathrm{E}[I_m] = \int_z^R P_1 r^{-\alpha_1} \frac{2r}{R^2 - z^2}\,\mathrm{d}r. \tag{3.39}$$

Proof.

$$\begin{aligned}\mathrm{E}[I_m] &= \int P_1 r^{-\alpha_1} f_R(r)\,\mathrm{d}r \\ &= \int_z^R P_1 r^{-\alpha_1} \frac{2r}{R^2 - z^2}\,\mathrm{d}r.\end{aligned} \tag{3.40}$$

□

UEs in Set A

In this section, the coverage probability for UEs in set A will be derived.

The probability density function (PDF) of the distance r between UEs in area A to the macrocell can be expressed as

$$f_R(r) = \frac{2r}{z^2}. \tag{3.41}$$

Proposition 1. *The coverage probability for UEs in area A can be given as:*

$$G_A = \int_0^z e^{-\mu T r^{\alpha_1} \sigma^2} \mathscr{L}_{I_s}(\mu T r^{\alpha_1}) \frac{2r}{z^2}\,\mathrm{d}r, \tag{3.42}$$

where $T = \frac{2^{\frac{UN_A}{W_A}} - 1}{P_1}$, *$N_A$ is the number of UEs in set A and can be expressed as:* $N_A = \lambda_2 \pi z^2$, *W_A is*

bandwidth allocated to all the UEs in set A, and the Laplace transform of I_s can be written as

$$\mathscr{L}_{I_s}(\mu T r^{\alpha_1}) = \exp\left(-\pi r^2 \lambda_2 (T * P_2)^{2/a_2}(\pi/2)\right) \exp\left(2\lambda_2 \int_{r-z}^{r+z} \frac{\arccos(\frac{r^2+\rho^2-z^2}{2r\rho})}{1+\frac{\rho^{\alpha_2}}{P_2 s}} \rho \, \mathrm{d}\rho + 2\lambda_2 \int_0^{r-z} \frac{\pi}{1+\frac{\rho^{\alpha_2}}{P_2 s}} \rho \, \mathrm{d}\rho\right), \tag{3.43}$$

where $s = \mu T r^{\alpha_1}$.

Proof. Proof see Appendix B.

UEs in Set U_1

In this section, the coverage probability for UEs in set U_1 will be derived. Just as shown in Fig. 3.9, set U_1 is the set of UEs connected to the macrocell in area B, and is expressed in (3.33).

The probability that a UE in set U_1 (in area B and connect to the macrocell) can be expressed as:

$$\begin{aligned} q_B^{U_1} &= \mathbb{P}(P_1 R_1^{-\alpha_1} \geq P_2 R_2^{-\alpha_2} B_2) \\ &= \int_z^R \mathbb{P}(R_2 \geq ((\frac{P_1}{P_2 B_2})^{-\frac{1}{\alpha_2}} R_1^{\frac{\alpha_1}{\alpha_2}}) f_{R_1}(r) \, \mathrm{d}r \\ &= \int_z^R e^{-\lambda_2 (\frac{P_1}{P_2 B_2})^{-\frac{2}{\alpha_2}} r^{\frac{2\alpha_1}{\alpha_2}}} \frac{2r}{R^2 - z^2} \, \mathrm{d}r. \end{aligned} \tag{3.44}$$

The number of users in this area connect to macrocell can be expressed as $N_B^{U_1} = q_B^{U_1} \pi (R^2 - z^2)$.

Proposition 2. *Assume the distance between the macrocell with a random UE in set U_1 is X_1. The PDF $f_{X_1}(x)$ can be expressed as:*

$$f_{X_1}(x) = \frac{dF_{X1}}{dx} = \begin{cases} 0, & x \leq z \\ \frac{1}{q_B^{U_1}} e^{(-\lambda_2 \pi (\frac{P_1}{P_2 B_2})^{-\frac{2}{\alpha_2}} x^{\frac{2\alpha_1}{\alpha_2}})} \frac{2x}{R^2 - z^2}, & R \geq x > z. \\ 0, & x > R \end{cases} \tag{3.45}$$

Proof. Proof see Appendix C.

Corollary 1. *The coverage probability of UEs in set U_1 can be expressed as:*

$$G_B^{U1} = \int_z^R e^{-\lambda_2 \pi (\frac{P_1}{P_2 B_2})^{-\frac{2}{\alpha_2}} x^{\frac{2\alpha_1}{\alpha_2}}} e^{-\mu T x^{\alpha_1} \sigma^2} \mathscr{L}_{I_s}(\mu T x^{\alpha_1}) \frac{2x}{q_B^{U_1}(R^2 - z^2)} \, \mathrm{d}x, \tag{3.46}$$

where $T = \frac{2^{\frac{UN_{U_1}}{W_B^{U_1}}} - 1}{P_1}$.

$W_B^{U_1}$is the bandwidth allocated to all the UEs in set U_1, $N_B^{U_1}$ is the number of users in set U_1 and can be expressed as :$N_B^{U_1} = q_B^{U_1}\frac{\lambda_u}{\lambda_2}$.

The proof of $G_B^{U_1}$ is expressed below:

Proof.

$$\begin{aligned}
G_B^{U_1} &= \mathbb{E}\{\mathbb{P}\left(\frac{W_B^{U_1}}{N_B^{U_1}}\log_2(1+\gamma_B^{U_1})\right) > U\} \\
&= \mathbb{E}_{x_1}\{\mathbb{P}\left(\frac{W_B^{U1}}{N_B^{U1}}\log_2(1+\frac{P_1 h x_1^{-\alpha_m}}{\mathrm{I_s}+\sigma^2})\right) > U\} \\
&= \int\left(\mathbb{P}\left(\frac{W_B^{U_1}}{N_B^{U_1}}\log_2(1+\frac{P_1 h x_1^{-\alpha_m}}{\mathrm{I_s}+\sigma^2})\right) > U\right) f_{X_1}(x)\,\mathrm{d}x \\
&= \int\mathbb{P}\left(h > \frac{(2^{\frac{UN_B^{U_1}}{W_B^{U_1}}}-1)(\mathrm{I_s}+\sigma^2)x^{\alpha_1}}{P_1}\right) f_{X_1}(x)\,\mathrm{d}x \\
&= \int e^{-\mu T r^{\alpha_1}\sigma^2}\mathscr{L}_{I_s}(\mu T r^{\alpha_1}) f_{X_1}(x)\,\mathrm{d}x,
\end{aligned} \tag{3.47}$$

where $f_{X_1}(x)$ is expressed in (3.45). □

$$\mathscr{L}_{I_s}(\mu T x^{\alpha_1}) = \exp(-\lambda_2\pi x^2(T*P_2)^{\alpha_2/2}(\frac{\pi}{2}-\mathrm{atan}(m\cdot T^{-\alpha_2/2})))\exp(\int_g^{r+z}\frac{2\pi l(\rho)}{1+\frac{\rho^{\alpha_2}}{P_2\cdot s}}\rho\mathrm{d}\rho), \tag{3.48}$$

where $l(\rho) = \frac{\lambda_2}{\pi}\arccos(\frac{x^2+\rho^2-z^2}{2x\rho})$, $m = (\frac{P_1}{P_2*B_2})^{-2/\alpha_2}$, $g = \max[x-z, (\frac{P_1}{P_2*B_2})^{-1/\alpha_2}\cdot x]$.

Proof. Proof see Appendix D.

UEs in Set U_2

In this section, an analysis of the coverage probability of UEs in set U_2 will be given. Just as shown in Fig. 3.9, set U_2 is the set of UEs close to small cells in area B, and is expressed in (3.33).

The probability that UEs in set U_2 is:

$$\begin{aligned}
q_B^{U_2} =& \mathbb{P}(P_2 R_2^{-\alpha_2} \geq P_1 R_1^{-\alpha_1}) \\
&= \int_z^R \mathbb{P}(R_2 \leq (\frac{P_1}{P_2})^{-\frac{1}{\alpha_2}} R_1^{\frac{\alpha_1}{\alpha_2}}) f_{R_1}(r)\,\mathrm{d}r \\
&= \int_z^R (1-e^{-\pi\lambda_2((\frac{P_1}{P_2})^{-\frac{2}{\alpha_2}} r^{\frac{2\alpha_1}{\alpha_2}})})\frac{2r}{R^2-z^2}\,\mathrm{d}r.
\end{aligned} \tag{3.49}$$

Proposition 3. *Suppose the distance between a random UE in set U_2 with its associated small cell is X_2. The pdf $f_{X_2}(x)$ can be written as:*

$$f_{X_2}(x) = \frac{dF_{X2}}{dx} = \begin{cases} \frac{1}{q_B^{U_2}}(2\pi\lambda_2 x e^{-\lambda_2\pi x^2}), & x \le x_1 \\ \frac{R^2-(\frac{P_2}{P_1})^{-\frac{2}{\alpha_1}}x^{\frac{2\alpha_2}{\alpha_1}}}{R^2-z^2}\frac{2\pi\lambda_2}{q_B^{U_2}} x e^{-\lambda_2\pi x^2}, & x_2 \ge x > x_1 \\ 0, & x > x_2, \end{cases} \tag{3.50}$$

where $x_1 = \frac{z}{(P2/P1)^{-0.25}}$ and $x_2 = \frac{R}{(P2/P1)^{-0.25}}$,

Proof. Proof see Appendix E.

Corollary 2. *The coverage probability of UEs in set U_2 can be expressed as:*

$$\begin{aligned} G_B^{U2} &= \int_0^{x_1} e^{-\lambda_2\pi x^2}\frac{2\pi\lambda_2 x}{q_B^{U_2}} e^{-\mu T x^{\alpha_2}(\mathrm{I_m}+\sigma^2)}\mathscr{L}_{I_s}(\mu T x^{\alpha_2})\,\mathrm{d}x \\ &+ \int_{x_1}^{x_2} e^{-\lambda_2\pi x^2}\frac{R^2-(\frac{P_2}{P_1})^{-\frac{2}{\alpha_1}}x^{\frac{2\alpha_2}{\alpha_1}}}{R^2-z^2}\frac{2\pi\lambda_2 x}{q_B^{U_2}} e^{-\mu T x^{\alpha_2}(\mathrm{I_m}+\sigma^2)}\mathscr{L}_{I_s}(\mu T x^{\alpha_2})\,\mathrm{d}x, \end{aligned} \tag{3.51}$$

where $T = (2^{(U*N_B^{U_2}/W_B^{U_2})}-1)/P_2$, $W_B^{U_2}$ is the bandwidth allocated to set U_2, $N_B^{U_2}$ is the average number of users in set U_2 and can be expressed as :$N_B^{U_2} = q_B^{U_2}\frac{\lambda_u}{\lambda_2}$.

Proof.

$$\begin{aligned} G_B^{U2} &= \mathbb{E}\{\mathbb{P}\left(\frac{W_B^{U_2}}{N_B^{U2}} log_2(1+\gamma_B^{U_2})\right) > U\} \\ &= \mathbb{E}_{x_2}\{\mathbb{P}\left(\frac{W_B^{U_2}}{N_B^{U_2}} log_2(1+\frac{P_2 h x_2^{-\alpha_2}}{\mathrm{I_s}+I_m+\sigma^2})\right) > U\} \\ &= \int\left(\mathbb{P}\left(\frac{W_B^{U_2}}{N_B^{U2}}\log_2(1+\frac{P_2 h x^{-\alpha_2}}{\mathrm{I_s}+I_m+\sigma^2})\right) > U\right) f_{X_2}(x)\,\mathrm{d}x \\ &= \int \mathbb{P}\left(h > \frac{(2^{\frac{UN_B^{U_2}}{W_B^{U_2}}}-1)(\mathrm{I_s}+I_m+\sigma^2)x^{\alpha_2}}{P_2}\right) f_{X_2}(x)\,\mathrm{d}x \\ &= \int e^{-\mu T x^{\alpha_2}(\sigma^2+I_m)}\mathscr{L}_{I_s}(\mu T x^{\alpha_2}) f_{X_2}(x)\,\mathrm{d}x, \end{aligned} \tag{3.52}$$

where $f_{X_2}(x)$ is expressed in (3.50). □

$$\mathscr{L}_{I_s}(\mu T x^{\alpha_2}) = \exp\left(-\pi\lambda_2 x^2 (T * P_2)^{2/\alpha_2} * (\pi/2 - \operatorname{atan}(T^{-2/\alpha_2}))\right) * \exp\left(2\lambda_2 \int_{x_l}^{x_u} \frac{\arccos \frac{(D_{oo'}^2 + \rho^2 - z^2)}{(2D_{oo'}\rho)}}{1 + \frac{\rho^{\alpha_2}}{P_2 s}} \rho \, \mathrm{d}\rho\right) \tag{3.53}$$

x_l can be written as $x_l = max(D_{oo'} - z, x)$, $x_u = D_{oo'} + z$, and it's noted that $D_{oo'}$ has the constraints which can be expressed as $D_{oo'} \leq (\frac{P_2}{P_1})^{-\frac{1}{\alpha_1}} x^{\frac{\alpha_2}{\alpha_1}}$, here the upper bound $D_{oo'} = (\frac{P_2}{P_1})^{-\frac{1}{\alpha_1}} x^{\frac{\alpha_2}{\alpha_1}}$ is selected.

The proof of (3.53) can be referred to Proof (G.1) based on Fig. G.1 in Appendix G. Moreover, it's worth noting that because UEs in set U_2 are likely close to small cells and far away from the macrocell, the approximation has a quite limited impact on the real results.

UEs in Set U_3

In this section, an analysis of the coverage probability of UEs in set U_3 will be given. Just as shown in Fig. 3.9, set U_3 is the set of UEs in the CRE area, and is expressed in (3.33).

The probability that the UEs in set U_3 can be expressed as:

$$\begin{aligned} q_B^{U_3} &= \mathbb{P}(P_1 R_1^{-\alpha_1} \leq P_2 R_2^{-\alpha_2} B_2 \cap P_1 R_1^{-\alpha_1} \geq P_2 R_2^{-\alpha_2}) \\ &= \int_z^R \mathbb{P}((\frac{P_1}{P_2 B_2})^{-\frac{1}{\alpha_2}} R_1^{\frac{\alpha_1}{\alpha_2}} \geq R_2 \geq (\frac{P_1}{P_2})^{-\frac{1}{\alpha_2}} R_1^{\frac{\alpha_1}{\alpha_2}}) f_{R_1}(r) \, \mathrm{d}r \\ &= \int_z^R (\exp(-\lambda_2 \pi (\frac{P_1}{P_2})^{-\frac{1}{\alpha_2}} R_1^{\frac{\alpha_1}{\alpha_2}}) - \exp(-\lambda_2 \pi (\frac{P_1}{P_2 B_2})^{-\frac{1}{\alpha_2}} R_1^{\frac{\alpha_1}{\alpha_2}})) \frac{2r}{R^2 - z^2} \, \mathrm{d}r. \end{aligned} \tag{3.54}$$

The average number of users in set U_3 connect to the small cell is :$N_B^{U_3} = q_B^{U_3} \frac{\lambda_u}{\lambda_2}$.

Proposition 4. *The probability of the distance from UEs to associated small cells in set U_3 in area B can be expressed as*

$$f_{X_3}(x) = \frac{dF_{X3}}{dx} = \begin{cases} 0, & x \leq x_1 \\ \frac{\rho_1^2 - z^2}{q_B^{U_3}(R^2 - z^2)} 2\pi\lambda_2 x e^{-\lambda_2 \pi x^2}, & x_1 \leq x < x_1^b \\ \frac{\rho_1^2 - \rho_2^2}{q_B^{U_3}(R^2 - z^2)} 2\pi \, \lambda_2 x e^{-\lambda_2 \pi x^2}, & x_1^b < x \leq x_2 \\ \frac{R^2 - \rho_2^2}{q_B^{U_3}(R^2 - z^2)} 2\pi \, \lambda_2 x e^{-\lambda_2 \pi x^2}, & x_2 < x \leq x_2^b, \end{cases} \tag{3.55}$$

where $x_1 = \frac{z}{(\frac{P_2}{P_1})^{-0.25}}$, $x_1^b = \frac{z}{(\frac{P_2 B_2}{P_1})^{-0.25}}$, $x_2 = \frac{R}{(\frac{P_2}{P_1})^{-0.25}}$, $x_2^b = \frac{R}{(\frac{P_2 B_2}{P_1})^{-0.25}}$. $\rho_1 = (\frac{P_2}{P_1})^{-0.25}$. $\rho_2 = (\frac{P_2 B_2}{P_1})^{-0.25}$.

Proof. Proof see Appendix E.

Corollary 3. *The coverage probability of UEs in set U_3 of area B can be expressed as:*

$$
\begin{aligned}
&G_B^{U_3} = \\
&\int_{x_1}^{x_1^b} e^{-\mu T x^{\alpha_2}\sigma^2} e^{-\lambda_2 \pi x^2} \mathscr{L}_{I_s}(\mu T x^{\alpha_2}) \frac{\rho_1^2 - z^2}{q_B^{U_3}(R^2 - z^2)} 2\pi\lambda_2 x \,\mathrm{d}x + \\
&\int_{x_1^b}^{x_2} e^{-\mu T x^{\alpha_2}\sigma^2} e^{-\lambda_2 \pi x^2} \mathscr{L}_{I_s}(\mu T x^{\alpha_2}) \frac{\rho_1^2 - \rho_2^2}{q_B^{U_3}(R^2 - z^2)} 2\pi\ \lambda_2 x \,\mathrm{d}x + \\
&\int_{x_2}^{x_2^b} e^{-\mu T x^{\alpha_2}\sigma^2} e^{-\lambda_2 \pi x^2} \mathscr{L}_{I_s}(\mu T x^{\alpha_2}) \frac{R^2 - \rho_2^2}{q_B^{U_3}(R^2 - z^2)} 2\pi\ \lambda_2 x \,\mathrm{d}x,
\end{aligned} \tag{3.56}
$$

where $x_1, x_2, x_1^b, x_2^b, \rho_1, \rho_2$ can be found in (3.55), $T = (2^{(U * N_B^{U_3}/W_B^{U_3})} - 1)/P2$, $W_B^{U_3}$ is the bandwidth allocated to UEs in set U_3, $N_B^{U_3}$ is the UEs in set U_3 and can be expressed as $N_3 = q_b^{U_3} * \frac{\lambda_u}{\lambda_2}$.

Proof.

$$
\begin{aligned}
G_B^{U_3} &= \mathbb{E}\{\mathbb{P}\left(\frac{W_B^{U_3}}{N_B^{U3}}\log_2(1+\gamma_B^{U_3})\right) > U\} \\
&= \mathbb{E}_{x_3}\{\mathbb{P}\left(\frac{W_B^{U_3}}{N_B^{U3}}\log_2(1+\frac{P_2 h x_3^{-\alpha_2}}{\mathrm{I_s}+\sigma^2})\right) > U\} \\
&= \int \left(\mathbb{P}\left(\frac{W_B^{U_3}}{N_B^{U_3}}\log_2(1+\frac{P_2 h x^{-\alpha_2}}{\mathrm{I_s}+\sigma^2})\right) > U\right) f_{X_3}(x)\,\mathrm{d}x \\
&= \int \mathbb{P}\left(h > \frac{(2^{\frac{UN_B^{U_3}}{W_B^{U_3}}} - 1)(\mathrm{I_s}+\sigma^2)x^{\alpha_2}}{P_2}\right) f_{X_3}(x)\,\mathrm{d}x \\
&= \int e^{-\mu T x^{\alpha_2}(\sigma^2 + I_m)} \mathscr{L}_{I_s}(\mu T x^{\alpha_2}) f_{X_3}(x)\,\mathrm{d}x,
\end{aligned} \tag{3.57}
$$

where $f_{X_3}(x)$ is expressed in (3.55). □

Here, an upper bound approximation of $\mathscr{L}_{I_s}$ is provided.

$$
\mathscr{L}_{I_s}(\mu T x^{\alpha_2}) = \exp\left(-\lambda_2 \pi x^2 (T * P2)^{0.5}(\pi/2 - \arctan(T^{-0.5}))\right) \exp\left(2\lambda_2 \int_{x_l}^{x_u} \frac{\arccos\frac{(D_{oo'}^2 + \rho^2 - z^2)}{(2D_{oo'}\rho)}}{1 + \frac{\rho^{\alpha_s}}{P_2(s)}} \rho\,\mathrm{d}\rho\right) \tag{3.58}
$$

where $x_l = max((\frac{P_2}{P_1})^{-\frac{1}{\alpha_1}} x^{\frac{\alpha_2}{\alpha_1}} - z, x), x_u = (\frac{P_2}{P_1})^{-\frac{1}{\alpha_1}} x^{\frac{\alpha_2}{\alpha_1}} + z, D_{oo'} = (\frac{P_2}{P_1})^{-\frac{1}{\alpha_1}} x^{\frac{\alpha_2}{\alpha_1}}$

Proof. Proof see Appendix F.

Table 3.2 System parameters of Sect 3.2

Macro/Small cell/UE distribution	hexagon/PPP/uniform distribution
Density of UEs (θ)	0.0004*[1,2,3,4,5,6]/m^2
Bandwidth allocation [Hz]	20M Hz
Power consumption of macrocells (P1) [W]	40
Power consumption of small cells (P2) [W]	1
Noise power (σ^2) [dbm]	-104
Macro/Small cell pathloss exponent (α_1/α_2)	4
P_{0M}, P_{0s} [W]	130, 6.8
Δ_{pm}, Δ_{ps}	4.7 ,4.0
P_{mM}, P_{mS} [W]	20.0, 0.5
$P_s(s)$ [W]	0
Date Rate Requirement (U) [Mbps]	0.64
Coverage Probability Threshold (η)	0.8
CRE bias factor for small cells (B_2)[db]	[0,4,8,12]
Size of the macrocell (Apothem of hexagon) (R) [m]	500

3.2.5 Validation of Coverage Probability Analysis

In this section, the developed analysis is verified, in particular Proposition 1, Corollary 1, Corollary 2 and Corollary 3. The simulation parameters are listed in Tab. 3.2.5. The UE density here is assumed to be $0.0008/m^2$, and the small cell density is assumed to be $0.0005/m^2$. The cell range expansion bias (B_2) is set to be 4dB. These values are selected randomly to verify the numerical results. The coverage probability of UEs is validated by sweeping over a range of allocated bandwidth.

Simulation Set-up

In this part, the simulation method used to verify the numerical results will be mainly introduced. The simulation tool used in this section is Matlab. In the simulation, the macrocell is deployed at the origin and its coverage area is assumed to be a circle with radius 500m. The UEs follow random distribution within the circle with density $5*10^{-4}/m^2$, and the small cells follow SPPP distribution with density $8*10^{-4}/m^2$ in area B, just as Fig 3.8 shows. The bias factor (B_2) is set to be 4 dB. These values are selected randomly to verify the numerical results. The received power in the simulation is written in the form of $P_r = P_t * K * \frac{d}{d_0}^{-\alpha} * h$, where P_t is the BS transmission power, K and d_0 are set to be 1, h is the Rayleigh fading and can be generated with $'exprnd'$ function. In the simulation, the coverage probability of UEs is expressed as: 'the number of UEs satisfy $\frac{W}{N} log_2(1+\gamma_u) > U$' over 'the total number of UEs'. The values of all the parameters used in the simulation can be found in Tab. 3.2. It is noted that Monte Carlo method is used in the simulation and the loop count is 2000 times.

UEs in Set A

It is supposed that all UEs in set A will be offloaded to the macrocell. Fig. 3.10 explains the relationship between the bandwidth allocated and the coverage probability. It can be easily see that with the increase of z, the coverage probability will decrease on a large scale. That is because with z increase, more UEs will be offloaded to the macrocell from the sleeping small cells. In that case, more bandwidth is needed from the macrocell to guarantee the coverage probability of its UEs.

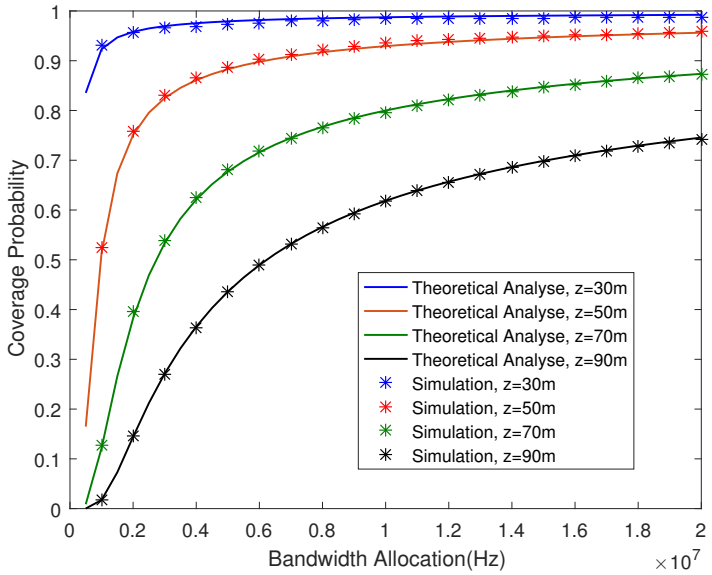

Fig. 3.10 Coverage probability obtained from simulation and Proposition 1(G_A) for UEs in set A

UEs in Set U_1

The relationship between the allocated bandwidth and the coverage probability of the UEs in set U_1 is shown in Fig. 3.11. It can be seen that as z increases, the coverage probability increases steadily, the major reason of which is that the number of UEs in set U_1 decreases with the increasing of z. Recalling that set U_1 is the set of UEs connected to macrocell outside the dashed circle, with the increase of z, the number of UEs in set U_1 declines. It is demonstrated as follows:

$$\begin{aligned} N_B^{U_1} &= \pi(R^2 - z^2) q_B^{U_1} \\ &= \pi(R^2 - z^2) \int_z^R e^{-\lambda_2 (\frac{P_1}{P_2 B_2})^{-\frac{2}{\alpha_2}} r^{\frac{2\alpha_1}{\alpha_2}}} \frac{2r}{R^2 - z^2} \mathrm{d}r, \end{aligned} \tag{3.59}$$

where $N_B^{U_1}$ is the number of UEs in set U_1, and $q_B^{U_1}$ is the association probability which can be found in (3.44). With numerical calculation, it can be found that N_{U_1} goes down rapidly with the increase

of z. Hence, the coverage probability will increase correspondingly.

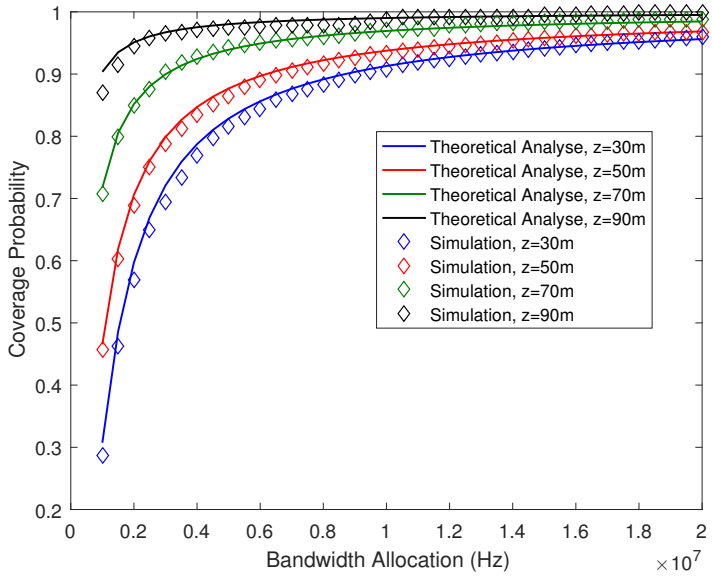

Fig. 3.11 Coverage probability obtained from simulation and Corollary 1($G_B^{U_1}$) for UEs in set U_1

UEs in Set U_2

The relationship between the allocated bandwidth and the coverage probability of UEs in set U_2 is shown in Fig. 3.12. It is noted that, in order to show the difference of coverage probability for each z significantly, I chose the maximum I_m here, $Im = P_1 z^{-\alpha_m}$. From Fig. 3.12, it can be seen that the coverage probability rises with the increase of z, the reason of which is the interference from the macrocell to UEs in set U_2 decreases with the increase of z, hence, the coverage probability will increase correspondingly.

UEs in Set U_3

The relationship between the allocated bandwidth and the coverage probability of UEs in set U_3 is illustrated in Fig. 3.13. It is noted that in this part, the inter-cell interference from small cells cannot be calculated accurately, hence, I provide an approximation of the upper bound of the interference. It can be seen that the coverage probability rises with the increase of z, this is because the number of UEs in set U_3 goes down with the increase of z. I demonstrate this as follows:

$$N_{U_3} = q_B^{U_3} \frac{\lambda_u}{\lambda_2}, \tag{3.60}$$

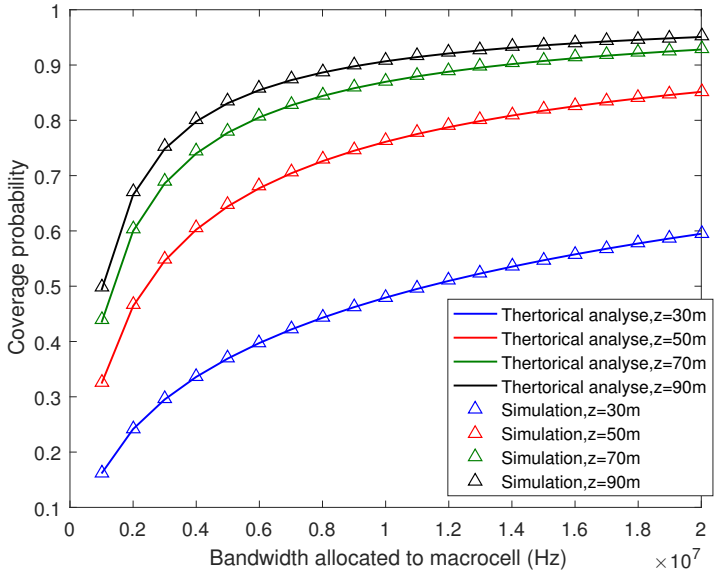

Fig. 3.12 Coverage probability obtained from simulation and Corollary 2($G_B^{U_2}$) for UEs in set U_2

where $q_B^{U_3}$ can be written as:

$$q_B^{U_3} = \int_z^R (\exp(-\lambda_2 \pi (\frac{P_1}{P_2})^{-\frac{1}{\alpha_2}} R_1^{\frac{\alpha_1}{\alpha_2}})) \frac{2r}{R^2 - z^2} \, \mathrm{d}r$$
$$- \int_z^R (\exp(-\lambda_2 \pi (\frac{P_1}{P_2 B_2})^{-\frac{1}{\alpha_2}} R_1^{\frac{\alpha_1}{\alpha_2}})) \frac{2r}{R^2 - z^2} \, \mathrm{d}r. \tag{3.61}$$

With numerical integration, it can be found that N_{U_3} decreases when z increases. Hence, the coverage probability will increase correspondingly.

3.2.6 Problems Analysis and Solutions

Based on the derived coverage constraints in the last section, the minimum power consumption with given user density will be proposed. The network power consumption can be written as :

$$P = \left(P_{0M} + \Delta_{pm} * P_{mM} * \frac{W_A + W_B^{U1}}{W} + (P_{0S} + \Delta_{ps} * P_{sS} * \frac{W_B^{U2} + W_B^{U3}}{W}) \lambda_2 \pi (R^2 - z^2) \right), \tag{3.62}$$

where $P_{0M} + \Delta_{pm} * P_{mM} * \frac{W_A + W_B^{U1}}{W}$ is the power consumption of the macrocell, and $(P_{0S} + \Delta_{ps} * P_{sS} * \frac{W_B^{U2} + W_B^{U3}}{W}) \lambda_2 \pi (R^2 - z^2)$ is the power consumption of all active small cells. Among them, W_A is the bandwidth required for UEs in set A, $W_B^{U_1}$ is the bandwidth required for UEs in set U_1, $W_B^{U_2}$ is the bandwidth required for UEs in set U_1, $W_B^{U_3}$ is bandwidth required for UEs in set U_3. P_{0M}, Δ_{pm}, P_{mM},

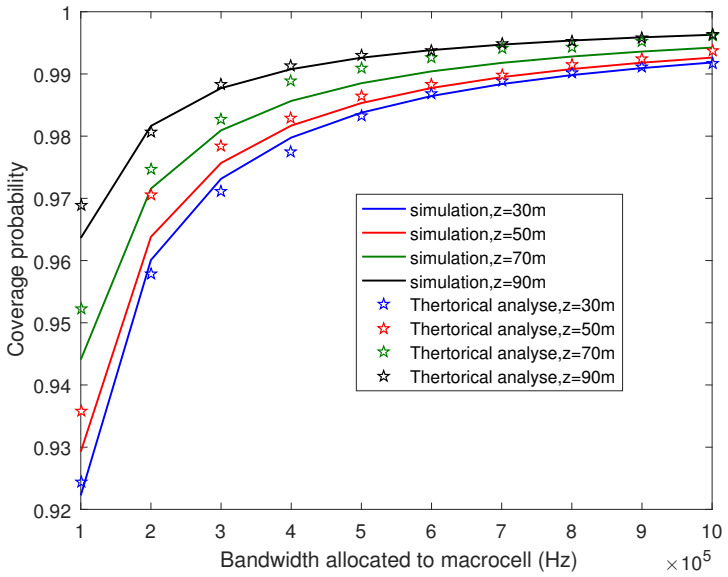

Fig. 3.13 Coverage probability obtained from simulation and Corollary 3($G_B^{U_3}$) for UEs in set U_3

Δ_{ps}, P_{sS} can be found in Tab. 3.2.

The problem can be formulated as bellow:

$$\text{OPT: } \min P(\lambda_2, z, B_2) \tag{3.63}$$

$$\text{s.t., } \frac{W_A}{\lambda_u \pi z^2}(1+\gamma(z,B_2,\lambda_2)) > \eta \tag{3.64}$$

$$\frac{W_B^{U_1}}{q_B^{U_1}\lambda_u \pi (R^2-z^2)}(1+\gamma(z,B_2,\lambda_2)) > \eta \tag{3.65}$$

$$\frac{W_B^{U_2}}{q_B^{U_2}\lambda_u/\lambda_2}(1+\gamma(z,\lambda_2)) > \eta \tag{3.66}$$

$$\frac{W_B^{U_3}}{q_B^{U_3}\lambda_u \pi (R^2-z^2)}(1+\gamma(z,B_2,\lambda_2)) > \eta \tag{3.67}$$

$$W_A + W_B^{U_1} + W_B^{U_3} \leq W_t \tag{3.68}$$

$$W_B^{U_2} + W_B^{U_3} \leq W_t \tag{3.69}$$

However, the problem is hard to solve as there is no closed-form expressions for W_A, $W_B^{U_1}$, $W_B^{U_2}$, $W_B^{U_3}$, which can be found in (B.5),(3.46),(3.51),(3.56) respectively, so the problem can be solved step by step.

Firstly, I calculate the lower bound and upper bound of z, which can be written as z_{min} and z_{max}.

Here, it is assumed that $z_{min} = 0$, and z_{max} can be calculated according to (3.65) and (3.66). Given $z_i = z_{min} + \Delta_z * i, z_i \leq z_{max}$, $\Delta_z = 5$, $i = [0,1,2,3,4...]$, I can analyse the minimum network energy consumption with each z_i.

Then, based on (3.66), it can be derived that the minimum of λ_2:$\lambda_2(min)$. It's noted that (3.68) and (3.69) also need to be satisfied. According to (3.64) and (3.68), the maximum of λ_2:$\lambda_2(max)$ can be derived. Given $\lambda_2(j) = \lambda_2(min) + \Delta_\lambda * j, \lambda_2(i) \leq \lambda_2(max)$, $\Delta_\lambda = 2 * 10^{-5}$, $j = [0,1,2,3,4...]$, the network power P in (3.62) can be solved with $\lambda_2(j)$ and corresponding B_2. Actually P is minimised when B_2 reaches maximum. By comparing network power P with given $\lambda_2(j)$, the minimum value of $P(z)$ can be found.

Finally, compare $P(z)$ with given $z(i)$ and found the minimum.

Below is the summary of the optimisation steps:

1. Let $z_{min} = 0$ and derive z_{max} according to (3.65) and (3.66).
2. Let $z_i = z_{min} + \Delta_z * i, z_i \leq z_{max}$, where $\Delta_z = 5$, $i = [0,1,2,3,4...]$.
3. Derive $\lambda_2(min)$ from (3.66), (3.68) and (3.69). Derive $\lambda_2(max)$ according to (3.64) and (3.68).
4. Let $\lambda_2(j) = \lambda_2(min) + \Delta_\lambda * j, \lambda_2(i) \leq \lambda_2(max)$, where $\Delta_\lambda = 2 * 10^{-5}$, $j = [0,1,2,3,4...]$.
5. Find the minimum value $P^*(z_i)$ of $\{P(z_i, \lambda_2(j))\}$ over λ_2 with each z_i.
6. Find the minimum value of $\{P^*(z_i)\}$.

3.2.7 Network Power Consumption

Fig. 3.14 and Fig .3.15 are generated based on the optimisation of (3.62). The parameters used are all listed in Tab. 3.2.

Fig. 3.14 illustrates the network energy consumption(P) with different z and different bias factor B_2 when $\theta = 0.0016/m^2$ and $\theta = 0.0008/m^2$. It's easy to see that the network has a higher power consumption with more UEs. In addition, the figure demonstrates that the network consumes lower power with larger bias factor (B_2). It can also be seen that, with CRE technique used, especially with large B, the network power consumption drops rapidly, that is because the small cell density outside the dashed circle is diluted in a large scale with CRE technique applied.

Fig. 3.15 represents the relationship between the network power consumption (P) with different UE density (θ) for three approaches. It's clear to see that the power consumption rises with the increase of the UE density. In addition, as expected, the proposed method has a much better performance compared with that of the conventional approach, especially with higher UE density. It can be seen from the figure that when the UE density reaches $2.4 * 10^{(-3)}/m^2$, the network power consumption of the conventional method exceeds 3000W, which is almost twice compared with that of the proposed approach. Moreover, both the proposed and conventional approaches outperform the random sleeping method significantly.

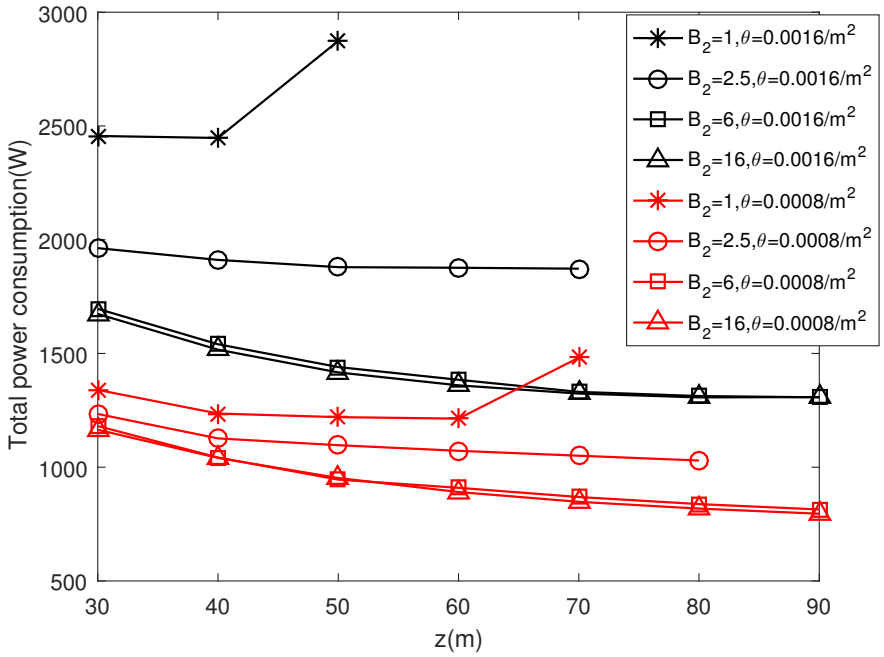

Fig. 3.14 Network power consumption with z

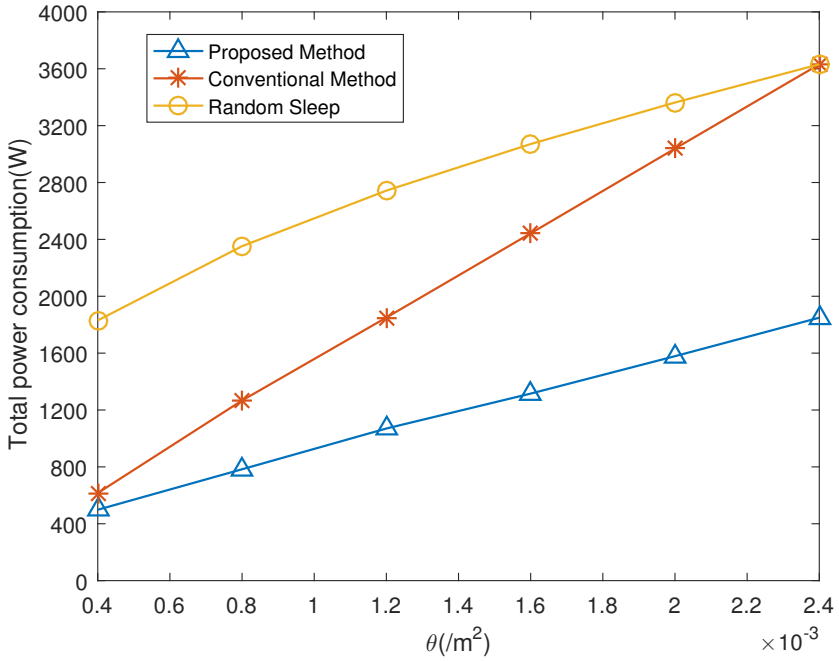

Fig. 3.15 Network power consumption with different UE density

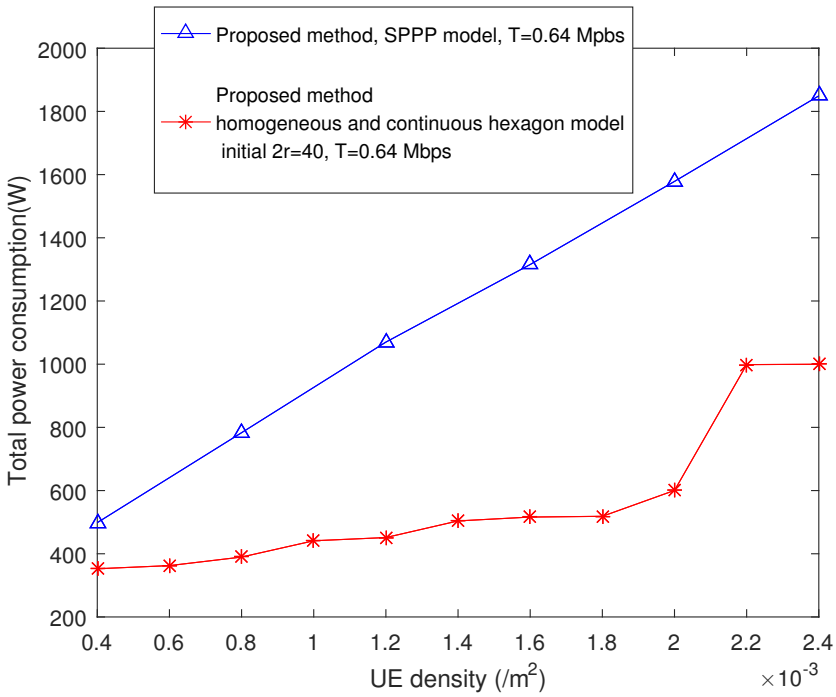

Fig. 3.16 Network power consumption comparison for different network models

3.3 Summary

In this chapter, a strategic small cell sleeping mechanism according to the dynamic traffic is proposed to minimise the HetNet power consumption. The proposed approach uses range expanded small cells and eICIC technique to cover the sleeping cells which are far from the macrocell and uses macrocell to serve the UEs from the sleeping cells close to it. The proposed mechanism is analysed in homogeneous and continuous hexagon network model in Sect. 3.1, as well as homogeneous SPPP based network model in Sect .3.2. The results in both sections demonstrate that the proposed scheme outperforms the conventional ones in a large scale.

Fig. 3.16 compares the results with same UE density when $T = 0.8Mbps$. It can be seen that when UEs are uniformly distributed in the entire area, the hexagon based network power consumption is lower than that of SPPP based network model. In fact, stochastic geometry is introduced in HetNets research because it is accurate in predicting probabilistic parameters of randomly designed HetNets such as SINR distribution, coverage probability, etc. Homogeneous SPPP based model is significantly more tractable than the traditional hexagon-based models, and appears to track the lower bound performance (e.g., coverage probability) of real deployment.

Chapter 4

Enhancing Small Cell and Network Capacity using Wireless Backhaul

4.1 Introduction

Recently, hyper dense small cells are proposed to meet the challenge of the tremendous increment in mobile data service requirement. To reduce the deployment cost as well as operating cost, these small cells are usually connected to limited backhauls, in which case the backhaul capacity may become the bottleneck in busy hours. In this chapter, I propose an optimal resource allocation scheme for the small cells to utilise the macrocell links as the wireless backhaul. The simulation results show that the proposed scheme can significantly improve the network performance in high traffic load scenarios.

To address the explosive growth in data demands driven by mobile phones, network operators have to significantly increase the capacity of their networks. Dense small cells deployment has been considered as a key technology to offer high throughput and continuous coverage rate. With limited backhaul capacity, the small cells could connect to the core network by low capacity backhaul links (e.g., DSL links). In this situation, the QoS of UEs may not be guaranteed. Therefore, if the capacity of the current backhaul link is insufficient, the wireless resources could be utilised to backhaul information for small cells.

Compared with fibre backhaul, wireless backhaul is cheaper and more flexible. However, wireless backhaul suffers from interference and the resource allocation and performance evaluation are challenging.

In this chapter, a scheme which uses macrocell link as wireless backhaul is proposed. In the proposed scheme, the capacity of small cells and the entire network is maximised. Both FDD and IB-FD approaches are used to verify the proposed maximisation. To the best of my knowledge, the numerical performance evaluation in terms of network throughput of the two methods has not been provided yet.

In FDD networks, wireless resources allocated to links between the Macrocell and small cells are orthogonal to that allocated for the data exchange between the small cell and its associated UEs, as shown in Fig. 4.1. Whereas in IB-FD networks, small cells are able to carry out the self-interference cancellation. Therefore, IF-FD is able to transmit and receive signals in the same time-frequency resource, as shown in Fig. 4.2. The detailed explanation of IB-FD technique has been provided in Sect .2.3.

The capacity enhancement with wireless backhaul is analysed under two scenarios: (1) In the first scenario, a single considered small cell that uses wireless backhaul is analysed in a two tier network. In this scenario, the traffic of some hot spots could increase significantly. Therefore, the wireless backhaul could only be needed in these selected hot spot areas. (2) In the second scenario, all small cells are assumed to utilise wireless backhaul, and the throughput of the entire network is analysed. Most of the papers in this area target on the optimisation of UEs' coverage probability, the researches about network throughput performance evaluation are insufficient. In this part, the detailed analysis of the network throughput will be proposed.

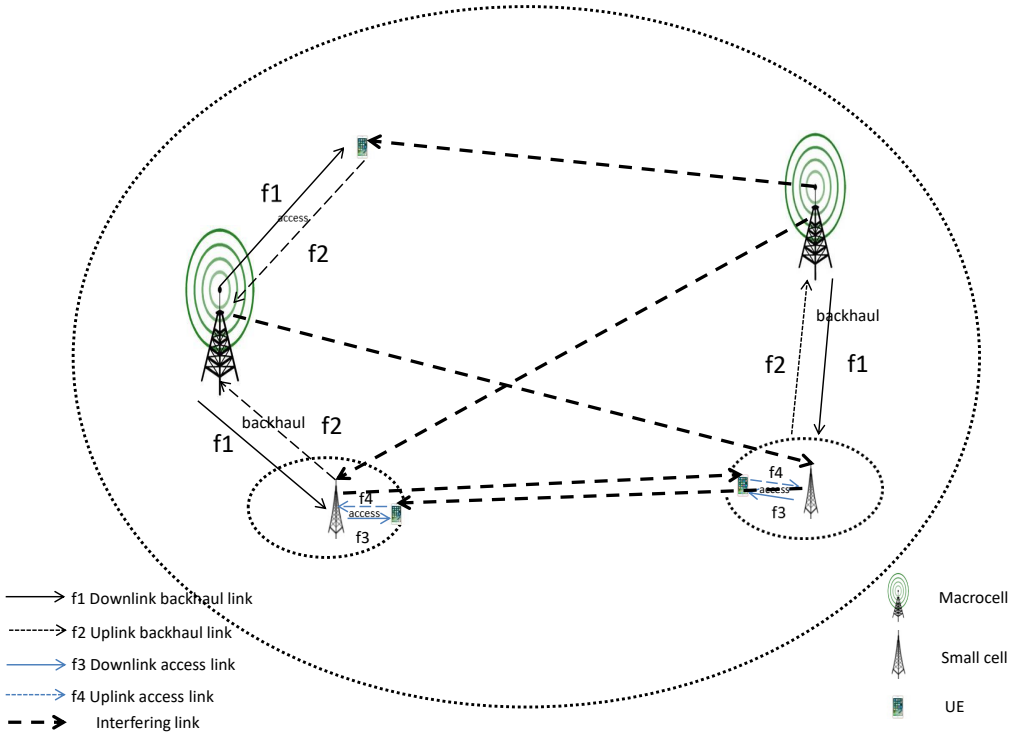

Fig. 4.1 FDD System Model

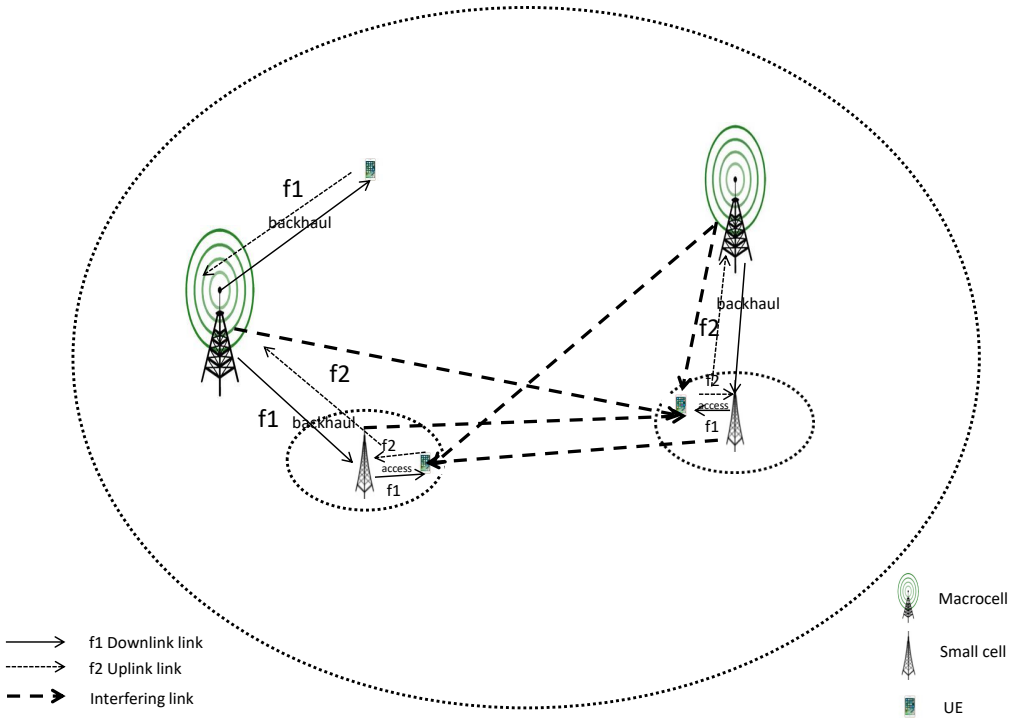

Fig. 4.2 IB-FD System Model

4.2 System Model and Problem Formulation

The system model consists of both macrocells and small cells deployed according to a homogeneous Spatial Poisson Point Process (SPPP) Φ with intensity λ_m and λ_s, respectively, in the Euclidean plane. The UEs are uniformly distributed within the entire area. The backhaul capabilities for the macrocells are assumed to be profound and the small cells are connected to limited backhauls. W denotes the whole bandwidth of the network. In the small cell, the spectrum is divided into subchannels each with bandwidth b. Suppose that N represents the number of available sub-channels in the network, if N servers are all busy simultaneously, then any new arrival requests would be dropped.

Considering a channel model consisting of distance dependent path loss and multipath fading, the channel gain g of a link can be expressed as:

$$g = d^{-\alpha}h, \tag{4.1}$$

where d is the distance between the transmitter and receiver, h is exponential distributed random variable with mean $(1/\gamma)$, representing Rayleigh fading, and α is the path loss exponent. It is assumed that the path loss exponents for macrocells and small cells are the same, $\alpha_s = \alpha_m = \alpha$.

For a typical UE l associated with a BS in tier k, its SINR Υ_l is

$$\Upsilon_l = \frac{g_{l,0}P_k}{\sum_{j=1}^{K}\sum_{i\in\mathscr{C}_j\setminus B_{k0}} g_{l,i}P_j + \sigma^2}, \tag{4.2}$$

where P_k, k=s *or* m is the transmit power of the serving BS, $g_{l,0}$ and $g_{l,i}$ are the channel gain (as defined in (4.1)) of the link from the serving BS to the UE l and the interfering links to the UE l, respectively, $\mathscr{C}_j$ is the set of BSs and σ^2 is the power of the additive white Gaussian noise (AWGN). For FDD approach, $K = 1$.

The SINR Υ_m for the link between macro-cell BS and the small cell BS is

$$\Upsilon_m = \frac{g_{m,0}P_m}{\sum_{j=1}^{K}\sum_{i\in\mathscr{C}_j\setminus B_{m0}} g_{s,i}P_j + \sigma^2}, \tag{4.3}$$

where P_m is the transmit power of macrocell, $g_{s,0}$ is the channel gain of the link from the macro BS to the target small cell, and $g_{s,i}$ are the channel gain (as defined in (4.1)) of interfering links from other BSs to the target small cell. $\mathscr{C}_j$ is the set of interfering BSs. For FDD approach, $K = 1$.

Denoting R_i as the capacity of UE i, the total requests of a small cell is $N(t)$ at time t and thus the total throughput (bits/s) of the small cell is

$$R_T = \sum_{i=0}^{N(t)} R_i = \sum_{i=0}^{N(t)} b\log_2(1+\Upsilon_i). \tag{4.4}$$

Consider a transmission time period T ($T \gg T_c$, where T_c is the coherence time, defined as a statistical measure of the time duration over which the channel impulse response is essentially invariant.) Assume that the perfect interleaving is fulfilled under certain coherence time as well as delay restrictions and the receiver has perfect Channel Quality Indicator, the fading channel can be transformed into an equivalent stochastic channel model, which is a strong stationary process [143]. In that case, the ergodic capacity can be used to represent the statistical expectation of the Shannon capacity over all fading states.

Suppose that at time t, $\rho(t)$ UEs move into the coverage area of the small cell A, and the number of available channels is expressed as N. The average number of UEs served by the small cell can be expressed as

$$\mathbb{E}[N(t)] = \min(\rho(t), N). \tag{4.5}$$

The average throughput of small cell A is

$$R_C = \mathbb{E}[R_T] = \mathbb{E}[\sum_{j=0}^{N(t)} R_i] = \mathbb{E}[N(t)]\mathbb{E}[R_i]. \tag{4.6}$$

Proof. Proof see [144, Chapter 3, pages 83-103].

As each small cell is connected to a limited backhaul, its backhaul capacity C_b might not be enough to sustain the total capacity R_C, i.e., $C_b < R_C$. Therefore, a portion of bandwidth (τB, $0<\tau \leq 1$) from the macrocell can be used as wireless backhaul link to support the traffic of the small cell. Nevertheless, the macrocell needs to serve its UEs simultaneously. The bandwidth can be used for the communication between the macrocell and small cells is τW for frequency division duplex (FDD) method, and W for IB-FD method. Thus, for a specific τ, $N = \lfloor (1-\tau)W/b \rfloor$ for the FDD, and $N = \lfloor W/b \rfloor$ for the IB-FD, where b is the number of channels a user occupies The average backhaul capacity the macrocell provides can be modelled as its ergodic capacity [42, 145]. It's noted that for FDD, the wireless backhaul is only interfered by other macrocells, however, for IB-FD, the wireless backhaul receives interference from both tiers, which is illustrated in Fig. 4.1 and Fig. 4.2.

4.3 Capacity Analysis for a Single Small Cell

In this part, I focus on analysing the capacity of a single small cell, denoted by small cell A, utilizing wireless backhaul from a macrocell. Both FDD and IB-FD schemes are compared in this section. The network model is illustrated in Fig. 4.3.

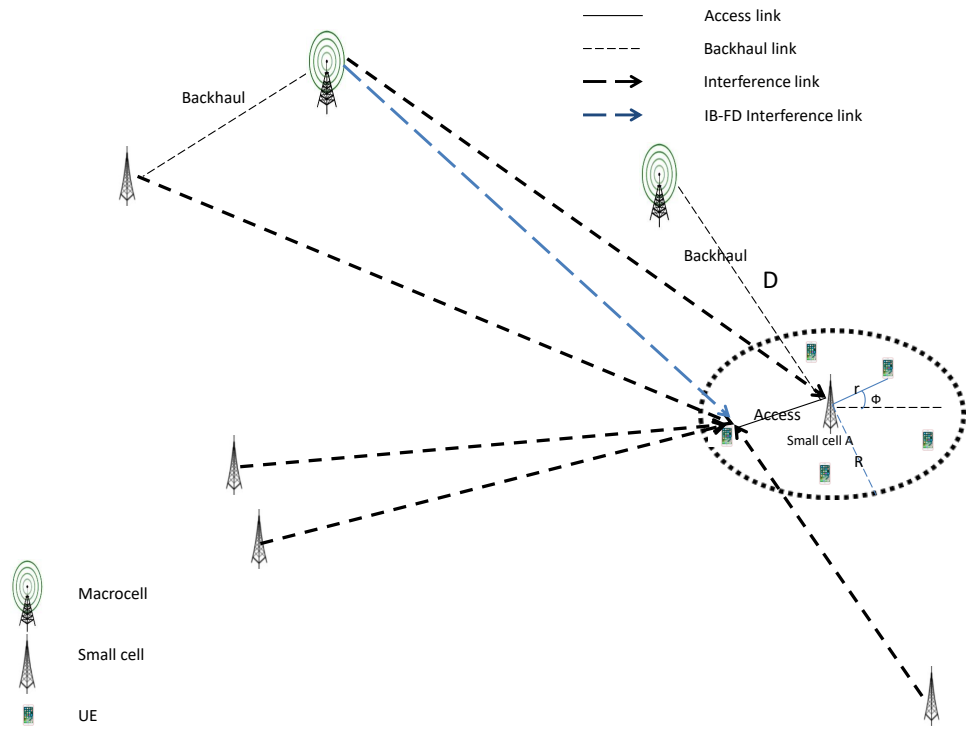

Fig. 4.3 Capacity Analysis of Small Cell A

Suppose adding the small cell A into the macro-cell coverage area, the distance between the

chosen macrocell and small cell A is denoted as D.

I calculate the capacity(C_m) of the wireless backhaul from macrocell to small cell A first:

Theorem 1. *The ergodic capacity C_m is:*

$$\begin{aligned} C_m =& W\left(\mathbb{E}\left[\log_2\left(1+\frac{P_m h D^{-\alpha_m}}{I_s+I_m+\sigma^2}\right)\right]\right) \\ =& W\left(\int_{t>0}\mathbb{P}\left[\log_2(1+\frac{P_m h D^{-\alpha_m}}{I_s+I_m+\sigma^2})>t\right]\,\mathrm{d}t\right) \\ =& W\left(\int_{t>0}\mathbb{P}\left[h>D^{\alpha_m}P_m(\sigma^2+I_m+I_s)(2^t-1)\right]\,\mathrm{d}t\right) \\ =& W\left(\int_{t>0}\mathbb{E}(\exp(-\frac{\mu D^{\alpha_m}}{P_m}(\sigma^2+I_m+I_s)(2^t-1))\,\mathrm{d}t\right) \\ =& W\left(\int_{t>0}e^{-\sigma^2\mu D^{\alpha_m}T}\mathscr{L}_{I_s}(\mu D^{\alpha_m}T)\mathscr{L}_{I_m}(\mu D^{\alpha_m}T)\,\mathrm{d}t\right), \end{aligned} \tag{4.7}$$

where $T=\frac{(2^t-1)}{P_m}$ for $\alpha_m=4$, and

$$\mathscr{L}_{I_m}(\mu T D^{\alpha_m})=\exp\left(-\pi\lambda_1 D^2(TP_m)^{2/\alpha_m}(\pi/2-atan((TP_m)^{-2/\alpha_m}))\right).$$

The proof of $\mathscr{L}_{I_m}(\mu T D^{\alpha_m})$ can be referred to (2.4). For the FDD approach, as the backhaul link and data links of small cells are in different frequency bands, the backhaul link is freed from the interference of small cells. In that case, $\mathscr{L}_{I_s}(\mu T D^{\alpha_m})=1$. For IB-FD approach, due to the reason that the backhaul link and data links of small cells share the same frequency band, the backhaul link suffers the interference from small cells. Hence, $\mathscr{L}_{I_s}(\mu T D^{\alpha_m})=\exp\left(-\pi\lambda_s D^2(TP_s)^{2/\alpha_s}(\pi/2)\right)$ when $\alpha_s=4$. The proof of $\mathscr{L}_{I_s}(\mu T D^{\alpha_m})$ can be referred to (2.4). The parameters μ, σ^2, P_s, P_m and λ_s can be found in Tab. 4.1.

The physical meaning of (4.7) is the capacity of the wireless backhaul link to small cell A based on Shannon's theorem. $\frac{P_m h D^{-\alpha_m}}{I_s+I_m+\sigma^2}$ is the SINR of the backhaul link from the macrocell to small cell A from (4.3).

In the FDD scheme, $\tau\in[0,1]$ denotes the ratio between the wireless backhaul bandwidth and all available bandwidth in the network. Thus the downlink average achievable throughput from the macrocell to the k th small cell is written as:

$$c_m=\tau C_m, \tag{4.8}$$

where C_m is expressed in (4.7), and $\tau=1$ for IB-FD method.

Then the ergodic capacity of a UE from small cell A will be computed. Assume that there are UEs continuously coming into the coverage area of small cell A. Without loss of generality, it is assumed that all these UEs are distributed uniformly in a circle inside the coverage area of A with radius R_A. Here, an approximation of the range of R_A will be provided. Firstly, the UEs inside the

coverage area will not be associated to the macrocell, that is, $P_m D^{-\alpha_m} < P_s R_A^{-\alpha_s}$, and it can be derived that $R_A < \frac{P_s}{P_m}^{\frac{1}{\alpha_s}} D^{\frac{\alpha_m}{\alpha_s}}$. Secondly, the UEs inside the coverage area will not connect to other small cells. Given the small cell density to be λ_s, the average distance between the two closest small cells is $\frac{1}{2\sqrt{\lambda_s}}$. Therefore, R_A can be approximated as $R_A = \min(\frac{1}{2\sqrt{\lambda_s}}, \frac{P_s}{P_m}^{\frac{1}{\alpha_s}} D^{\frac{\alpha_m}{\alpha_s}})$

Theorem 2. *The ergodic capacity of a UE from small cell A is approximated as*

$$\begin{aligned}
\mathbb{E}[R_i] &= \mathbb{E}[\log_2(1+SINR)] \\
&= \int_0^{2\pi}\int_0^{R_A} \mathbb{E}\left[log_2\left(\frac{P_s h r^{-\alpha_s}}{I_s+I_m+I_{mD}+\sigma^2}\right)\right] r\,\mathrm{d}r\mathrm{d}\phi \\
&= \int_0^{2\pi}\int_0^{R_A}\int_{t>0} \mathbb{P}\left[\log_2\left(\frac{P_s h r^{-\alpha_s}}{I_s+I_m+I_{mD}+\sigma^2} > t\right)\right] \mathrm{d}t r\mathrm{d}r\mathrm{d}\phi \\
&= \int_0^{2\pi}\int_0^{R_A}\int_{t>0} \mathbb{E}\left(e^{-\mu r^{\alpha_s}(\sigma^2+I_s+I_m+I_{mD})(2^t-1)/P_s}\right) \mathrm{d}t r\mathrm{d}r\mathrm{d}\phi \\
&= \int_0^{2\pi}\int_0^{R_A}\int_{t>0} e^{-\mu r^{\alpha_s}(\sigma^2+I_{mD})(2^t-1)/P_s} \mathscr{L}_{I_s}(\mu r^{\alpha_s}(\frac{2^t-1}{P_s}))\mathscr{L}_{I_m}(\mu r^{\alpha_s}(\frac{2^t-1}{P_s}))\,\mathrm{d}t r\mathrm{d}r\mathrm{d}\phi, \quad (4.9)
\end{aligned}$$

where $\frac{P_s h r^{-\alpha_s}}{I_s+I_m+I_{mD}+\sigma^2}$ is the SINR expression of the UE from small cell A from (4.2). ϕ is the angle of the x-axis and the line between small cell A and UE. I_s is the interference from other small cells. I_{mD} is the interference from the macrocell which communicates with small cell A. I_m is the interference from other macrocells.

The Laplace transform of I_s is :

$$\mathscr{L}_{I_s}(\mu r^{\alpha_s}(\frac{2^t-1}{P_s})) = exp\left(-\pi\lambda_2 r^2((\frac{2^t-1}{P_s})P_s)^{2/\alpha_s} * (\pi/2 - atan(((\frac{2^t-1}{P_s})P_s)^{-2/\alpha_s}))\right). \quad (4.10)$$

The proof of $\mathscr{L}_{I_s}(\mu r^{\alpha_s}(\frac{2^t-1}{P_s}))$ can be referred to (2.4).

For IB-FD, I_{mD} can be expressed as:

$$I_{mD} = P_m(D^2 + r^2 - 2Drcos(\phi+\pi/2))^{-\alpha_s/2}. \quad (4.11)$$

The Laplace transform of I_m is :

$$\mathscr{L}_{I_m}(\mu r^{\alpha_s}(\frac{2^t-1}{P_s})) = exp\left(-\pi\lambda_1 r^2((\frac{2^t-1}{P_s})P_m)^{2/\alpha_m} * (\pi/2 - atan((D/r)^2 \cdot (\frac{2^t-1}{P_s})P_m)^{-2/\alpha_m}))\right). \quad (4.12)$$

The proof of $\mathscr{L}_{I_m}(\mu r^{\alpha_s}(\frac{2^t-1}{P_s}))$ can be referred to (2.4).

For FDD, $\mathscr{L}_{I_m}(\mu r^{\alpha_s}(\frac{2^t-1}{P_s})) = 1$. $I_{mD} = 0$. The parameters μ, σ^2, P_s and λ_s are assigned in Tab. 4.1.

4.3.1 Problem Formulation and Solution for FDD Approach

It is noted that for IB-FD approach, $\tau = 1$ as all bandwidth of the macrocell is utilized as wireless backhaul to support small cell A. Hence, I only need to provide the solution for *Optimal (OPT)* of FDD method in this section.

Definition 1. *The total capacity of the small cell is defined as*

$$C_\tau = \min\{R_C, C_b + c_m\}. \tag{4.13}$$

Here the aim is to maximise the capacity of the small cell

$$\text{OPT:} \qquad \arg\max_{\tau} C_\tau \tag{4.14}$$

$$\text{s.t.,} \qquad \tau \leq \tau^\dagger \tag{4.15}$$

where $\tau^\dagger$ is the maximum portion of bandwidth can be utilised for wireless backhaul. In this thesis, it is assumed that $\tau^\dagger = 1$.

Proposition 5. *The solution τ^* to* OPT *is the solution τ_s of the following equation*

$$R_C = C_b + c_m, \tag{4.16}$$

if $\tau_s \leq \tau^\dagger$, otherwise $\tau^* = \tau^\dagger$, where R_C is in (4.6) and (4.9), C_b is the backhaul capacity, and c_m is in (4.7) and (4.8).

Proof. It is easy to prove that c_m defined in (4.7) (Theorem 2) strictly increases with τ. In addition, it can be seen that R_C strictly decreasing with τ. Thus when $\tau < \tau_s$, $c_m + C_b < R_C$ and $C_\tau = c_m + C_b$, while $\tau > \tau_s$, $c_m + C_b > R_C$ and $C_\tau = R_C$. It is easy to find that C_τ increases with τ for $\tau \in [0, \tau_s]$ and decreases with τ for $\tau \in [\tau_s, 1]$. With these discussions, I conclude that C_τ reaches its maxima at τ_s. Thus it is known that $\tau^* = \tau_s$ if $\tau_s < \tau^\dagger$, otherwise $\tau^* = \tau^\dagger$. □

It is worth noting that, (4.16) can be efficiently solved by numerical algorithms, such as Brent's method [146].

4.3.2 Numerical Results Analysis

Based on (4.7), (4.9), (4.6), (4.16), the maximum capacity of small cell A can be derived. The major parameters utilised in the simulation can be found in Tab. 4.1. $\tau^\dagger$ is chosen to be 1 here.

Fig. 4.4 and Fig. 4.5 can be obtained from the optimisation of (4.16). Both figures illustrate the capacity of small cell A with FDD and IB-FD methods. It can be seen that FDD method outperforms the IB-FD method significantly, which is due to two reasons: (1) In IB-FD method, the spectrum

Table 4.1 System parameters of chapter 4

Macro/Small cell/UE distribution	PPP/PPP/uniform distribution
Density of macrocells(λ_m)	$1.5^{-6}/m^2$
Density of small cells(λ_s)	$6^{-5}/m^2$
Density of UEs (θ)	0.0004*[1,2,3,4,5,6,7]/m^2
Number of UEs to small cell A (ρ)	10*[2,3,4,5,6,7,8,9]
Bandwidth allocation (W)	10M Hz
Power consumption of macrocells (P_m)	40W
Power consumption of small cells (P_s)	1W
Macro/Small cell pathloss exponent (α_m/α_s)	4
Original wired backhaul(C_b)	$2*10^6$ Hz, $6*10^6$ Hz
Noise power (σ^2) [dbm]	-104
Bandwidth of Resource Block (RB) [Hz]	180K

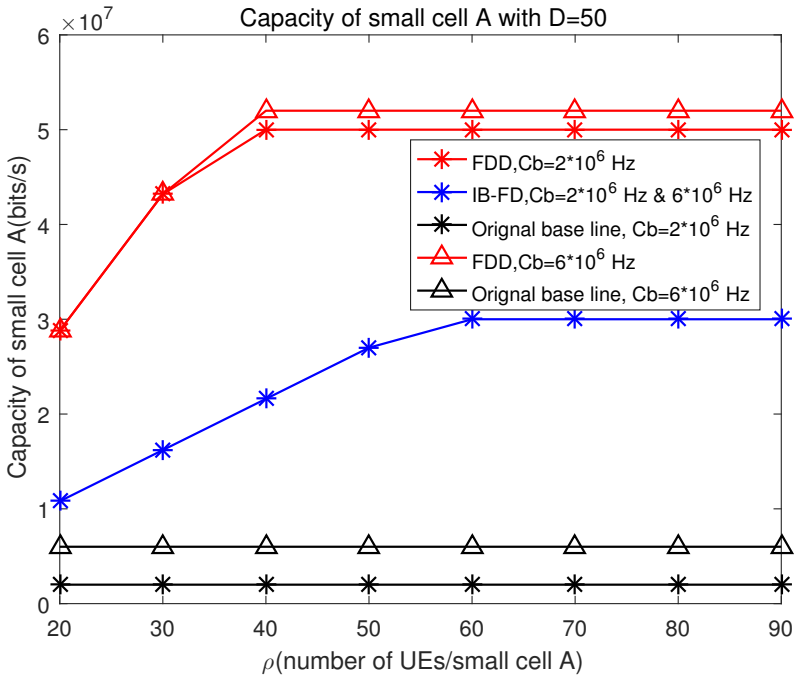

Fig. 4.4 Capacity of small cell A with D=50

efficiency of UEs' data links and wireless backhaul links degrade in a large scale due to the cross-tier interference. (2) For FDD method, the whole spectrum can be utilised to communicate with small cell A ($\tau^{\dagger} = 1$) especially when the UE density is low, which means enough bandwidth can be allocated to small cell A as its wireless backhaul link to serve its traffic. Furthermore, it's obvious to see that both FDD and IB-FD achieve much better performance than the original base line. In addition, the enhancement of the wireless backhaul falls down with the increase of D.

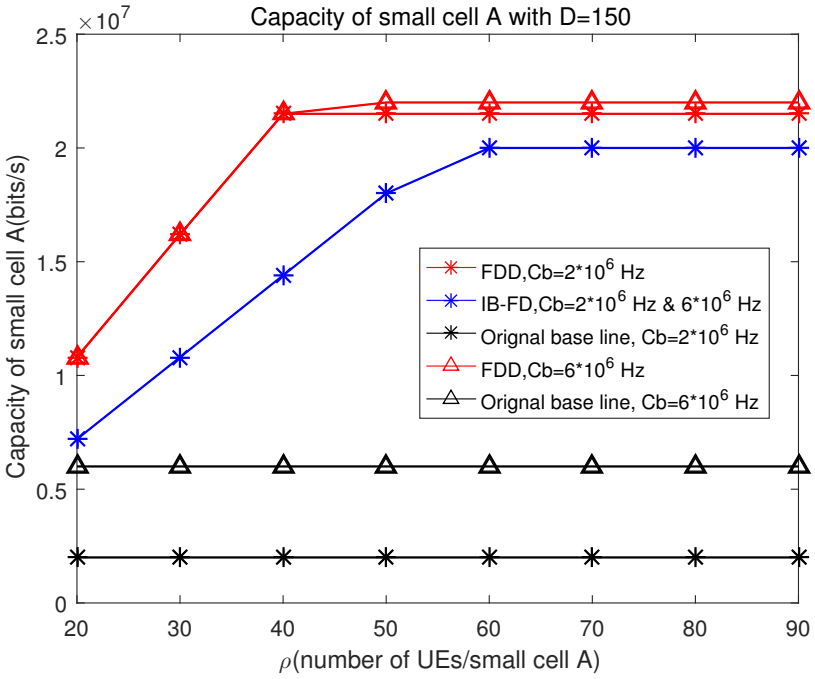

Fig. 4.5 Capacity of small cell A with D=150

4.4 Network Capacity Analysis

In this part, I will provide a numerical analysis of the network throughput, including small cells and the macrocell. The throughput of the small cells can be divided into two groups: (1) Group A: the traffic of the small cell is beyond of the capacity of wired and wireless backhaul. (2) Group B: the traffic of the small cell can still be supported by the wired and wireless backhaul.

4.4.1 Numerical Analysis of Network Throughput

Numerical Analysis of Throughput of Small Cells in Group A

Lemma 1. *Given a random variable X, and a constant a, then* $\mathbb{E}[X \cdot \mathbf{1}\{x \leq a\}] = a\mathbb{P}\{x \leq a\} - \int_0^a \mathbb{P}\{x \leq t\}\,\mathrm{d}t$

Proof. Proof see Appendix G.

The average throughput $\mathbb{E}[R_A]$ of a small cell in group A can be calculated as

$$\mathbb{E}[R_A] = \mathbb{E}[C_{backhaul}\mathbf{1}\{C_{backhaul} \leq C_S\}], \tag{4.17}$$

where $C_{backhaul}$ is the average backhaul capacity and can be expressed as

$$C_{backhaul} = W\tau \log 2(1+\gamma) + C_b, \tag{4.18}$$

where $W\tau\log_2(1+\gamma)$ is the expression of the capacity of the wireless backhaul, C_b is the expression of the capacity of wired backhaul.

C_S is the sum of UEs' data rate of a small cell and can be expressed as:

$$C_S = R_s * \mathbb{E}[N_s(t)], \tag{4.19}$$

where that R_s is the average data rate of small cell UEs, which can be found in [147], and the average number of UEs of each small cell is $n_s = \lambda_u * A_2/\lambda_s$. A_2 is the UE association probability to small cells, which can also be found in [147]. Based on (4.5), the average UEs served by the small cells can be written as $\mathbb{E}[N_s(t)] = \min(n_s, N)$, where N is the number of available channels and is defined in section 4.2, here, it is assumed that for FDD, each small cell UE occupies one RB and each macrocell UE occupy 1/4 RB, for IB-FD, because both backhaul links and data links suffer signal degradation due to the cross-tier interference received, for fair comparison, it is assumed that each small cell UE occupies 2 resource blocks (RBs), also each macrocell UE occupies 1/3 RB.

According to lemma(1), (4.17) can be derived as:

$$\begin{aligned}
\mathbb{E}[R_A] &= \mathbb{E}[C_{backhaul} \cdot \mathbf{1}\{C_{backhaul} \leq C_S\}] \\
&= \mathbb{E}[(W_b\tau\log_2(1+\gamma) + C_b) \cdot \mathbf{1}\{W_b\tau\log_2(1+\gamma) + C_b \leq R_s * \mathbb{E}[N_s(t)]\}] \\
&\overset{(a)}{=} R_s * \mathbb{E}[N_s(t)] * q_A - \int_0^{R_s * n_s} \mathbb{P}(W_b\tau\log_2(1+\gamma) + C_b \leq t)\,\mathrm{d}t,
\end{aligned} \tag{4.20}$$

where (a) follows lemma (1). q_A is the probability that a small cell is in group A, which can be written as:$q_A = \mathbb{P}\{W_b\tau log2(1+\gamma) + C_b \leq R_s * \mathbb{E}[N_s(t)]\}$. γ is the SINR of small cell UEs, for FDD, it can be expressed as $\gamma_F = \frac{P_m r^{-\alpha_m} h}{I_m + \sigma^2}$, and for IB-FD, it can be expressed as $\gamma_Z = \frac{P_m r^{-\alpha_m} h}{I_m + I_s + \sigma^2}$. In this section the bandwidth is assumed to be equally divided to allocate to each wireless backhaul link, therefore, $W_b = \frac{W}{\lambda_s/\lambda_m}$.

q_A can be further derived as:

$$\begin{aligned}
q_A &= \mathbb{P}\{W_b\tau log2(1+\gamma) + C_b \leq R_s * \mathbb{E}[N_s(t)]\} \\
&= \int_0^{+\infty} (1 - e^{-\sigma^2\mu r^{\alpha_m} T_1} \mathscr{L}_{I_m}(\mu T_1 r^{\alpha_m}) * \mathscr{L}_{I_s}(\mu T_1 r^{\alpha_m})) 2\pi\lambda_1 r exp(-\lambda_1\pi r^2)\,\mathrm{d}r.
\end{aligned} \tag{4.21}$$

Based on (4.20), $\mathbb{E}[R_A]$ can be derived as:

$$\begin{aligned}&\mathbb{E}[R_A]\\&= R_s * \mathbb{E}[N_s(t)] * q_A -\\&\int_{r>0}\int_0^{R_s*\mathbb{E}[N_s(t)]} (1-e^{-\sigma^2\mu r^{\alpha_m}T_2}\mathscr{L}_{I_m}(\mu T_2 r^{\alpha_m}) * \mathscr{L}_{I_s}(\mu T_2 r^{\alpha_m}))2\pi\lambda_1 r exp(-\lambda_1\pi r^2)\,\mathrm{d}t\,\mathrm{d}r,\end{aligned} \tag{4.22}$$

where $\mathscr{L}_{I_m}(\mu T_1 r^{\alpha_m}) = exp\left(-\pi\lambda_1 r^2 (T_1 * P_m)^{2/\alpha_m} * (\pi/2 - atan((T_1 * P_m)^{-2/\alpha_m}))\right)$. $\mathscr{L}_{I_s}(\mu T_2 r^{\alpha_m}) = exp\left(-\pi\lambda_2 r^2 (T_2 * P_s)^{2/\alpha_m} * (\pi/2))\right)$ for IB-FD, and $\mathscr{L}_{I_s}(\mu T_2 r^{\alpha_m}) = 1$ for FDD. $T_1 = \frac{2^{\frac{R_s*\mathbb{E}[N_s(t)]-Cb}{W_b\tau}}-1}{P_m}$ ($\tau = 1$ for IB-FD) and $T_2 = \frac{2^{\frac{t-Cb}{W_b\tau}}-1}{P_m}$.

The proof can be referred to (2.4).

The total throughput of small cells in group A (T_A) is:

$$\begin{aligned}T_A =& \mathbb{E}[R_A] * \mathbb{E}[N_A]\\&= \mathbb{E}[R_A] * q_A * \lambda_s/\lambda_m,\end{aligned} \tag{4.23}$$

where $\mathbb{E}[R_A]$ is expressed in (4.22), q_A is expressed in (4.21), $\mathbb{E}[N_A]$ is the number of small cells in group A, and is expressed as: $\mathbb{E}[N_A] = q_A * \lambda_s/\lambda_m$.

Numerical Analysis of Throughput of Small Cells in Group B

The throughput of small cells in group B is derived in this section. According to the definition mentioned in the beginning of Sect. (4.4), the traffic of the small cell in group B can still be supported by its wired and wireless backhaul. In that case, the throughput of a small cell in group B $\mathbb{E}[R_B]$ can be expressed as:

$$\begin{aligned}\mathbb{E}[R_B] &= \mathbb{E}[C_S \cdot \mathbf{1}\{C_S \le C_{backhaul}\}]\\&= C_S.\end{aligned} \tag{4.24}$$

The total throughput of small cells in group B (T_B) is :

$$\begin{aligned}T_B &= \mathbb{E}[R_B] * \mathbb{E}[N_B]\\&= C_S * ((1-q_A) * \lambda_s/\lambda_m),\end{aligned} \tag{4.25}$$

where the expressin of C_S can be found in (4.19). $\mathbb{E}[N_B]$ can be written as$((1-q_A) * \lambda_s/\lambda_m)$.

Network Throughput Analysis

Based on (4.23) and (4.25), the small cell network total throughput T_s can be derived:

$$\begin{aligned} T_s &= T_A + T_B \\ &= \mathbb{E}[R_A] * \mathbb{E}[N_A] + \mathbb{E}[R_B] * \mathbb{E}[N_B] \\ &= \mathbb{E}[R_A] * q_A * \lambda_s/\lambda_m + C_S * (1-q_A) * \lambda_s/\lambda_m. \end{aligned} \tag{4.26}$$

The throughput of the macrocell can be written as: $T_m = R_m * \lambda_u * (1-A_2)/\lambda_1$, where R_m is the average data rate of the macrocell UEs, A_2 is the UE association probability to small cells, the expression of which can be found in [147], λ_1 is the density of macrocells.

Finally the average total throughput of all the BSs in one macrocell coverage area can be derived as :

$$\begin{aligned} T &= T_s + T_m \\ &= T_s + R_m * \mathbb{E}[N_m] \\ &= \mathbb{E}[R_A] * q_A * \lambda_s/\lambda_m + C_S * (1-q_A) * \lambda_s/\lambda_m + R_m * \lambda_u * (1-A_2)/\lambda_1. \end{aligned} \tag{4.27}$$

4.4.2 Results Analysis and Validation

The numerical results derived from (4.26) are verified with the simulation results in Fig.4.6 and Fig.4.7. In addition, the maximum network throughput derived from (4.27) is illustrated in Fig. 4.8 and Fig. 4.9 with different UE density.

Simulation Set-up

In this part, a brief introduction of the simulation used Fig. 4.6 and Fig. 4.7 will be provided. Matlab is used as the simulation too. In the simulation, the small cells as well as UEs are distributed in a circle area with radius 500 m, and the macrocell is deployed at the centre of the area. The small cells follow SPPP distribution with density $6 * 10^{-5}/m^2$ and the UEs follow uniform distribution with density $4 * 10^{-4}/m^2, 8 * 10^{-4}/m^2, 12 * 10^{-4}/m^2$ respectively. The received power in the simulation is written in the form $P_r = P_t * K * \frac{d}{d_0}^{-\alpha} * h$, where P_t is the BS transmission power, K and d_0 are set to be 1, h is the Rayleigh fading and can be generated with $'exprnd'$ function. The values of all the parameters used in the simulation can be found in Tab. 4.1. In the simulation, the actual throughput of the small cell can be obtained from (4.13), where $C_b + c_m$ is backhaul capacity of the small cell, and R_c is the UEs' capacity of the small cell. It is noted that Monte Carlo method is used in the simulation and the loop count is 2000 times.

Small Cell throughput Analysis and Validation

Fig. 4.6 and Fig. 4.7 depict the relationship of the throughput of all small cells (in a macrocell coverage) with given τ. It can be seen from the figures that numerical results from (4.26) excellently match the simulations. It's obvious that the throughput of small cells decreases rapidly when τ is quite large, that is because only a small amount of spectrum is left for the data links of small cells and can serve quite a few UEs. Furthermore, comparing both figures, it can be seen that the throughput of small cells increases with the rise of C_b.

Network Throughput Analysis

Fig. 4.8 illustrates the relationship of the whole network throughput with varying UE density when $C_b = 2 * 10^6$. It can be seen that FDD outperforms the IB-FD method with a lower UE density ($< 0.8 * 10^{-3}$). The reason is explained as follows: When UE density is low, the network throughput has a closer relationship with the sum of UEs' data rate. Considering that in IB-FD system, UEs' average data rate is lower than that in FDD system due to the cross-tier interference suffered, the FDD system will have a better performance with lower UE density.

Fig.4.9 compares the performance of IB-FD and FDD when $C_b = 6 * 10^6$. Similar to Fig. 4.8, it can be seen that FDD approach achieves a better performance with lower UE density. However, the throughput starts declining rapidly when the UE density is larger than $1.2 * 10^{-3}$, that is because due to the rise of the UE density, the macrocell needs to allocate more resource (large τ) to serve its UEs, on the contrary, only quite a small amount of the resource ($(1-\tau)$) is left for small cells to serve UEs, which results in a low throughput of small cells.

4.5 Summary

In this chapter, a strategy to utilise wireless backhaul which is able to maximise the network throughput is proposed. Using stochastic geometry based network model, the numerical analysis of the capacity of the target small cell and the throughput of the whole networks is proposed. The FDD and IB-FD schemes are comprehensively compared while using wireless backhauls. To draw a conclusion, when only a few small cells need to utilise the wireless backhaul of the macrocell, the FDD performs better than the IB-FD in terms of the small cell capacity. On the contrary, when the macrocell needs to communicate with a large number of small cells, especially when UE density is high, the IB-FD performs better than the FDD.

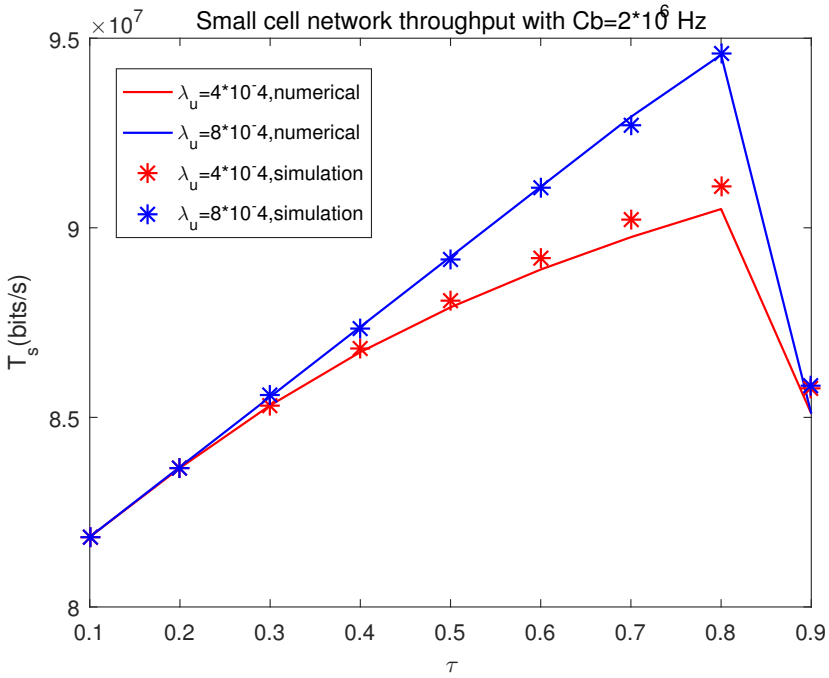

Fig. 4.6 Small cell network throughput with Cb=$2*10^6$ based on FDD

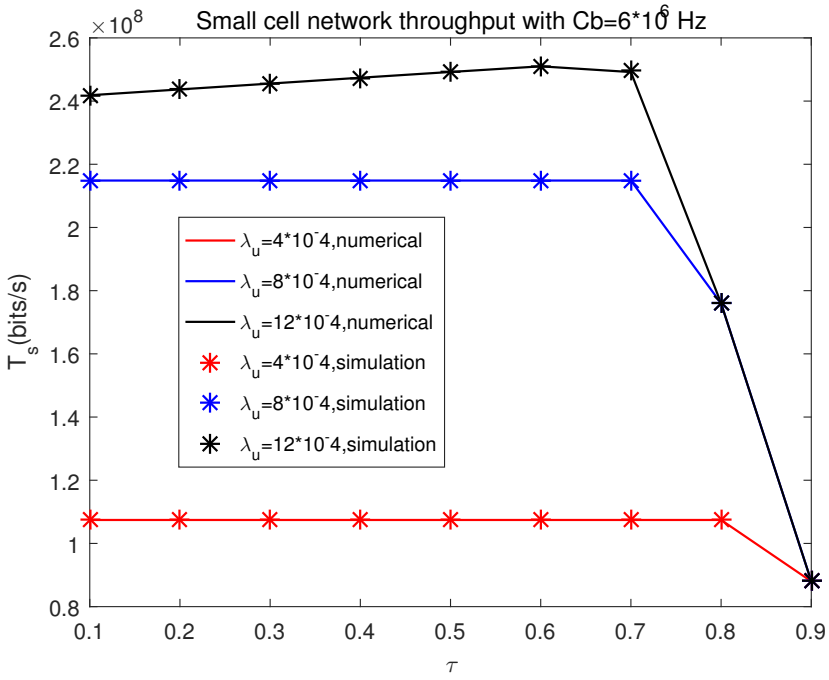

Fig. 4.7 Small cell network throughput with Cb=$6*10^6$ based on FDD

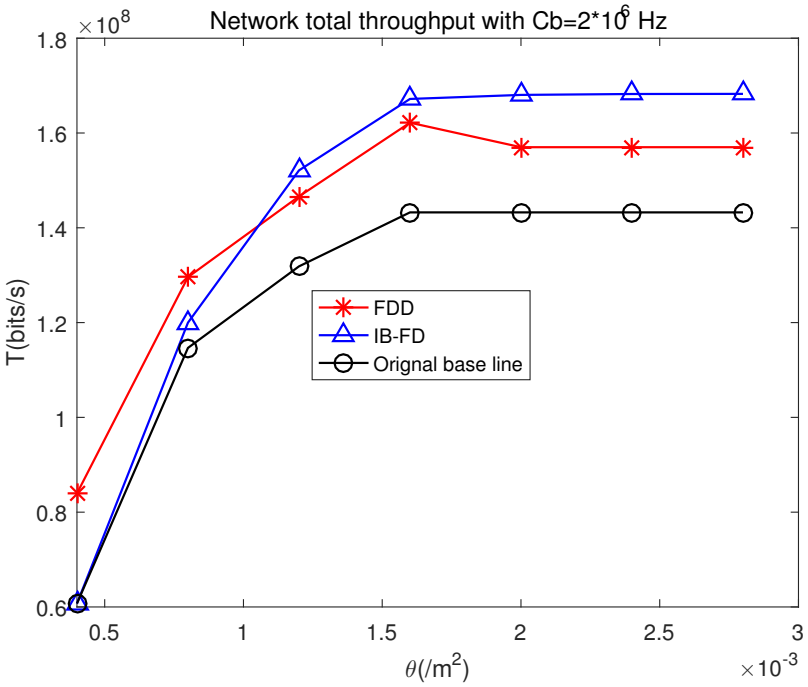

Fig. 4.8 Network throughput with Cb=$2 * 10^6$

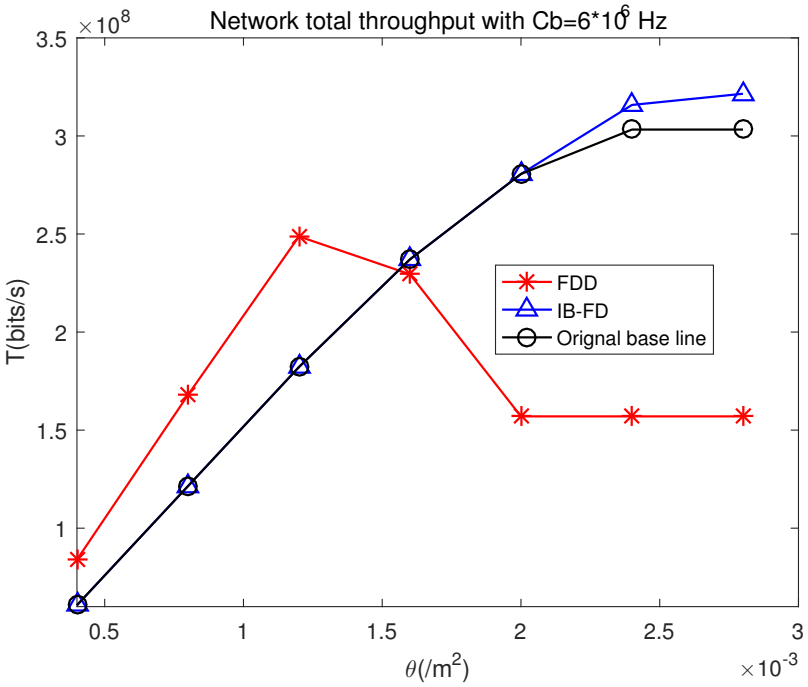

Fig. 4.9 Network throughput with Cb=$6 * 10^6$

Chapter 5

Mobility Management Analysis in HetNets and in LTE-LAA Networks

The handover process allows a UE to move freely through the network while maintaining QoS. Handover is a core element in planning and deploying mobile networks , as it ensures continuous and seamless connectivity to mobile UEs. In this section, the MM in ultra-dense small cell networks and outdoor LTE-LAA networks will be introduced.

5.1 Mobility Management in Small Cell Networks

Dense small cell deployment has been widely considered as a promising technique to cope with the forecasted 1000x increase in wireless capacity demands by 2030. Dense deployment of small cells will offload large amounts of traffic from macrocells to the small cells.

In this part, an analysis of the handover in dense small cell HetNets will be given. Handover process is one of the key factors, as it guarantees the continuous connectivity to mobile UEs. In conventional homogeneous macrocell networks, mobile UEs normally use the same set of handover parameters, and due to the large coverage area of macrocells, the parameters do not need to be adjusted frequently. However, in dense HetNets, using the same set of handover parameters for all small cells/UEs will degrade the handover performance. For instance, high mobility macrocell UEs may run deep into the small cell coverage area before TTT expires, which will probably result in handover failure due to the high interference from the small cells (low SINR). Moreover, due to the large number of small cells, the high-mobility UEs may suffer a large number of PPHOs when they quickly move across the small cells. In such a situation, the need for the self-optimisation of handover parameters is imposed. The definition of PPHO can be referred to Sect. 2.4.2.

SONs aim to raise the level of automated operation (including planning, configuration, management, optimisation and healing) in the next generation of networks. One of the application in this field is the optimisation of the handover process, which involves a trade-off between the PPHO and

the QoS of UEs, e.g., handover failure rate. My purpose is to optimise the handover parameters, e.g., PPHO in an efficient way based on the current network performance, meanwhile, the QoS of UEs need to be guaranteed. The challenge is to find optimal values for the handover parameters because reducing the PPHO will lead to the increase of the outage probability, and vice versa.

In the following parts, a detailed analysis of the proposed handover mechanism will be presented. Specifically, the signalling flows for handovers between the macrocell and the small cell will be introduced first, then, an analysis of the proposed optimisation algorithm will be provided. Finally, the comparison between the proposed strategy and the conventional one will be given.

5.1.1 Handover Call Flow in HetNets

The handover procedures can be divided into three phases: handover preparation phase (information gathering, handover decision), handover execution phase, and handover completion phase[148]. During the information collecting process, the UE gathers information about the handover candidates. In handover decision phase, the best candidate BS to switch is determined. Finally, the target cell informs the source cell of the successful completion of the handover and triggers the resource release of the source cell. The biggest challenge during the handover process is to select the best target small cell from the candidates. In HetNets, the size of the candidate cell list is negatively impacted by the dense deployment and the short coverage of small cells [149]. In the proposed mechanism, the assumption is made that the macrocells have the function of selecting the best candidate cell by considering UE's speed; open or close access of small cells and radio resource control, etc.

Fig. 5.1 depicts the basic handover scenario from the macrocell to the small cell. The handover from the macrocell to small cell is quite complicated as there are many possible candidate small cells. The UE needs to select the most appropriate target small cell.

5.1.2 The Proposed Optimisation Algorithm

In my work, the optimisation of PPHO rate with the guarantee of handover failure rate. PPHO is introduced in Sect. 2.4.2. The detailed explanation of PPHO and handover failure can be found in [150].

The contributions of the work are highlighted below. Firstly, the exponential weighted algorithm is used to average the optimisation objectives: PPHO and handover failure rate, so that the sudden fluctuation of the output PPHO can be avoid. Secondly, a new self-optimisation PPHO control programme for LTE networks is presented. By adjusting the TTT and HM, PPHO rate can be optimised and a balance between PPHO rate and handover failure rate can be finally obtained. Thirdly, the adjustment of HM and TTT is independent, for the reason that adjusting TTT and HM simultaneously can easily cause fluctuations of the system.

The PPHO rate use exponential weighted history in case of sudden fluctuations, which can be

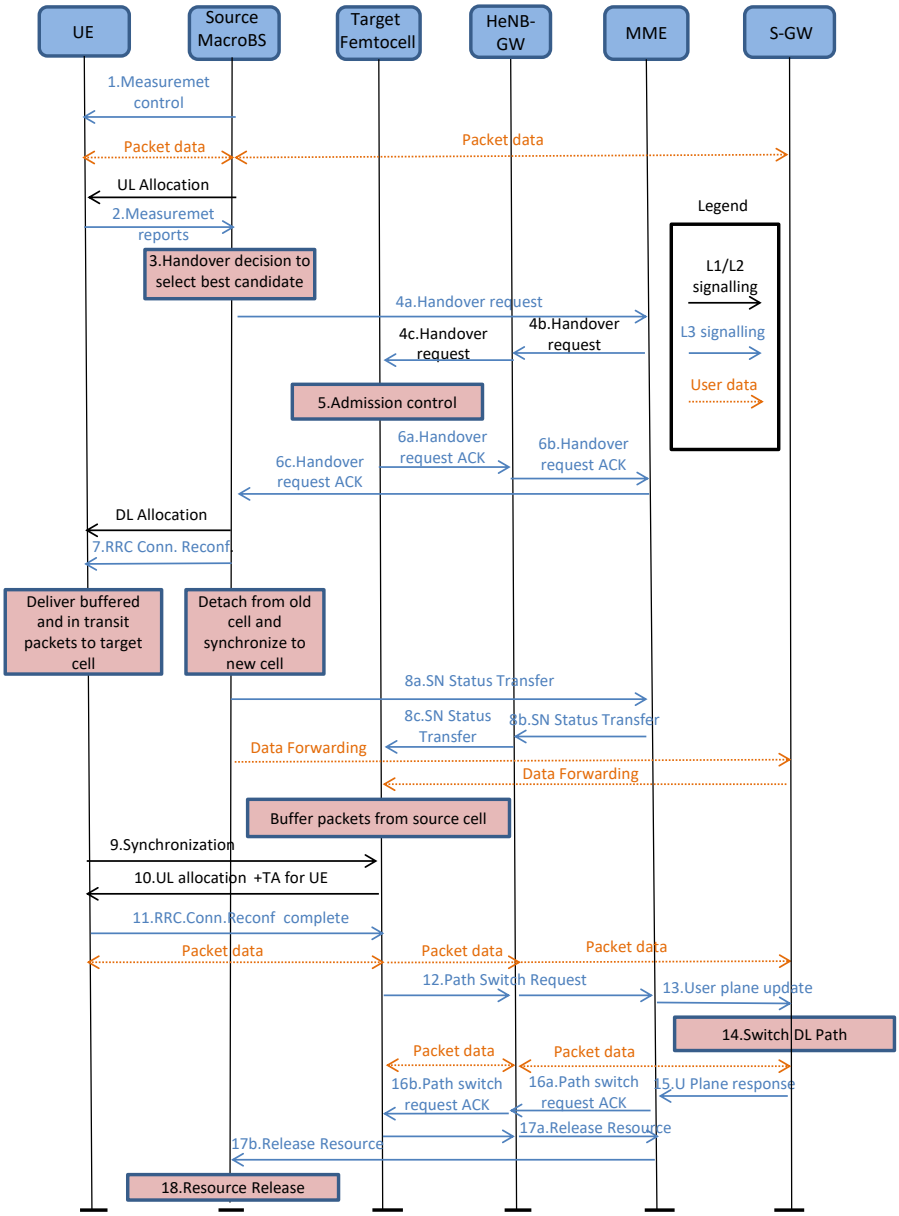

Fig. 5.1 Handover from macro BS to femtocell

seen in (5.1).

$$PPHO_w = \alpha_w(PPHO_n + (1-\alpha_w)PPHO_{n-1} + (1-\alpha_w)^2 PPHO_{n-2} + (1-\alpha_w)^3 PPHO_{n-3}) \quad (5.1)$$

$PPHO_n$ is the current PPHO rate , and $PPHO_{n-1}, PPHO_{n-2}, PPHO_{n-3}$ are the past PPHO rates. It can be seen that, with larger n applied, more past PPHO performance is considered. Here, n is set to be 4, which means four values (three past values included) are weighted and averaged. In

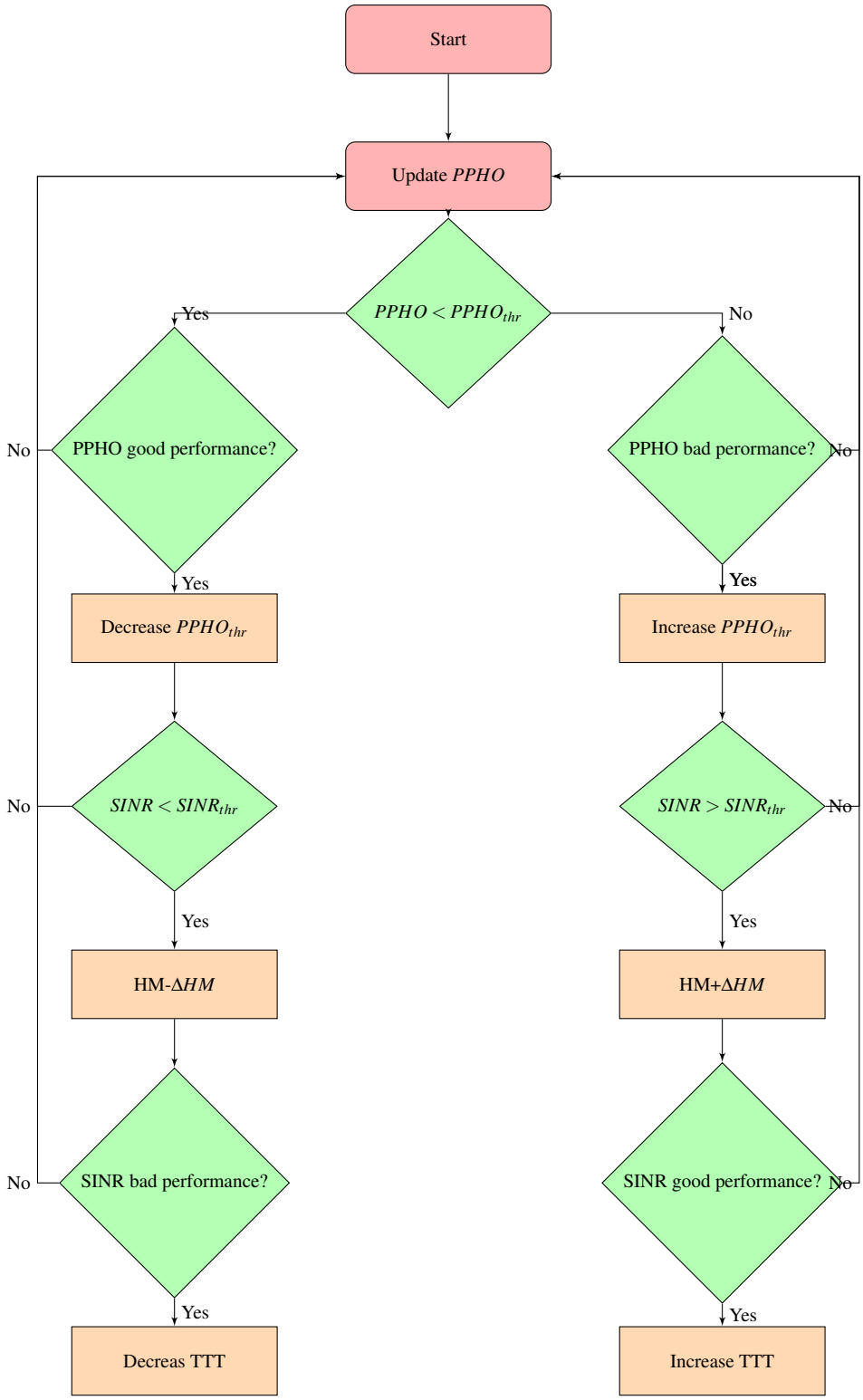

Fig. 5.2 Ping-Pong handover optimisation flowchart

addition, the parameter α is the weighting coefficient of current and past PPHO rates. The range of α_w is $0 \leq \alpha_w \leq 1$. Here it's set to be 0.5.

Fig.5.2 describes the optimisation procedure: whether the procedure will go into the PPHO bad performance or good performance region is decided by the difference of the current PPHO and the PPHO threshold. After that, if the procedure comes into the bad performance or good performance region, the PPHO threshold will increase ($PPHP_{thr} + 0.01$) or decrease ($PPHO_{thr} - 0.01$) correspondingly. Here, it is assumed that if the conditions ($PPHO_i < PPHO_{i-1}$, $PPHO_i < PPHO_{i-2}$, $PPHO_i < PPHO_{i-3}$ and $PPHO_i < PPHO_{i-4}$) are all satisfied, it means that the system comes into the PPHO good performance area. On the contrary, if the conditions ($PPHO_i > PPHO_{i-1}$, $PPHO_i > PPHO_{i-2}$, $PPHO_i > PPHO_{i-3}$ and $PPHO_i > PPHO_{i-4}$) are all satisfied, it means that the system comes into the PPHO bad performance region.

Then, the HM will increase or decrease according to the comparison of the SINR and SINR threshold. Similarly, when the conditions ($SINR_i < SINR_{i-1}$, $SINR_i < SINR_{i-2}$, $SINR_i < SINR_{i-3}$ and $SINR_i < SINR_{i-4}$) are all satisfied, the system comes into the SINR bad performance region. When the conditions ($SINR_i > SINR_{i-1}$, $SINR_i > SINR_{i-2}$, $SINR_i > SINR_{i-3}$ and $SINR_i > SINR_{i-4}$) are all satisfied, it means that the system comes into the SINR good performance region.

Finally, the system will decide how to adjust TTT based on whether the system is in SINR good or bad performance region.

The main advantage of the self optimisation procedure above is that it avoids adjusting the TTT and HM simultaneously at each transmission time interval (TTI), which makes the system more stable. Furthermore, it's not sensitive to the initial pairing of TTT and HM.

5.1.3 System Simulation and Results

In the simulation, the proposed method is compared with the conventional one [33]. The conventional approach can be explained as: The optimisation target HPI is the combination of handover failure failure, PPHO, dropped calls performance. First, the HPI performance is compared with the threshold, whether the system will increase good performance time depends on the comparing result. Then, if the system is in bad performance region, the handover operating point will be changed. If the system is in good performance, the HPI threshold will decrease.

Simulation Set-up

In this part, a Matlab based simulation is presented. Tab. 5.1 summarizes the configuration used in the simulation. The pathloss of macrocells is defined as: $128.1 + 37.6 * log_{10}(d)$ and the pathloss of small cells is defined as:$140.7 + 36.7 * log_{10}(d)$. A hexagon layout with 3 eNBs and 9 sectors with an ISD distance of 300m is considered. There are 18 small cells deployed in 3 clusters within each sector area. 50 mobile UEs are initially randomly distributed in a circle area around the macrocell with radius 100m and then do Brownian motion with a given speed [151]. It's noted that when a UE

Simulation Parameter	Value
Simulation time [s]	100
TTI [s]	0.05
Initial TTT [TTI]	4
Initial HM	3 (5m/s), 4(10m/s)
Δ_{HM}	0.5
$\Delta_{TTT}[5TTI]$	5
SINR threshold 1 [dB]	-4
SINR threshold 2 [dB]	0
UE Thermal Noise Figure (σ^2) [dBm/Hz]	-174
UE walking model	Brownian motion
UE walking speed [m/s]	5,10
Femtocell TX power [dBm]	20
α_w	0.5
Q_{out} [dB]	-7
ISD [m]	300
Frequency [G Hz]	2.6
Number of femtocells	54
Number of UEs	50

Table 5.1 System parameters of Sect 5.1

hits the boundary of the simulation area, it will turn back and move towards a new randomly selected direction. The simulation time is 75s and the operation point for the HM is 3dB (5m/s), 4dB (10m/s), the initial time to trigger (TTT) is set to be 200ms. Moreover, it's worth noting that when the UE's speed exceeds 10m/s, it will be connected to the macrocell. The algorithm of the proposed method can be found in Fig. 5.2 and the pseudocode is presented in Algorithm 1. Monte Carlo method is used in the simulation and the loop account is 300 times. The values of all the parameters used in the simulation can be found in Tab. 5.1.

Results Analysis

Figure 5.3 below describes the motion trail of UEs and the distribution of the small cells. The green points represent small cells in cluster distribution. The blue points describe the users' moving trajectory.

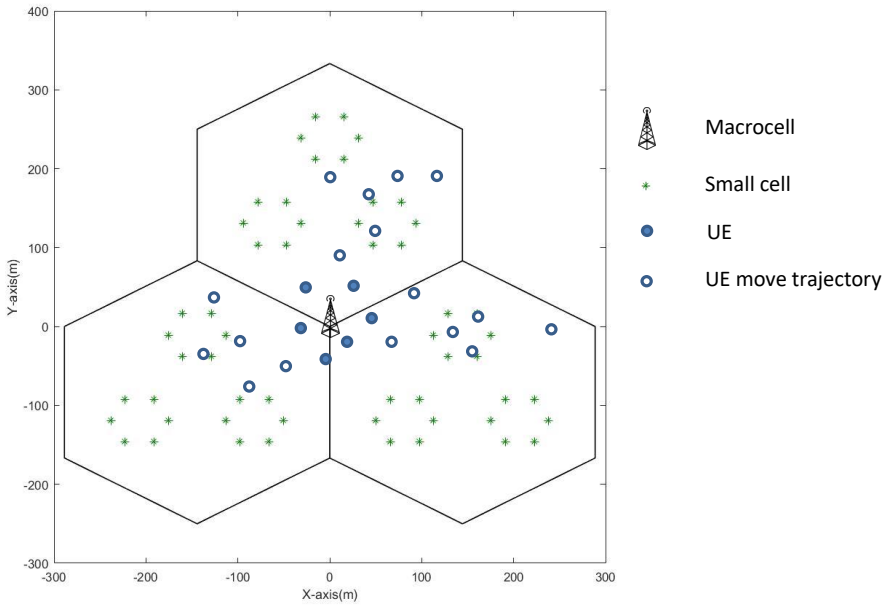

Fig. 5.3 Femtocell distribution and Users move trajectory

Fig. 5.4 evaluates the PPHO probability performance of the proposed method, conventional method and the approach without optimisation(HM=3, TTT=200ms) with UE speed 5m/s. It is noticed that the proposed method outperforms the conventional approach [33] in most of the time.

Algorithm 1 Handover optimisation algorithm pseudocode in small cell networks

Require: PPHO rate, Handover failure rate, $PPHO_{thr}$, $SINR_{thr}$, Δ_{HM}, TTT, HM
Ensure: Optimised PPHO ratio, Optimised handover failure rate

```
Update PPHO
if PPHO < PPHO_thr then
    if PPHO good performance then
        Decrease PPHO_thr
    else
        return Update PPHO
    end if
    if SINR < SINR_thr then
        HM − Δ_HM
        if SINR bad performance then
            Decrease TTT
        else
            return Update PPHO
        end if
    else
        return Update PPHO
    end if
end if
if PPHO > PPHO_thr then
    if PPHO bad performance then
        Increase PPHO_thr
    else
        return Update PPHO
    end if
    if SINR > SINR_thr then
        HM + Δ_HM
        if SINR good performance then
            Increase TTT
        else
            return Update PPHO
        end if
    else
        return Update PPHO
    end if
end if
```

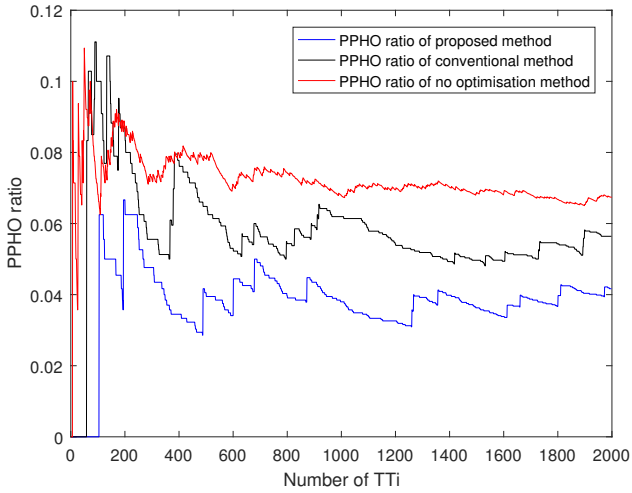

Fig. 5.4 Ping-Pong handover performance with v=5m/s

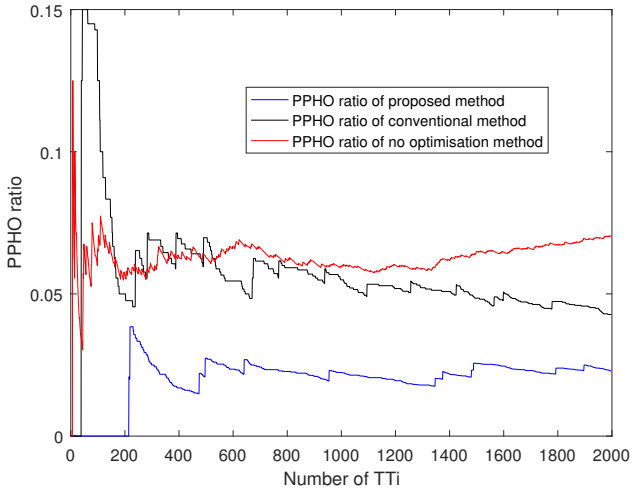

Fig. 5.5 Ping-Pong handover performance with v=10m/s

More specifically, the PPHO probability declines about 20% and 50% receptively compared with conventional and no optimisation methods.

Fig.5.5 compares the PPHO probability performance of the proposed method, conventional method and approach without optimisation (HM=4, TTT=200ms) with UE speed 10m/s. It can be seen that the proposed method has a much better performance compared with the conventional one. To be more specific, the PPHO probability declines around 35% and more than 50% respectively compared with conventional and no optimisation methods.

Fig. 5.6 depicts the handover failure rate of the proposed method, conventional method and the

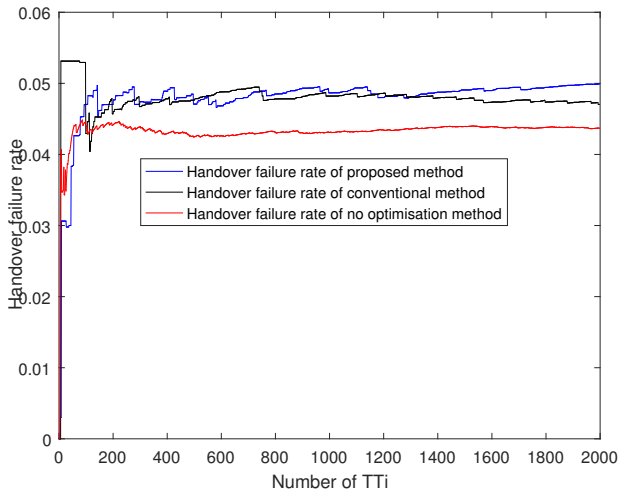

Fig. 5.6 Handover failure rate performance with v=5m/s

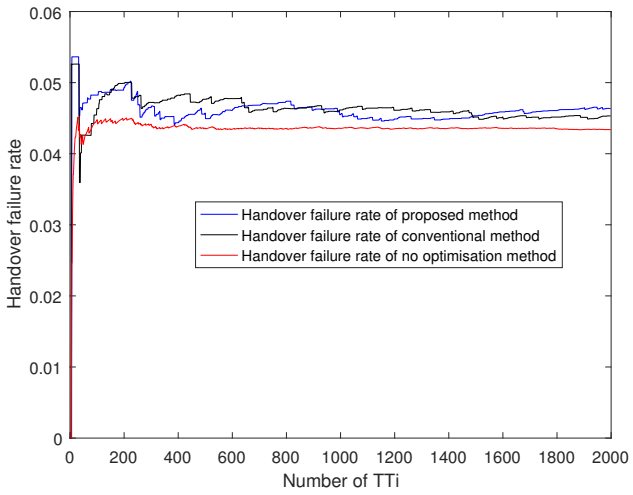

Fig. 5.7 Handover failure rate performance with v=10m/s

approach without optimisation (HM=3, TTT=200ms) with UE speed 5m/s. Here, it can be seen that the handover failure rate of the proposed method increases to around 5% from 4.8% of the conventional method.

Fig.5.7 illustrates the comparison of handover failure rate of the the proposed method, conventional method and the approach without optimisation (HM=3, TTT=200ms) with UE speed 10m/s. It is noted that the handover failure rate increases to around 4.6% from 4.5% of the conventional method.

5.2 Handover Mechanism and Performance Evaluation for LTE-LAA systems

5.2.1 Introduction

As the use of mobile devices has grown rapidly over the past few years, the wireless data demand has increased exponentially. Due to the extremely high price of licensed spectrum, License Assisted Access (LAA) has been proposed to provide high capacity by extending LTE transmissions to the unlicensed spectrum that Wi-Fi systems operate. Due to the coexistence with Wi-Fi systems, mobility management has become a critical problem in LTE-LAA networks. Compared with handover in conventional LTE networks that would only be triggered by user mobility in licensed bands, in LTE-LAA networks, handover can also be triggered due to the availability of unlicensed band in the serving cell. In this section, a new handover scheme is proposed and analysed in details for LTE-LAA networks, including handover triggering and handover procedure, then the simulation is presented to evaluate the performance of the proposed handover scheme by considering the availability of the unlicensed spectrum. The detailed explanation of the simulation is presented in Sect. 5.2.5. The simulation results show that by introducing the proposed handover mechanism, the unlicensed spectrum handover ratio, which can be defined as times of handover to unlicensed spectrum over total handover times, has a significant improvement, meaning that a more efficient utilisation of unlicensed spectrum can be achieved, while the handover failure rate will relatively increase. Thus, a parameter denoted as "availability threshold" is introduced to control the handover failure rate.

5.2.2 LTE-LAA Networks Model

In LTE-LAA systems, the aggregation of licensed and unlicensed spectrum can provide small cell UEs with high speed and seamless broadband multimedia services. In the transmission of LTE-LAA system, a user can access to the primary component carrier (PCC) in license band and several secondary component carrier (SCC) in unlicensed band simultaneously. As mentioned in Sect. 2.5, the control signal is always transmitted on PCC in licensed band for security and safety, and the data signal can be transmitted either on PCC in licensed bands or on SCC in unlicensed bands. Meanwhile, in this section, the concept of splitting control of control plane (C-plane) and user plane (U-plane) is applied here to reduce the delay in handover procedure, specifically, C-plane is provided by macrocell in a low frequency licensed spectrum to maintain a good connectivity and mobility, meanwhile the U-plane is provided by small cells in a high frequency licensed band or unlicensed bands to boost user capacity. Users can access to PCCs of licensed spectrum and SCCs of unlicensed spectrum simultaneously. It's also noted that the small cells are called Phantom Cells [39] which are only intended to carry user traffic. The Radio Resource Control (RRC) connection procedures between the UE and a Phantom Cell are managed by the macrocell.

In LTE-LAA system, many recent researches like[153] have demonstrated that if LTE-LAA

systems directly inherits MAC protocol of LTE without any coexistence measures, the Wi-Fi systems will be severely and continuously interfered and the back off will be frozen. To allow coexistence with Wi-Fi systems and UEs friendly, a load based LBT system is needed in the proposed handover mechanism. The detailed explanation of LBT technique is presented in Sect. 2.5.2 .

5.2.3 Handover Mechanism for LTE-LAA

As mentioned above, the proposed handover scheme consists of mobility triggered handover and availability triggered handover based on the trigger event. Furthermore, LBT technology is also used in the handover mechanism to guarantee the QoS of UEs.

Handover Procedure

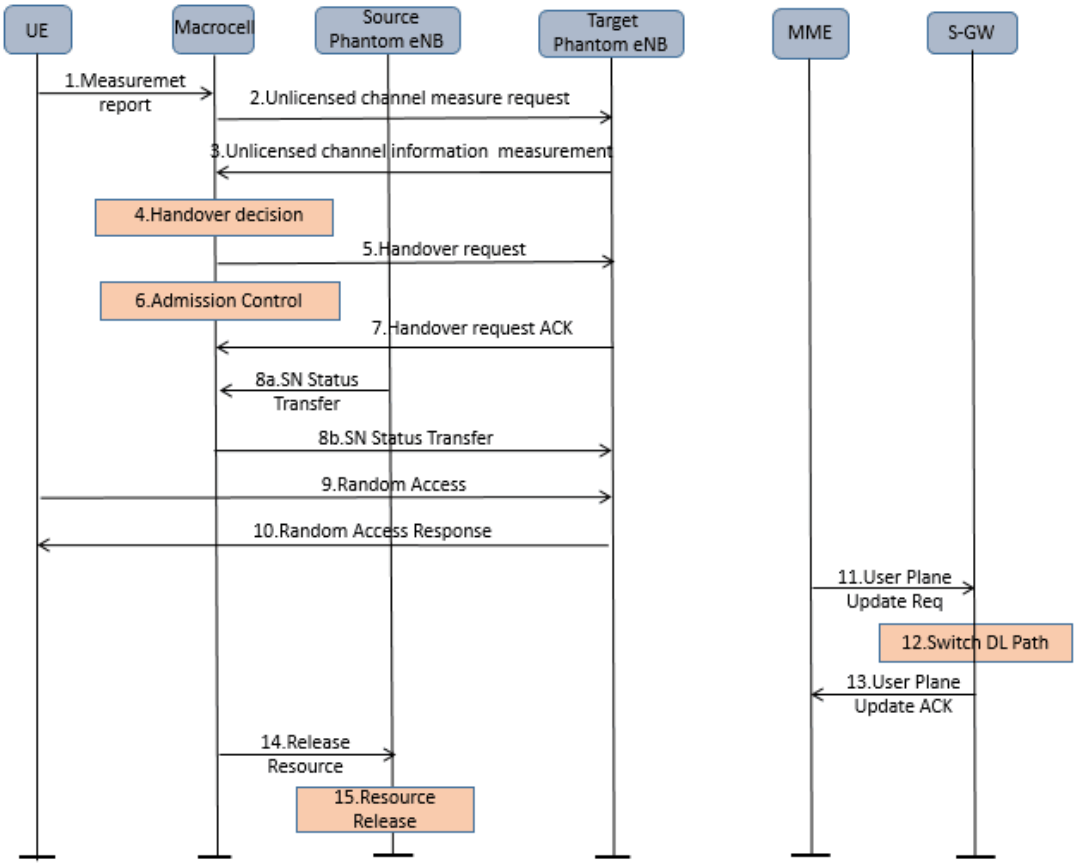

Fig. 5.8 LTE-LAA small cell networks handover procedure

The handover procedure in LAA systems is introduced in Fig. 5.8. It's noted that in the handover preparation phase, UEs send (1) measurement reports to the macrocell periodically, the candidate small cells list will be generated according to the measurement reports received by the macrocell.

Then, LBT technology is processed in (2) and (3) to sense the availability of the unlicensed channels. After receiving the unlicensed channel measurement request from the macrocell(2), the candidate small cells will send the unlicensed channel state information to the macrocell (3). The macrocell will select the target cell with its handover decision algorithm (4), then send the handover request (5) to the target cell. After receiving the handover request, the macrocell prepared for the required resource for the admission control (6) and the target small cell send the handover request acknowledgement (ACK) (7) back to the macrocell. Then, the sequence number (SN) (8) will be transferred to the target small cell to prevent the data packet being lost during the handover. The synchronisation procedures to target small cells are performed in (9)-(10). At last, the handover completion phase is processed between (11) to (13). Mobility management entity (MME) is informed that the UE has changed and serving-gateway (S-GW) switches user plane. At the final step (14-15), the source small cell is noticed to release the resource by the macrocell.

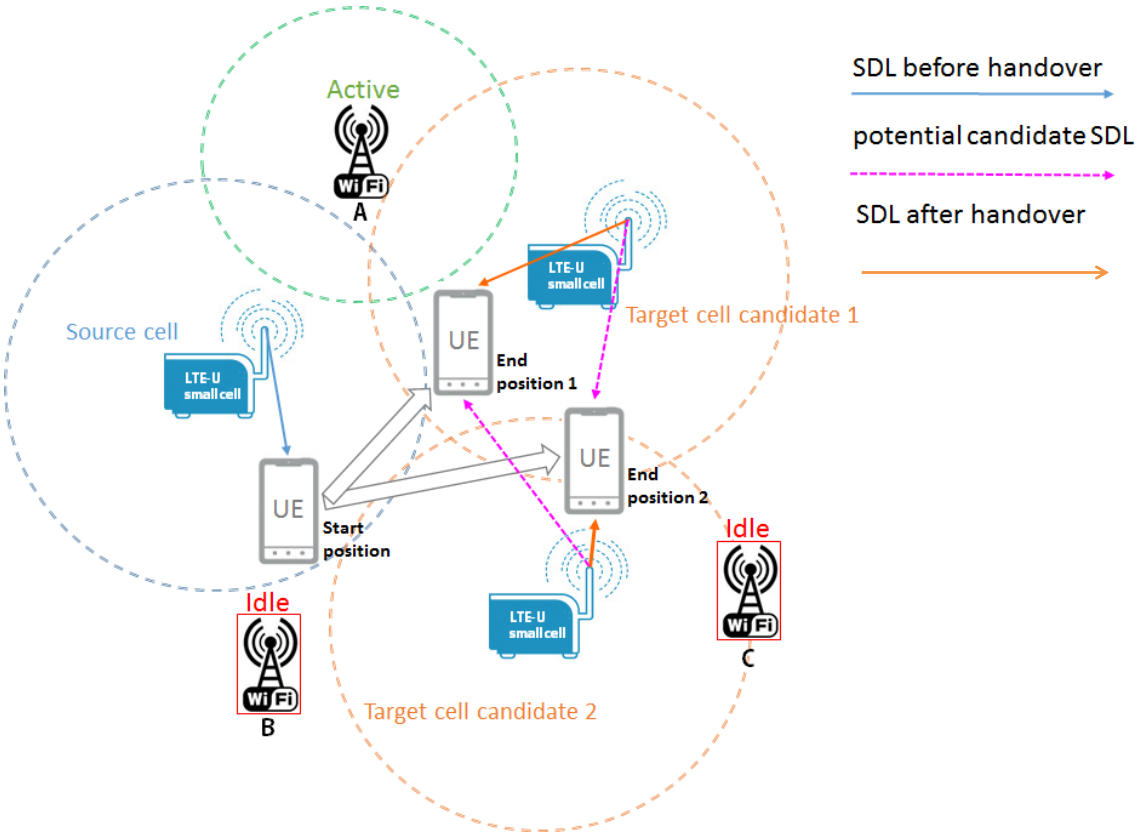

Fig. 5.9 LAA Mobility-triggered SDL handover scenario.

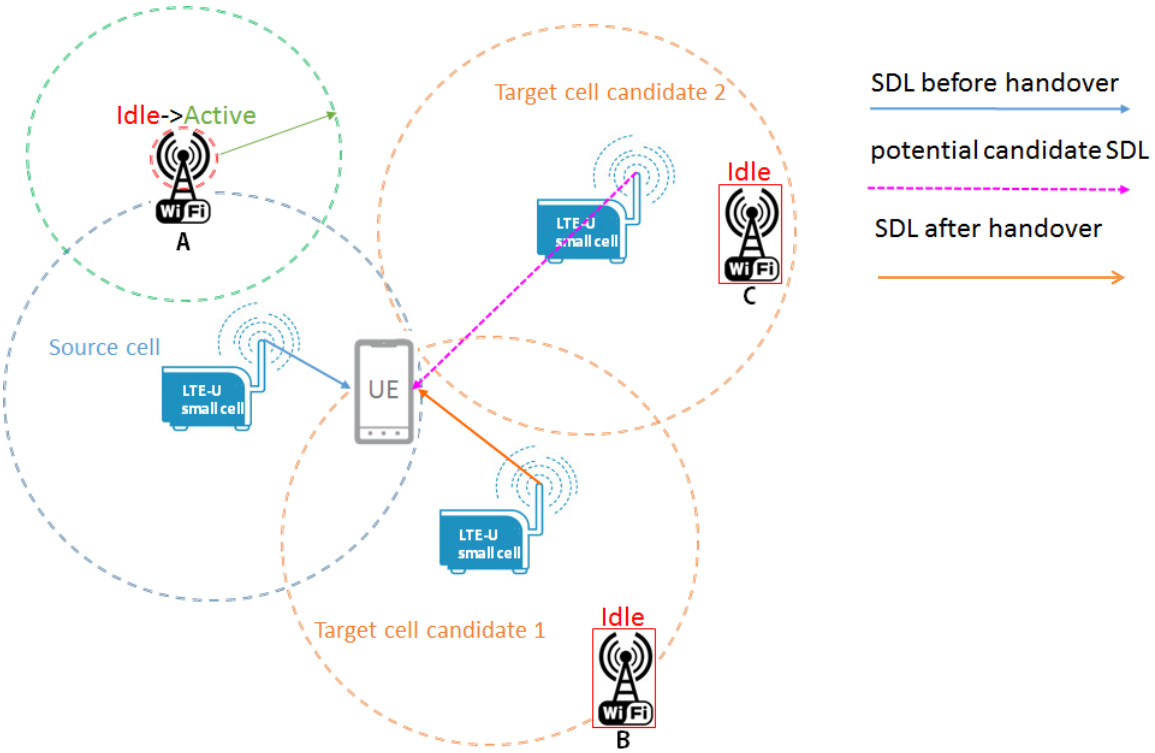

Fig. 5.10 LAA Availability-triggered SDL handover scenario.

Mobility Triggered Handover

In this section, an analysis of trigger event and channel selection will be provided. Just like handover in conventional networks, this type of handover is triggered due to the UE moving from the coverage of one cell to that of another cell. The similarity is that the handover is triggered by the change of received signal quality reported in UE measurement report. And the difference is that, in conventional LTE networks, the target BS is the cell that provides the best signal quality, while for LAA networks, the selection of the target cell should consider the availability of the unlicensed spectrum. Fig.5.9 illustrates the mobility triggered handover scenario in LAA networks.

- The UE measurement reports about target cell candidate 1 and target cell candidate 2 are sent to the source serving cell.
- When the UE moves to the end position 1, the downlink received signal quality from target cell candidate 1 is significantly better than that from target cell candidate 2. In this case, even though the target cell candidate 1 does not have access to the unlicensed bands at that time because of a nearby actively transmitting Wi-Fi AP, the UE will still handover to it as the poor

signal quality provided by target cell candidate 2 may very likely lead to the transmission failure.

- When the UE moves to the end position 2 which is in coverage overlap area of both target cell candidates, the downlink received signal qualities from both cells are good enough. In this case, the UE will handover to target cell candidate 2 due to lack of surrounding active Wi-Fi AP occupying the unlicensed bands.

It's noted that when mobility handover is needed, the unlicensed bands in target candidates are priority searched for handover with LBT technology. Only when no unlicensed bands are available in the selected target candidates, in case of signal outage, the UE (both its UL and DL) will be associated to licensed bands of the cell that provides the best signal quality.

Availability Triggered Handover

Due to the coexistence of Wi-Fi APs and LTE system, the availability triggered handover is necessary in LAA system to avoid the QoS degradation of UEs' experience. The availability-triggered handover scenario is illustrated in fig. 5.10.

- The UE will try to leave the source cell when the nearby Wi-Fi AP A starts to transmit so that the unlicensed band previously occupied by the source cell becomes unavailable, even that the UE is still in the coverage of the source cell.

- The UE selects target cell candidate 1 because it provides the best signal quality. It's noted that when there are more than one target cell candidates that have sufficient and available unlicensed spectrum resources, the one which provides the best signal quality will be selected as the target cell.

To summarize, in this system, When the unlicensed band of the serving cell becomes unavailable, the UE will start to select the target cell with sufficient unlicensed spectrum from its candidates. The type of handover is call 'availability triggered handover' in this work.

It's worth noting that the availability-triggered handover can only take place when there are other nearby target cell candidates whose unlicensed bands are not occupied by Wi-Fi APs. Moreover, For availability triggered handover, the PCC can still remain in the source cell and SCC will be moved to the target cell for SDL transmission.

5.2.4 Performance Evaluation

The handover failure rate as well as handover times to unlicensed bands which reflects unlicensed spectrum utilisation are evaluated with variable Wi-Fi APs density in the proposed and conventional handover schemes (without availability triggered handover introduced).

5.2.5 Simulation Setup and Parameters

In the previous section, the handover procedure scheme is provided for LAA network. In this section, the handover performance will be analysed by simulation. It is assumed that all UEs have Brownian motion with the speed 5m/s in a simulation time of 100s. The layout of the scenario is configured of a macrocell with radius 300 m and there are 30 small cells and 40 UEs which are uniformly distributed in each macrocell coverage area. It's noted that I only consider the handover occurred between small cells due to the reason that the SCC in unlicensed spectrum can only be provided by small cells. The parameters of the simulation are summarized in Tab. 5.2, among which the definition of parameters 'CW_{min}' and 'CW_{max}' can be referred to[154], and parameters 'Q_{out}' is set according to [155].

It's noted that in the proposed handover scheme, to avoid the QoS degrading of the UEs, the assume is made that if the UE is in the outage state continuously for a certain time which is defined as delay threshold here, and no other small cells with available unlicensed spectrum can be associated, it will make handover attempt to the licensed band of the target small cell with the strongest signal. Furthermore, I introduce the parameter' availability threshold' which is defined as the minimum time interval between two consecutive availability handover to control the times of availability handover.

The pseudocode of the proposed handover algorithm is presented in Algorithm 2, where S_s is the serving small cell, $S_{i,i=1\sim n}$ is the group of other small cells, M_s is signal of the serving small cell, $M_{i,i=1\sim n}$ is the group of received signal of other small cells, U is the group of target small cells' indices, t_u is the time that the UE stays within the unlicensed band. N is the number of handovers, and N_u is the number of handovers to unlicensed band.

Analysis of Handover Performance

In this part, the performance of the proposed handover strategy will be evaluated from the following three aspects: (1) Unlicensed band handover ratio. The unlicensed band handover is defined as the number of handovers to unlicensed band over the total number of handovers. (2) The number of availability triggered handovers. (3) Handover failure rate. The unlicensed band handover ratio and the number of availability triggered handovers are selected as the outputs because they are important matrix to evaluate the improvement of UEs' data rate.

Fig. 5.11 illustrates the handover performance for conventional and the proposed handover schemes. It can be seen from the upper one of Fig. 5.11 that the number of handovers to unlicensed bands of the proposed scheme (availability threshold is set to be 5 here) is significantly higher than that of conventional scheme due to the introducing of availability triggered handover. Moreover, it 's noted that the number of handovers to licensed bands of the proposed scheme is also lower compared with the conventional scheme.

The lower one of Fig.5.11 presents a comparison of ratio of handover to unlicensed bands. Firstly, it's apparent that the unlicensed band handover ratio keeps declining with the increase of Wi-Fi AP density, which means that the unlicensed spectrum utilisation is influenced with Wi-Fi AP density strongly. Secondly, it's easy to see that the proposed handover scheme performs better than

Table 5.2 System parameters of Sect 5.2

Parameter	Value
Macrocell radius [m]	300
Total number of small cells	30
Total number of UEs	40
Pathloss Exponent (WiFi, small cell)	2, 3.67
Tx.power of small cell [dBm]	23
Tx.power of WiFi[dBm]	23
Center frequency of LTE [Hz]	2.6 G
Center frequency of WIFI [Hz]	5 G
Simulation time [s]	100
Delay threshold [ms]	10
Availability threshold [ms]	1,5,9
HM [dB]	2
Q_{out} [dB]	-8
WiFi slot time [s]	9
$T_{attempt}$ [ms]	1
T_{cellTx} [ms]	5
$T_{sensing}$	2 WiFi slot time
CWMin/CWMax	15/255

Algorithm 2 LTE-LAA handover optimisation algorithm pseudocode

Require: S_s, $S_{i,i=1\sim n}$, M_s, $M_{i,i=1\sim n}$, U, HM, t_u
Ensure: N_u, N
Update S_s, M_s, S_i, M_i
for i= 1:n **do**,
  if $M_i > M_s + HM$ & S_i has available unlicensed band **then**
    Add i to U
  end if
end for
if $U \neq \emptyset$ **then**
  $i^* = \arg\max_U(M_i)$
  Handover from S_s to S_{i^*}
  $N_u = N_u + 1$
  N=N+1;
  Update S_s, M_s, S_i, M_i
else
  $i^* = \arg\max(M_i)$
  Handover from S_s to S_{i^*}
  N=N+1;
  Update S_s, M_s, S_i, M_i
end if
if unlicensed band of S_s becomes unavailable & t_u>availability threshold **then**
  $i^* = argmax(M_{si})$
  Handover from S_s to S_{i^*}
  $N_u = N_u + 1$
  N=N+1;
  $t_u = 0$;
  Update S_s, M_s, S_i, M_i , t_u
end if

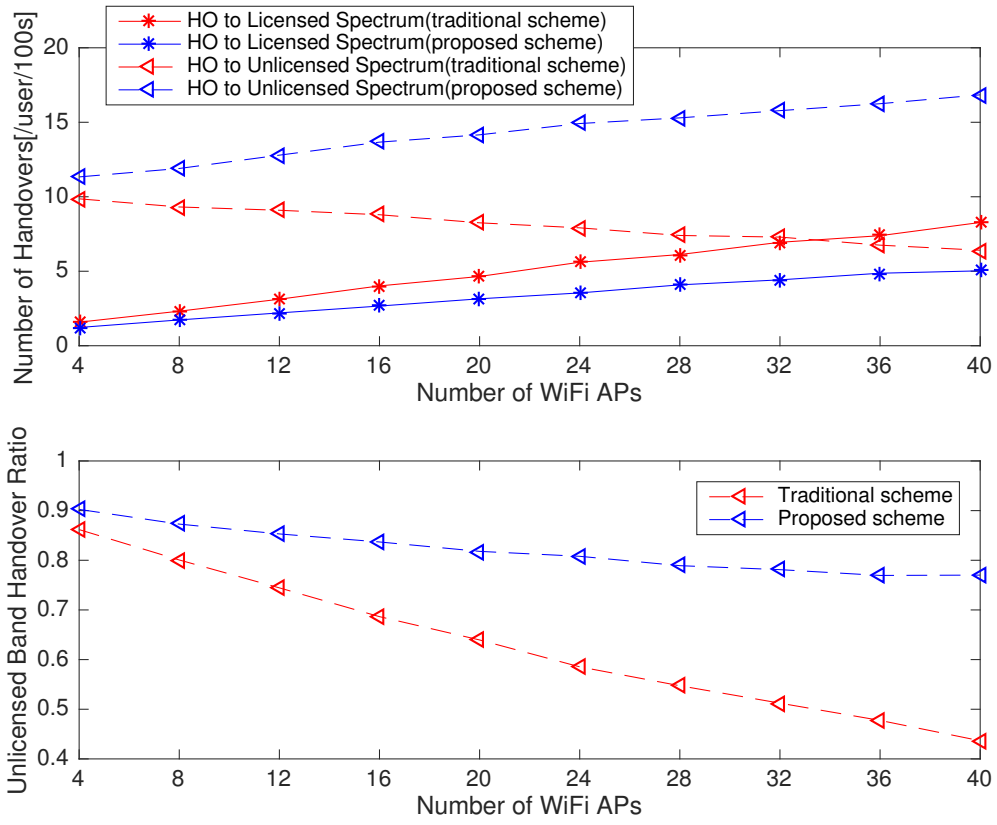

Fig. 5.11 Comparison of handover performance with the proposed and conventional handover scheme.

that of the conventional scheme, especially when the Wi-Fi AP density is high. Specifically, compared with the conventional scheme, the proposed handover scheme has a significant improvement of unlicensed spectrum handover ratio from about 0.05 to 0.35 when Wi-Fi AP number grows from 4 to 40.

From Fig. 5.11, it can be seen that the unlicensed handover ratio can be improved by introducing availability triggered handover. However, redundant handovers will cost large amount of overhead signalling and lead to a low energy efficiency, hence, in the proposed scheme, the number of availability handover can be controlled by adjusting the threshold. Here, the threshold is defined as the period that the serving unlicensed band is occupied by a Wi-Fi AP.

Fig. 5.12 compares the number of availability handover with different availability threshold. It's obviously that availability handover rate decreases with the increase of the availability threshold. The number of availability handover will almost have a 100% increase when Wi-Fi AP density doubles. Moreover, it also can be seen that the availability triggered handover rate grows with the increase of availability threshold.

Fig. 5.13 compares the handover failure rate of the conventional handover scheme and that of

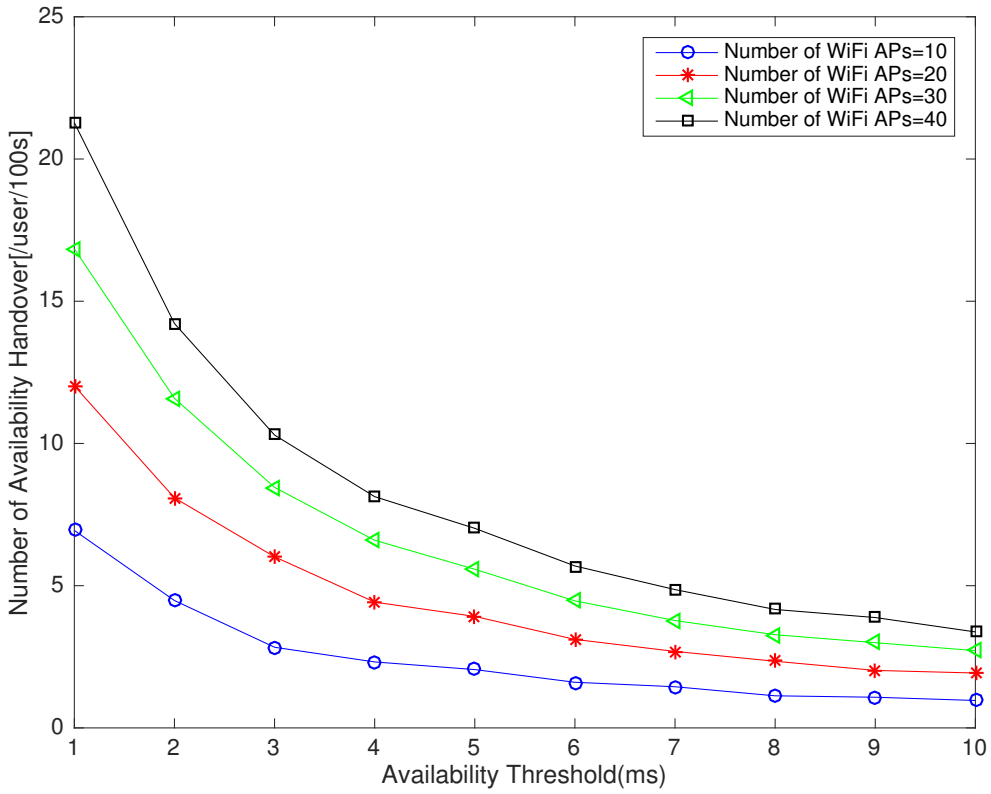

Fig. 5.12 Number of availability handover with different availability threshold.

the proposed scheme with different availability threshold. Firstly, it is noticeable that the handover failure rate will increase with the Wi-Fi AP density. The black curve that represents conventional handover scheme shows that the handover failure rate increases almost 40% when the number of Wi-Fi APs grows from 4 to 40. The reason is that the number of small cells with available unlicensed channel declines with the increase of Wi-Fi APs density, hence the UEs will have fewer opportunities to access the unlicensed bands and will keep waiting until connected to the available unlicensed channel or licensed channel. During this time, UEs will probably experience the signal quality degradation and lead to handover failure. Secondly, it's noted that handover failure rate goes higher for the proposed handover scheme with availability triggered handover, it can be seen that when the number of Wi-Fi APs is 40, the handover failure rate is about 0.2 for conventional handover scheme and 0.4 for the proposed handover scheme with availability threshold equalling 1. The reason is that users will try to associate to small cells with available unlicensed channel but lower signal quality, which will lead to a relatively high handover failure rate. Availability threshold is introduced in this section to achieve the balance between the enhancement of UEs capacity and handover failure rate.

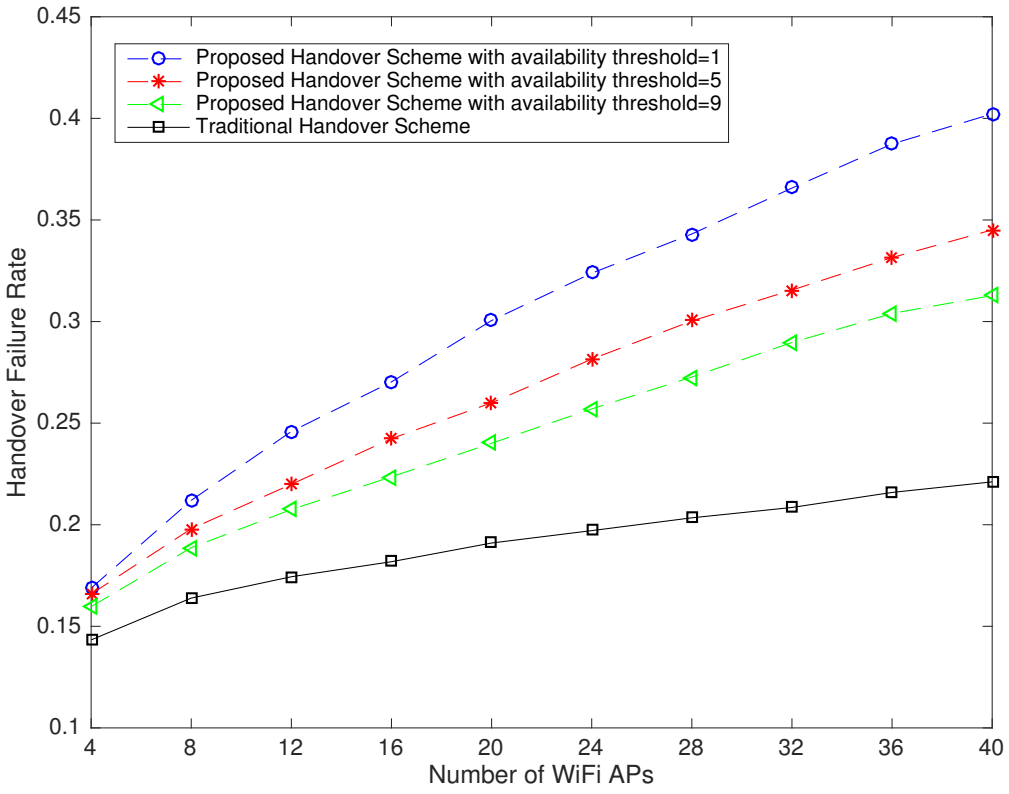

Fig. 5.13 Comparison of handover failure rate with the proposed and conventional handover scheme.

5.2.6 Summary

In Sect. 5.1, a self optimisation handover scheme is proposed to change the network performance by adjusting the values of HM and TTT in an automatic way. The results show that the proposed handover scheme outperforms the conventional one significantly in terms of PPHO ratio, meanwhile, the handover failure rate are controlled in an acceptable range.

In Sect. 5.2, I designed a handover scheme for LTE-LAA networks. Comparing with handover in traditional LTE networks, the proposed handover scheme combines mobility triggered handover and availability triggered handover together to enhance UEs' throughput. A detailed analysis of trigger event, channel selection and handover procedure is also presented for the proposed handover scheme. The results show that, for the proposed handover scheme with availability handover introduced, the utilisation of unlicensed spectrum will have a significant increase, meanwhile, the parameter 'availability threshold' is designed to control the handover failure rate of UEs.

Chapter 6

Conclusion and Future Work

6.1 Conclusion

To summarize, the work in this thesis can be classified in three groups. In Chapter 3, an energy saving small cell sleeping mechanism is proposed. With CRE technique introduced, the proposed algorithm achieves a significant improvement compared with conventional methods. IB-FD and FDD based small cell wireless backhaul strategies are analysed in Chapter 4 to enhance the small cells' capacity. The results show that IB-FD is more effective to improve the throughput of the whole network. The MM in HetNets and LTE-LAA networks is provided in Chapter 5. I develop a self optimisation mechanism to optimise the PPHO parameters while guaranteeing the handover failure rate of UEs. For mobility management in LTE-LAA networks, I provide a detailed analysis of handover trigger events, channel selection, and handover procedure. In addition, the results demonstrate that the proposed handover mechanism can enhance the throughput of UEs significantly.

In Chapter 3, an energy saving small cell sleeping strategy in HetNets is proposed. Compared with conventional methods that the small cell is switched off when it needs to save energy and all its traffic is handed over to the macrocell, I use the small cell to cover sleeping cells, which are far away from the macrocell to achieve more energy saving. It's worth noting that the eICIC technique is applied to ensure UEs' QoS requirement. The proposed mechanism is verified under both hexagon and stochastic geometry based system models. In hexagonal based networks, I provide several optimal BS sleeping point based on the four BS switching off patterns given. This is quite important as it can maximise the energy saving of the whole network when the number of cell sleeping times is limited. In stochastic geometry based model, based on the numerical coverage probability provided, the network energy saving is optimised. The results in both network models prove that the proposed strategy can achieve better performance compared with conventional ones.

In Chapter 4, both IB-FD and FDD based small cell wireless backhaul strategies are proposed to enhance the small cell capacity. Using stochastic geometry based HetNets model, a numerical analysis of the target small cell capacity and throughput of the whole network is provided. The results

show that when a number of small cells need to utilize the backhaul of the macrocell, especially when the UE density is high, IB-FD can be a much better choice. Inversely, FDD can achieve a better performance only when macrocell has enough resource to be utilized.

In Chapter 5, I mainly research the MM in HetNets and LTE-LAA networks. The handover procedure from macrocell to the small cell is provided. In addition, a self optimisation algorithm is proposed to optimise PPHO in HetNets. It's worth noting that the HM and TTT are adjusted separately in case of the sudden fluctuations of the system. The results demonstrate that the proposed algorithm achieves better results compared to the conventional methods. In LTE-LAA networks, the proposed handover scheme is combined with conventional mobility triggered handover and newly introduced availability triggered handover to enhance UEs' capacity performance. The results show that the unlicensed spectrum handover ratio of THE proposed scheme is significantly higher than that of conventional schemes, especially in a dense Wi-Fi system scenario , which means a significant improvement of UEs' throughput. Moreover, a detailed trigger event and handover procedures are also presented.

6.2 Future Work

For the research work in Chapter 3, I believe that my work can be improved from the following three areas:

- In the work of Chapter 3, I provide an upper bound of Laplace transform of interference ($\mathscr{L}_{I_s}$) of the CRE UEs, and I believe a more accurate approximation of ($\mathscr{L}_{I_s}$) can be obtained.
- I mainly consider the relationship between the small cell energy saving with its distance to the macrocell. However, the number of its associated UEs is another important factor impacting the energy saving. In future works, I will consider to optimise both factors.
- Inhomogeneous SPPP model will be used to analyse the network performance.

For the research in Chapter 4, I believe that my work can be improved from the following two aspects:

- In my work, the resource used for wireless backhaul from the macrocell is allocated equally to the small cells. I will target the resource allocation to the small cells to maximise the network throughput.
- I will analyse mm-Wave wireless backhaul in the future.

For the research in Chapter 5, I consider that our work can be extended from the two areas:

- I will use stochastic geometry SPPP model to evaluate the handover performance in the future.
- The handover procedure can be simplified in a further step to lower the signalling overhead.

Appendix A

A comparison of coverage probability between two network models

In this part, UEs' coverage probability is analysed in both homogeneous hexagon small cell network as well as the network where small cells follow traffic hot spots.

The network where small cells follow traffic hot spots is illustrated in Fig. A.1. It can be seen that small cells follow hexagon distribution with various density(λ_s) in different region in the macrocell's coverage area. There are total 126 small cells deployed. The ISD of the macrocell is 1000m, and the ISD of small cells is $200/\sqrt{(}3)$, $120/\sqrt{(}3)$, $100/\sqrt{(}3)$ respectively. The UEs are uniformly distributed in each area with density (λ_u) according to the corresponding λ_s. Here, two scenarios $\lambda_u = 2\lambda_s$ and $\lambda_u = 4\lambda_s$ are considered.

The homogeneous and continuous hexagon small cell network model is illustrated in Fig. 3.4. For fair comparison, the number of small cells is assumed to be the same for both network models.

Fig. A.2 illustrates the simulation based comparison of coverage probability with increasing allocated bandwidth. Assume that the macrocell and all small cells share the same frequency, the coverage probability P(c) can be written as:

$$\mathrm{P}(c) = \mathbb{P}[W/n * \log_2(1+\gamma) \geq T], \tag{A.1}$$

where W is the network bandwidth and n is the number of UEs of the small cell. $\gamma = \frac{P_i d^{-\alpha_i} h}{I_m + I_s + \sigma^2}$. Where i=s or m, representing small cell or macrocell. $T = 0.6M$ bps, which is the UEs' data rate requirement. h is exponential distributed random variable with mean ($\mu = 1$), representing Rayleigh fading. The value of P_s, P_m,α_s, α_m and σ^2 can be referred to Tab. 3.1.

Software Matlab is used to simulate the results. Monte Carlo method is used in the simulation and the loop count is 1000 times.

Fig. A.2 depicts the UEs' coverage probability performance for both network models. It's apparently that, when small cells are deployed following traffic hot spots, the networks will have a better performance in terms of UEs' coverage probability.

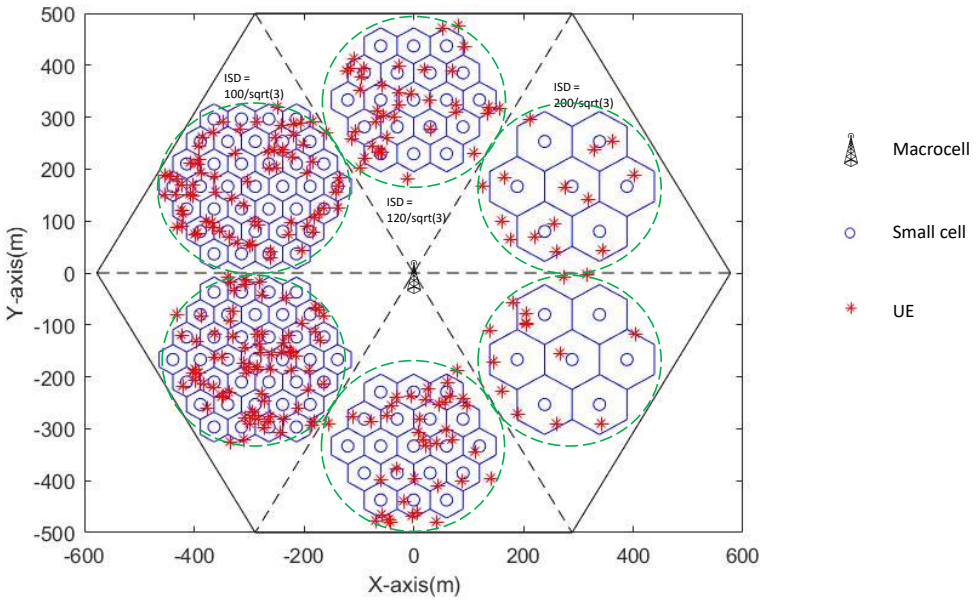

Fig. A.1 Network Where Small Cells Follow Traffic Hot Spots

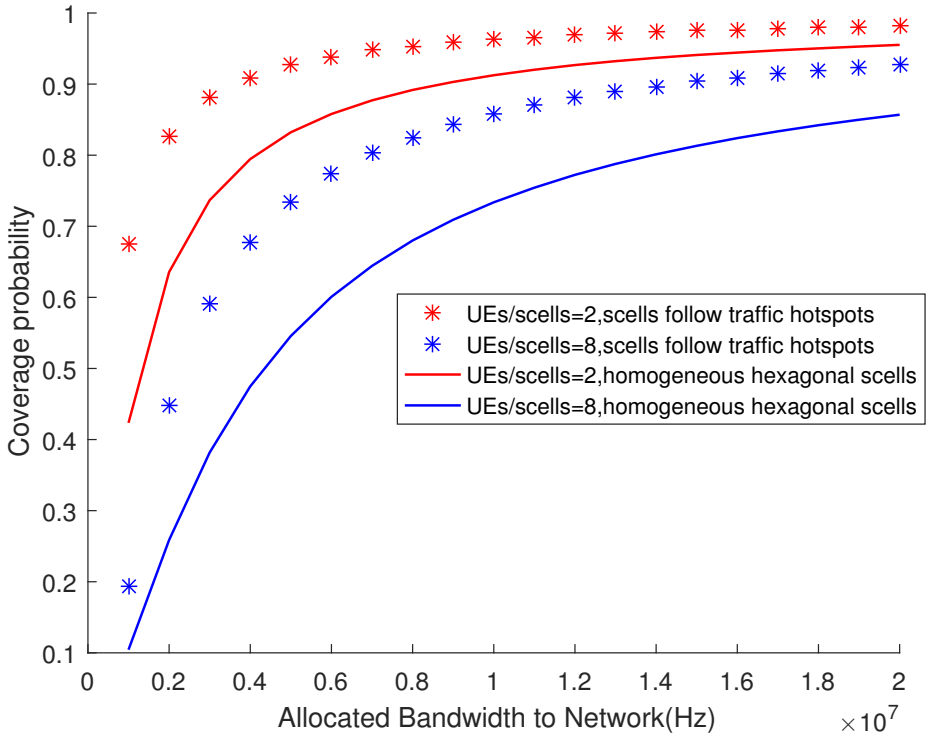

Fig. A.2 Coverage Probability Comparison

Appendix B

Proof of Proposition 1

The coverage probability of UEs in area A can be written as:

$$\begin{aligned}
G_A &= \mathbb{E}\{\mathbb{P}\left(\frac{W_A}{N_A} log_2(1+\gamma_A)\right) > U\} \\
&= \mathbb{E}_r\{\mathbb{P}\left(\frac{W_A}{N_A} log_2(1+\frac{P_1 h r^{-\alpha_m}}{I_s+\sigma^2})\right) > U\} \\
&= \int \left(\mathbb{P}\left(\frac{W_A}{N_A} log_2(1+\frac{P_1 h r^{-\alpha_m}}{I_s+\sigma^2})\right) > U\right) f_R(r)\,\mathrm{d}r \\
&= \int \mathbb{P}\left(h > \frac{(2^{\frac{UN_A}{W_A}}-1)(I_s+\sigma^2) r^{\alpha_1}}{P_1}\right) \frac{2r}{z^2}\,\mathrm{d}r \\
&= \int_0^z e^{-\mu T r^{\alpha_1}\sigma^2} \mathscr{L}_{I_s}(\mu T r^{\alpha_1}) \frac{2r}{z^2}\,\mathrm{d}r
\end{aligned} \tag{B.1}$$

Here I provide the proof of $\mathscr{L}_{I_s}(\mu T r^{\alpha_1})$, based on (2.4)

$$\begin{aligned}
\mathscr{L}_{I_s}(s) &= \mathbb{E}\left(exp\left(-s \sum_{x\in\phi\cap b^c(o',z)} P_2 h_{x,o} ||x||^{-\alpha_2}\right)\right) \\
&= \mathbb{E}_\phi\left(\prod_{x\in\phi\cap b^c(o',z)} \mathbb{E}_{h_{x,o}}[exp(-sP_2 h_{x,o})||x||^{-\alpha_2})]\right) \\
&= \mathbb{E}_\phi\left(\prod_{x\in\phi\cap b^c(o',z)} \frac{1}{1+sP_2||x||^{-\alpha_s}}\right) \\
&= \exp\left(-\lambda_2\left(\int_{\mathbb{R}^2} \frac{1}{1+||x||^{\alpha_2}/(sP_2)}\,\mathrm{d}x - \int_{b^c(o',z)} \frac{1}{1+||x||^{\alpha_2}/(sP_2)}\,\mathrm{d}x\right)\right)
\end{aligned} \tag{B.2}$$

The physical meaning of (B.2) is the Laplace transform of sum of the interference from the active small cells, which can be seen as the Laplace transform of the difference between the sum of the interference of all the small cells and the sum of the interference from sleeping small cells.

$exp(-\lambda_2(\int_{\mathbb{R}^2} \frac{1}{1+||x||^{\alpha_2}/(sP_2)}\,\mathrm{d}x))$ is the Laplace transform of sum of interference from all the small cells, which can be derived from (2.4). $\int_{b(o',z)} \frac{1}{1+||x||^{\alpha_2}/(sP_2)}\,\mathrm{d}x$ can be derived according to Fig. B.1.

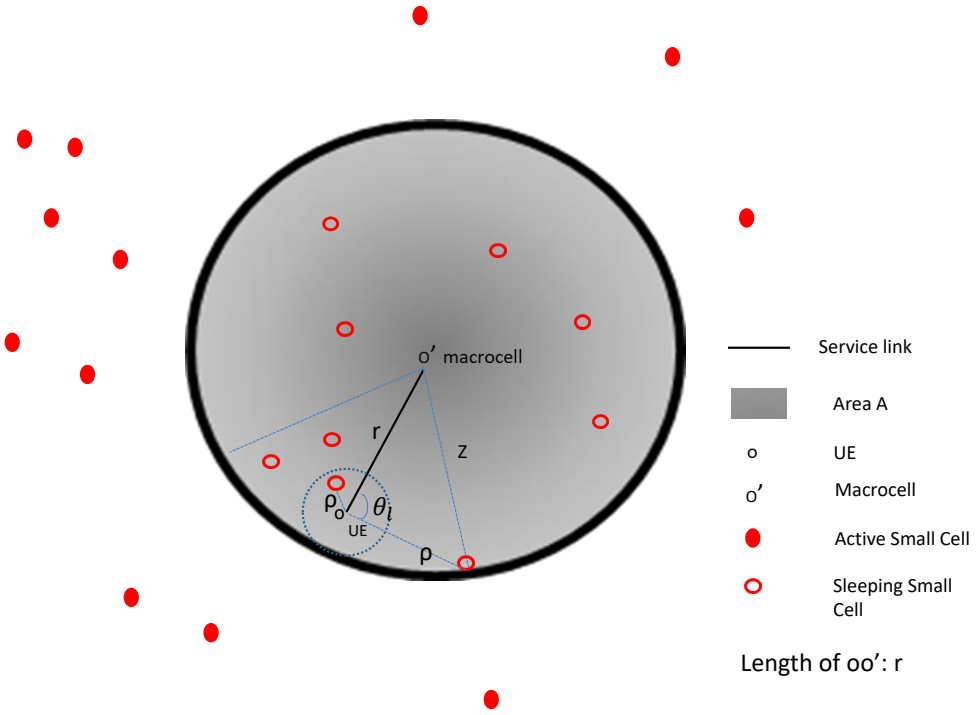

Fig. B.1 Illustration of interference Laplace transform proof

In Fig. B.1, o' is the location of macrocell, and o is the location of UE, the distance between o and o' is r. For $\int_{b^c(o',z)} \frac{1}{1+||x||^{\alpha_2}/(sP_2)}\,\mathrm{d}x$, $b^c(o',z)$ is the disk with centre o' and radius z, x is the coordinate of the small cell. Convert the integration $\int_{b(o',z)} \frac{1}{1+||x||^{\alpha_2}/(sP_2)}\,\mathrm{d}x$ from Cartesian to polar coordinates with origin o, then:

$$\begin{aligned}\int_{b(o',z)} \frac{1}{1+||x||^{\alpha_2}/(sP_2)} &= \int_{b(o',z)} \frac{1}{1+\rho^{\alpha_2}/(sP_2)}\rho d\rho d\theta \\ &= \int_0^{z-r}\int_{-\pi}^{\pi} \frac{1}{1+\rho^{\alpha_2}/(sP_2)}\rho d\rho d\theta + \int_{z-r}^{z+r}\int_{-\theta_l}^{\theta_l} \frac{1}{1+\rho^{\alpha_2}/(sP_2)}\rho d\rho d\theta \\ &= \int_0^{z-r} \frac{2\pi}{1+\frac{\rho^{\alpha_2}}{P_2 s}}\rho\,\mathrm{d}\rho + \int_{z-r}^{z+r} \frac{2\theta_l}{1+\frac{\rho^{\alpha_2}}{P_2 s}}\rho\,\mathrm{d}\rho, \end{aligned} \tag{B.3}$$

where $\theta_l = \arccos(\frac{r^2+\rho^2-z^2}{2r\rho})$.

When $\alpha_2 = 4$, according to (2.4)

$$exp\left(-\lambda_2\left(\int_{\mathbb{R}^2}\frac{1}{1+||x||^{\alpha_2}/(sP_2)}\,\mathrm{d}x\right)\right) = exp\left(-s^{2/\alpha_2}\frac{2\pi^2 csc(\frac{2\pi}{\alpha_2})}{\alpha_2}\lambda_2 P_2^{2/\alpha_2}\right)$$
$$= exp\left(-\pi r^2\lambda_2(T*P_2)^{2/a_s}(\pi/2)\right) \tag{B.4}$$

Then, $\mathscr{L}_{I_s}(s)$ in Proposition 1 is expressed as:

$$\mathscr{L}_{I_s}(s)$$
$$= \exp\left(-\pi r^2\lambda_2(T*P_2)^{2/a_2}(\pi/2)\right)\exp\left(2\lambda_2\int_{r-z}^{r+z}\frac{\arccos(\frac{r^2+\rho^2-z^2}{2r\rho})}{1+\frac{\rho^{\alpha_2}}{P_2 s}}\rho\,\mathrm{d}\rho + 2\lambda_2\int_0^{r-z}\frac{\pi}{1+\frac{\rho^{\alpha_2}}{P_2 s}}\rho\,\mathrm{d}\rho\right), \tag{B.5}$$

where $s = \mu T r^{\alpha_1}$.

Appendix C

Proof of Proposition 2

Assume the distance between the macrocell with a random UE in set U_1 is X_1, and the distance between the macrocell and a random UE is R_1.

Since the event of $X_1 > x$ is the event of $R_1 > x$, given the typical user's association with the first tier(n=1), the probability of $X_1 > x$ can be given as:

$$\mathbb{P}[X_1 > x] = \frac{\mathbb{P}[R_1 > x, n = 1]}{[n = 1]} \tag{C.1}$$

Where [n=1] is the probability of UEs in set U_1, which is given in (3.44). The joint probability of $R_1 > x$ and n=1 is:

$$\begin{aligned}
&\mathbb{P}[R_1 > x, n = 1] \\
&= \mathbb{P}[R_1 > x, P_1 R_1^{-\alpha_1} \geq P_2 R_2^{-\alpha_2} B_2)] \\
&= \int \mathbb{P}[R_1 > x, (R_2 \geq ((\frac{P_1}{P_2 B_2})^{-\frac{1}{\alpha_2}} R_1^{\frac{\alpha_1}{\alpha_2}})] f_{R_1}(r)\, \mathrm{d}r \\
&= \int_z^R \mathbb{P}[r > x, (R_2 \geq ((\frac{P_1}{P_2 B_2})^{-\frac{1}{\alpha_2}} r^{\frac{\alpha_1}{\alpha_2}})] \frac{2r}{R^2 - z^2}\, \mathrm{d}r
\end{aligned} \tag{C.2}$$

Solving (C.2), $\mathbb{P}[R_1 > x, n = 1]$ can be derived as:

$$\mathbb{P}[R_1 > x, n = 1] = \begin{cases} \int_z^R e^{(-\lambda_2 \pi (\frac{P_1}{P_2 B_2})^{-\frac{2}{\alpha_2}} r^{\frac{2\alpha_1}{\alpha_2}})} \frac{2r}{R^2 - z^2}\, \mathrm{d}r, x \leq z \\ \int_x^R e^{(-\lambda_2 \pi (\frac{P_1}{P_2 B_2})^{-\frac{2}{\alpha_2}} r^{\frac{2\alpha_1}{\alpha_2}})} \frac{2r}{R^2 - z^2}\, \mathrm{d}r, R \geq x > z \\ 0, \quad x > R \end{cases} \tag{C.3}$$

Plugging (C.3) into (C.1), $\mathbb{P}[X1 > x]$ can be easily derived:$\mathbb{P}[X1 > x] = \frac{1}{\frac{U_1}{q_B}} \mathbb{P}[R1 > x, n = 1]$.

The Cumulative density function (CDF) of the distance between a typical UE in set U_1 to its

associated macrocell can be expressed as:

$$\begin{aligned} F_{X_1}(x) &= 1 - \mathbb{P}[X_1 > x] \\ &= 1 - \frac{1}{q_B^{U_1}} \mathbb{P}[R_1 > x, n = 1] \end{aligned} \tag{C.4}$$

The pdf is :

$$f_{X_1}(x) = \frac{dF_{X1}}{dx} = \begin{cases} 0, & x \leq z \\ \frac{1}{q_B^{U_1}} e^{(-\lambda_2 \pi (\frac{P_1}{P_2 B_2})^{-\frac{2}{\alpha_2}} x^{\frac{2\alpha_1}{\alpha_2}})} \frac{2x}{R^2 - z^2}, & R \geq x > z \\ 0, & x > R \end{cases} \tag{C.5}$$

The result of (3.45) can be obtained.

Appendix D

Proof of $\mathscr{L}_{I_s}(\mu T r^{\alpha_1})$ in Corollary 1

.

According to (2.4), $\mathscr{L}_{I_s}(s)$ in Corollary 1 can be written as:

$$\begin{aligned}
\mathscr{L}_{I_s}(s) &= \mathbb{E}\left(exp\left(-s\sum_{x'\in\phi\cap b^c(o',z)} P_2 h_{x,o}||x'||^{-\alpha_2}\right)\right) \\
&= \mathbb{E}_\phi\left(\prod_{x'\in\phi\cap b^c(o',z)\setminus sl} \mathbb{E}_{h_{x',o}}[exp(-sP_2 h_{x',o})||x'||^{-\alpha_2})]\right) \\
&= \mathbb{E}_\phi\left(\prod_{x'\in\phi\cap b^c(o',z)\setminus sl} \frac{1}{1+sP_2||x'||^{-\alpha_2}}\right) \\
&= \exp\left(-\lambda_2\left(\int_{\mathbb{R}^2\setminus sl}\frac{1}{1+||x'||^{\alpha_2}/(sP_2)}\,\mathrm{d}x' - \int_{b^c(o',z)}\frac{1}{1+||x'||^{\alpha_2}/(sP_2)}\,\mathrm{d}x'\right)\right) \qquad \text{(D.1)}
\end{aligned}$$

Where $s=\mu T x^{\alpha_1}$. sl is the set of the small cells whose distance to the UE is smaller than $(\frac{P_1}{P_2B_2})^{-\frac{1}{\alpha_2}}x$, this is derived according to (C.1).

The physical meaning of (D.1) is the Laplace transform of sum of the interference from the active small cells, which can be seen as the Laplace transform of the difference between the sum of the interference of all the small cells and the sum of the interference from sleeping small cells. $\exp(-\lambda_2(\int_{\mathbb{R}^2\setminus sl}\frac{1}{1+||x'||^{\alpha_2}/(sP_2)}\,\mathrm{d}x')$ is the Laplace transform of sum of interference from the small cells whose distance to the UE is larger than $(\frac{P_1}{P_2B_2})^{-\frac{1}{\alpha_2}}x$, which can be derived from (2.4). $\int_{b^c(o',z)}\frac{1}{1+||x'||^{\alpha_2}/(sP_2)}\,\mathrm{d}x'$ can be derived according to Fig. D.1.

when $\alpha_2=4$, according to (2.4)

$$\exp\left(-\lambda_2\left(\int_{\mathbb{R}^2\setminus sl}\frac{1}{1+||x'||^{\alpha_2}/(sP_2)}\,\mathrm{d}x'\right)\right) = \exp(-\lambda_2\pi x^2(T\cdot P_2)^{\alpha_2/2}(\frac{\pi}{2}-\mathrm{atan}((\frac{P_1}{P_2B_2})^{-0.5}\cdot T^{-\alpha_2/2}))) \qquad \text{(D.2)}$$

The detailed proof procedure can be found in [157].

In Fig. D.1, o' is the position of macrocell, o is the position of UE, because the user is served by the macrocell, the distance between o and o' is x. For $\int_{b^c(o',z)} \frac{1}{1+||x'||^{\alpha_2}/(sP_2)}\,\mathrm{d}x'$, $b^c(o',z)$ is the disk with centre o' and radius z, x' is the coordinate of the small cell. Convert the integration $\int_{b^c(o',z)} \frac{1}{1+||x'||^{\alpha_2}/(sP_2)}\,\mathrm{d}x'$ from Cartesian to polar coordinates with origin o, then:

$$\begin{aligned}\int_{b^c(o',z)} \frac{1}{1+||x'||^{\alpha_2}/(sP_2)}\,\mathrm{d}x' &= \int_{b^c(o',z)} \frac{1}{1+\rho^{\alpha_2}/(sP_2)}\rho d\rho d\theta \\ &= \int_g^{x+z}\int_{-\theta_l}^{\theta_l} \frac{1}{1+\rho^{\alpha_2}/(sP_2)}\rho d\rho d\theta \\ &= \int_g^{x+z} \frac{2\theta_l}{1+\rho^{\alpha_2}/(sP_2)}\rho d\rho, \end{aligned} \tag{D.3}$$

where $\theta_l = \arccos(\frac{x^2+\rho^2-z^2}{2x\rho})$, and $g = \max((\frac{P_1}{P_2 * B_2})^{-1/\alpha_2}\cdot x, x-z)$.

Then, $\mathscr{L}_{I_s}$ in Corollary 1 is:

$$\mathscr{L}_{I_s}(s) = \exp(-\lambda_2\pi x^2(T*P_2)^{\alpha_2/2}(\frac{\pi}{2} - \operatorname{atan}(m\cdot T^{-\alpha_2/2})))\exp(2\lambda_2\int_g^{r+z}\frac{\theta_l}{1+\frac{\rho^{\alpha_2}}{P_2\cdot s}}\rho\mathrm{d}\rho), \tag{D.4}$$

where $m = (\frac{P_1}{P_2 B_2})^{-0.5}$.

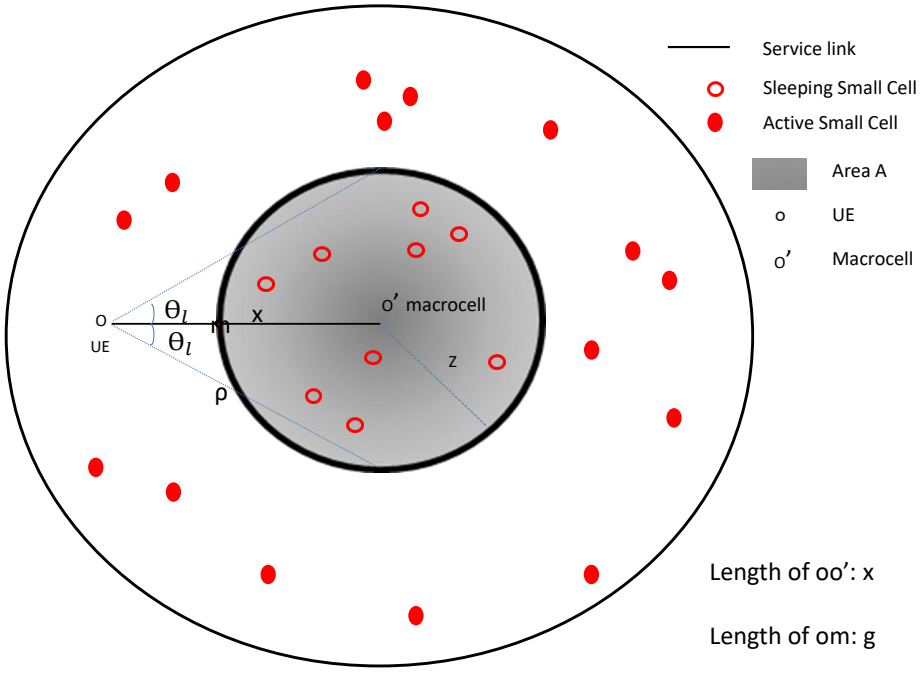

Fig. D.1 Illustration of interference Laplace transform proof

Appendix E

Proof of Proposition 3

Assume the distance between a random UE in set U_2 with its associated small cell is X_2, and the distance between a random UE with its nearest small cell is R_2.

Since the event of $X_2 > x$ is the event of $R_2 > x$, given the typical user's association with the first tier(n=2), the probability of $X_2 > x$ can be given as:

$$\mathbb{P}[X_2 > x] = \frac{\mathbb{P}[R_2 > x, n = k]}{[n = k]} \tag{E.1}$$

Where [n=2] is the probability that UEs in set U_2, which is expressed in (3.49). The joint probability of $R_2 > x$ and n=2 is:

$$\begin{aligned}
&\mathbb{P}[R_2 > x, n = 2] \\
&= \mathbb{P}[R_2 > x, P_2 R_2^{-\alpha_2} \geq P_1 R_1^{-\alpha_1})] \\
&= \int \mathbb{P}[R_2 > x, (R_1 \geq ((\frac{P_2}{P_1})^{-\frac{1}{\alpha_1}} R_2^{\frac{\alpha_2}{\alpha_1}})] f_{R_2}(r)\,\mathrm{d}r \\
&= \int \mathbb{P}[r > x, (R_1 \geq ((\frac{P_2}{P_1})^{-\frac{1}{\alpha_1}} r^{\frac{\alpha_2}{\alpha_1}})] 2\pi\lambda_2 r e^{-\lambda_2 \pi r^2}\,\mathrm{d}r
\end{aligned} \tag{E.2}$$

Solving (E.2), $\mathbb{P}[R_2 > x, n = 2]$ can be derived as:

$$\mathbb{P}[R_2 > x, n = 2] = \begin{cases}
\int_{x_1}^{x_2} \frac{R^2 - (\frac{P_2}{P_1})^{-\frac{2}{\alpha_1}} r^{\frac{2\alpha_2}{\alpha_1}}}{R^2 - z^2} 2\pi\lambda_2 r e^{-\lambda_2 \pi r^2}\,\mathrm{d}r \\
+ \int_{x}^{x_1} 2\pi\lambda_2 r e^{-\lambda_2 \pi r^2}, \quad x \leq x_1 \\
\int_{x}^{x_2} \frac{R^2 - (\frac{P_2}{P_1})^{-\frac{2}{\alpha_1}} r^{\frac{2\alpha_2}{\alpha_1}}}{R^2 - z^2} 2\pi\lambda_2 r e^{-\lambda_2 \pi r^2}\,\mathrm{d}r, \quad x_2 \geq x > x_1 \\
0, \quad x > x_2
\end{cases} \tag{E.3}$$

Plugging (E.3) into (E.1), $\mathbb{P}[X2 > x]$ can be easily derived:$\mathbb{P}[X2 > x] = \frac{1}{q_B^{U_2}} \mathbb{P}[R2 > x, n = 2]$.

The CDF of X_2 $F_{X_2}(x)$ is :

$$\begin{aligned} F_{X_2}(x) &= 1 - \mathbb{P}[X_2 > x] \\ &= 1 - \frac{1}{q_B^{U_2}} \mathbb{P}[R_2 > x, n = 2] \end{aligned} \tag{E.4}$$

The pdf of X_2 $f_{X_2}(x)$ is :

$$f_{X_2}(x) = \frac{dF_{X2}}{dx} = \begin{cases} \frac{1}{q_B^{U_2}} (2\pi\lambda_2 x e^{-\lambda_2 \pi x^2}), & x \leq x_1 \\ \frac{R^2 - (\frac{P_2}{P_1})^{-\frac{2}{\alpha_1}} x^{\frac{2\alpha_2}{\alpha_1}}}{R^2 - z^2} \frac{2\pi\lambda_2}{q_B^{U_2}} x e^{-\lambda_2 \pi x^2}, & x_2 \geq x > x_1 \\ 0, & x > x_2 \end{cases} \tag{E.5}$$

Appendix F

Proof of Proposition 4

Assume the distance between a random UE in set U_3 with its associated small cell is X_3, and the distance between a random UE with its nearest small cell is R_2.

Since the event of $X_3 > x$ is the event of $R_2 > x$, given the typical user's association with the first tier(n=3), the probability of $X_3 > x$ can be given as:

$$\mathbb{P}[X_3 > x] = \frac{\mathbb{P}[R_2 > x, n = 3]}{[n = 3]} \tag{F.1}$$

The joint probability of $R_2 > x$ and n=3 is:

$$\begin{aligned}
&\mathbb{P}[R_2 > x, n = 3] \\
&= \mathbb{P}[R_2 > x, P_1 R_1^{-\alpha_1} \leq P_2 R_2^{-\alpha_2} B \cap P_1 R_1^{-\alpha_1} \geq P_2 R_2^{-\alpha_2}] \\
&= \int \mathbb{P}[P_1 R_1^{-\alpha_1} \leq P_2 R_2^{-\alpha_2} B \cap P_1 R_1^{-\alpha_1} \geq P_2 R_2^{-\alpha_2}] 2\pi\lambda_2 r e^{-\pi\lambda_2 r^2} \, \mathrm{d}r \\
&= \int \mathbb{P}((\frac{P_2}{P_1})^{-\frac{1}{\alpha_1}} r^{\frac{\alpha_2}{\alpha_1}} \geq R_1 \geq (\frac{P_2 B}{P_1})^{-\frac{1}{\alpha_1}} r^{\frac{\alpha_2}{\alpha_1}}) 2\pi\lambda_2 r e^{-\pi\lambda_2 r^2} \, \mathrm{d}r
\end{aligned} \tag{F.2}$$

Solving (F.2), $\mathbb{P}[R_2 > x, n = 3]$ can be derived as:

$$\mathbb{P}[R_2 > x, n = 3] = \begin{cases}
\int_{x_1}^{x_1^b} \frac{\rho_1^2 - z^2}{R^2 - z^2} 2\pi\lambda_2 r e^{-\lambda_2 \pi r^2} \, \mathrm{d}r + \int_{x_1^b}^{x_2} \frac{\rho_1^2 - \rho_2^2}{R^2 - z^2} 2\pi \, \lambda_2 r e^{-\lambda_2 \pi r^2} \, \mathrm{d}r + \int_{x_2}^{x_2^b} \frac{R^2 - \rho_{1b}^2}{R^2 - z^2} 2\pi \, \lambda_2 r e^{-\lambda_2 \pi r^2} \, \mathrm{d}r, x < x_1 \\
\int_{x}^{x_1^b} \frac{\rho_1^2 - z^2}{R^2 - z^2} 2\pi\lambda_2 r e^{-\lambda_2 \pi r^2} \, \mathrm{d}r + \int_{x_1^b}^{x_2} \frac{\rho_1^2 - \rho_2^2}{R^2 - z^2} 2\pi \, \lambda_2 r e^{-\lambda_2 \pi r^2} \, \mathrm{d}r + \int_{x_2}^{x_2^b} \frac{R^2 - \rho_{1b}^2}{R^2 - z^2} 2\pi \, \lambda_2 r e^{-\lambda_2 \pi r^2} \, \mathrm{d}r, x_1 < x < x_1^b \\
\int_{x_1^b}^{x_2} \frac{\rho_1^2 - \rho_2^2}{R^2 - z^2} 2\pi \, \lambda_2 r e^{-\lambda_2 \pi r^2} \, \mathrm{d}r + \int_{x_2}^{x_2^b} \frac{R^2 - \rho_2^2}{R^2 - z^2} 2\pi \, \lambda_2 r e^{-\lambda_2 \pi r^2} \, \mathrm{d}r, x_1^b < x < x_2 \\
\int_{x_2}^{x_2^b} \frac{R^2 - \rho_2^2}{R^2 - z^2} 2\pi \, \lambda_2 r e^{-\lambda_2 \pi r^2} \, \mathrm{d}r, x_2 < x < x_2^b \\
0, \quad x > x_2^b
\end{cases} \tag{F.3}$$

Plugging (F.3) into (F.1), $\mathbb{P}[X3 > x]$ can be easily derived:$\mathbb{P}[X3 > x] = \frac{1}{\frac{U_3}{q_B}}\mathbb{P}[R2 > x, n = 3]$.
The CDF of X_k is :

$$\begin{aligned} F_{X_3}(x) &= 1 - \mathbb{P}[X_3 > x] \\ &= 1 - \frac{1}{q_B^3}\mathbb{P}[R_2 > x, n = 3] \end{aligned} \tag{F.4}$$

The pdf is :

$$f_{X_3}(x) = \frac{dF_{X3}}{dx} = \begin{cases} 0, \quad x \leq x_1 \\ \frac{\rho_1^2 - z^2}{\frac{U_3}{q_B}(R^2 - z^2)} 2\pi\lambda_2 x e^{-\lambda_2 \pi x^2}, x_1 \leq x < x_1^b \\ \frac{\rho_1^2 - \rho_2^2}{\frac{U_3}{q_B}(R^2 - z^2)} 2\pi\ \lambda_2 x e^{-\lambda_2 \pi x^2}, \quad x_1^b \leq x < x_2 \\ \frac{R^2 - \rho_2^2}{\frac{U_3}{q_B}(R^2 - z^2)} 2\pi\ \lambda_2 x e^{-\lambda_2 \pi x^2}, \quad x_2 \leq x < x_2^b \end{cases} \tag{F.5}$$

Appendix G

Proof of $\mathscr{L}_{I_s}(\mu T x^{\alpha_2})$ in Corollary 3

According to (2.4), $\mathscr{L}_{I_s}(s)$ in Corollary 3 can be written as:

$$\begin{aligned}
\mathscr{L}_{I_s}(s) &= \mathbb{E}\left(exp\left(-s\sum_{x\in\phi\cap b^c(o',z)\setminus o} P_2 h_{x,o}||x||^{-\alpha_s}\right)\right] \\
&= \mathbb{E}_\phi\left(\prod_{x\in\phi\cap b^c(o',z)\setminus o} \mathbb{E}_{h_{x,o}}[exp(-sP_2 h_{x,o})||x||^{-\alpha_s})]\right) \\
&= \mathbb{E}_\phi\left(\prod_{x\in\phi\cap b^c(o',z)\setminus o} \frac{1}{1+sP_2||x||^{-\alpha_2}}\right) \\
&= exp\left(-\lambda_2\left(\int_{\mathbb{R}^2\setminus o}\frac{1}{1+||x||^{\alpha_2}/(sP_2)}\,\mathrm{d}x - \int_{b^c(o',z)}\frac{1}{1+||x||^{\alpha_2}/(sP_2)}\,\mathrm{d}x\right)\right) \qquad \text{(G.1)}
\end{aligned}$$

when $\alpha_2 = 4$, according to (2.4)

$$\begin{aligned}
\exp\left(-\lambda_2\left(\int_{\mathbb{R}^2\setminus o}\frac{1}{1+||x||^{\alpha_2}/(sP_2)}\,\mathrm{d}x\right)\right) &= \exp\left(-2\pi\lambda_2\int_x^{+\infty}(\frac{T}{T+(v/x)^\alpha}v\mathrm{d}v\right) \\
&= exp\left(-\lambda_2\pi x^2(T*P_2)^{0.5}(\pi/2-\arctan(T^{-0.5}))\right); \qquad \text{(G.2)}
\end{aligned}$$

In Fig G.1, o' is the location of macrocell and o is location of UE. The distance between the associated small cell s and UE in o is x, and I assume that the distance between o and o' is $D_{oo'}$. It's worth noting that based on (F.2), $D_{oo'}$ must satisfy the condition that $((\frac{P_2}{P_1})^{-\frac{1}{\alpha_1}}x^{\frac{\alpha_2}{\alpha_1}} \geq D_{oo'} \geq (\frac{P_2 B}{P_1})^{-\frac{1}{\alpha_1}}r^{\frac{\alpha_2}{\alpha_1}})$. For $\int_{b^c(o',z)}\frac{1}{1+||x||^{\alpha_2}/(sP_2)}\,\mathrm{d}x$, $b^c(o',z)$ is the disk with centre o' and radius z, x is the coordinate of the small cell. Convert the integration $\int_{b^c(o',z)}\frac{1}{1+||x||^{\alpha_2}/(sP_2)}\,\mathrm{d}x$ from Cartesian to polar coordinates with

origin o, then:

$$\begin{aligned}\int_{b^c(o',z)} \frac{1}{1+||x||^{\alpha_2}/(sP_2)}\,\mathrm{d}x &= \int_{b^c(o',z)} \frac{1}{1+\rho^{\alpha_2}/(sP_2)}\rho d\rho d\theta \\ &= \int_{x_l}^{x_u}\int_{-\theta_l}^{\theta_l} \frac{1}{1+\rho^{\alpha_2}/(sP_2)}\rho d\rho d\theta \\ &= \int_{x_l}^{x_u} \frac{2\theta_l}{1+\rho^{\alpha_2}/(sP_2)}\rho d\rho, \end{aligned} \tag{G.3}$$

where $\theta_l = \arccos\frac{(D_{oo'}^2+\rho^2-z^2)}{(2D_{oo'}\rho)}$, x_u can be expressed as $x_u = D_{oo'}+z$, and x_l can be written as $x_l = \max(D_{oo'}-z,x)$, also, it can be seen that the upper bound of $\mathscr{L}_{I_s}(s)$ is $D_{oo'} = (\frac{P_2}{P_1})^{-\frac{1}{\alpha_1}}x^{\frac{\alpha_2}{\alpha_1}}$, and lower bound is $(\frac{P_2B_2}{P_1})^{-\frac{1}{\alpha_1}}x^{\frac{\alpha_2}{\alpha_1}}$. I chose upper bound here.

Then, $\mathscr{L}_{I_s}(s)$ in Corollary 3 is expressed as:

$$\mathscr{L}_{I_s}(s) = \exp\left(-\lambda_2\pi x^2(T*P2)^{0.5}(\pi/2-\arctan(T^{-0.5}))\right)\exp\left(2\lambda_2\int_{x_l}^{x_u}\frac{\arccos\frac{(D_{oo'}^2+\rho^2-z^2)}{(2D_{oo'}\rho)}}{1+\frac{\rho^{\alpha_2}}{sP_2}}\rho\,\mathrm{d}\rho\right) \tag{G.4}$$

where $x_l = max((\frac{P_2}{P_1})^{-\frac{1}{\alpha_1}}x^{\frac{\alpha_2}{\alpha_1}}-z,x), x_u = (\frac{P_2}{P_1})^{-\frac{1}{\alpha_1}}x^{\frac{\alpha_2}{\alpha_1}}+z, D_{oo'} = (\frac{P_2}{P_1})^{-\frac{1}{\alpha_1}}x^{\frac{\alpha_2}{\alpha_1}}$

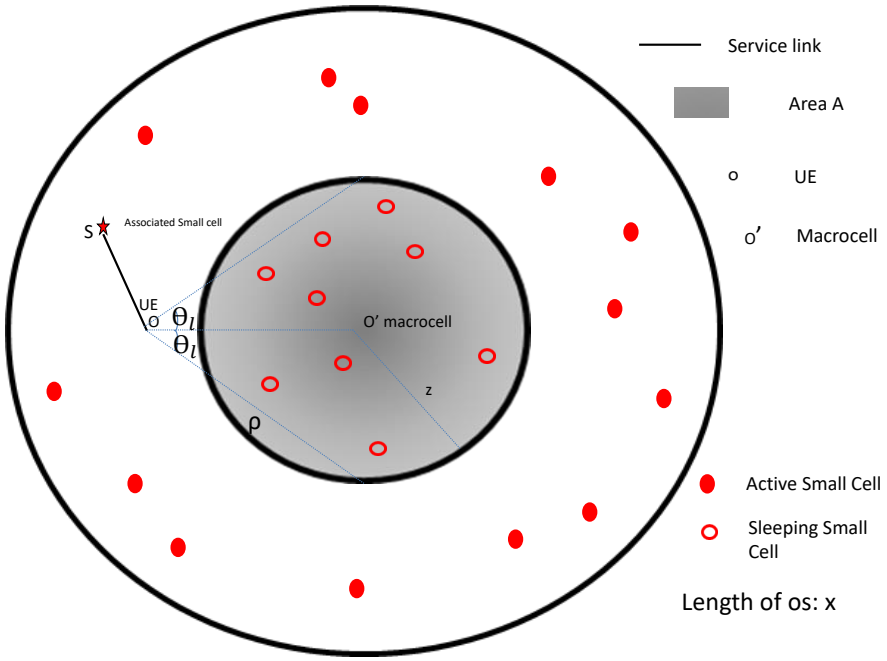

Fig. G.1 Illustration of interference Laplace transform proof

Appendix H

Proof of Lemma 1. in Sect. 4.4.

$$\begin{aligned}\mathbb{E}[X \cdot \mathbf{1}\{x \leq a\}] &= \mathbb{E}[a \cdot \mathbf{1}\{x \leq a\}] - \mathbb{E}[(a-x)\mathbf{1}\{x \leq a\}] \\ &= a\mathbb{P}\{x \leq a\} - \int_0^a \mathbb{P}\{x \leq t\}\,\mathrm{d}t \end{aligned} \tag{H.1}$$

From $\mathbb{E}[(x)] = \int_0^{+\infty} \mathbb{P}\{x > t\}\,\mathrm{d}t$, I can derive that $\mathbb{E}[(a-x)\mathbf{1}\{x \leq a\}] = \int_0^a \mathbb{P}\{x \leq t\}\,\mathrm{d}t$.

Lemma 1 has been proved.

References

[1] I. Hwang, B. Song, and S. S. Soliman, "A holistic view on hyper-dense heterogeneous and small cell networks," *IEEE Communications Magazine*, vol. 51, no. 6, pp. 20–27, 2013.

[2] S. Hur, T. Kim, D. J. Love, J. V. Krogmeier, T. A. Thomas, A. Ghosh *et al.*, "Energy aware radio and network technologies (earth)."

[3] H. Hu, J. Weng, and J. Zhang, "Coverage performance analysis of feicic low-power subframes," *IEEE Transactions on Wireless Communications*, vol. 15, no. 8, pp. 5603–5614, 2016.

[4] T. D. Assefa, R. Hoque, E. Tragos, and X. Dimitropoulos, "Sdn-based local mobility management with x2-interface in femtocell networks," in *Computer Aided Modeling and Design of Communication Links and Networks (CAMAD), 2017 IEEE 22nd International Workshop on*. IEEE, 2017, pp. 1–6.

[5] S. on integrated access and backhaul, "3gpp," *Technical Report 3GPP TR 38.874*, 2017.

[6] M. Mozaffari, W. Saad, M. Bennis, and M. Debbah, "Drone small cells in the clouds: Design, deployment and performance analysis," in *Global Communications Conference (GLOBECOM), 2015 IEEE*. IEEE, 2015, pp. 1–6.

[7] T. Langedem, "Reducing the carbon footprint of ict devices, platforms and networks," *GreenTouch, Amsterdam, The Netherlands*, Nov. 2012.

[8] J. Wu, Y. Zhang, M. Zukerman, and E. K.-N. Yung, "Energy-efficient base-stations sleep-mode techniques in green cellular networks: A survey," *IEEE communications surveys & tutorials*, vol. 17, no. 2, pp. 803–826, 2015.

[9] M. A. Marsan, L. Chiaraviglio, D. Ciullo, and M. Meo, "Optimal energy savings in cellular access networks," in *Communications Workshops, 2009. ICC Workshops 2009. IEEE International Conference on*. IEEE, 2009, pp. 1–5.

[10] L. M. Correia, D. Zeller, O. Blume, D. Ferling, Y. Jading, I. Gódor, G. Auer, and L. Van Der Perre, "Challenges and enabling technologies for energy aware mobile radio networks," *IEEE Communications Magazine*, vol. 48, no. 11, 2010.

[11] S. Chia, M. Gasparroni, and P. Brick, "The next challenge for cellular networks: Backhaul," *IEEE Microwave Magazine*, vol. 10, no. 5, 2009.

[12] Y. Yang, T. Q. Quek, and L. Duan, "Backhaul-constrained small cell networks: Refunding and qos provisioning," *IEEE Transactions on Wireless Communications*, vol. 13, no. 9, pp. 5148–5161, 2014.

[13] M. Paolini, L. Hiley, F. Rayal, and S. Fili, "Small-cell backhaul: Industry trends and market overview," *Senza Fili Consulting*, pp. 1–120, 2013.

[14] D. Bojic, E. Sasaki, N. Cvijetic, T. Wang, J. Kuno, J. Lessmann, S. Schmid, H. Ishii, and S. Nakamura, "Advanced wireless and optical technologies for small-cell mobile backhaul with dynamic software-defined management," *IEEE Communications Magazine*, vol. 51, no. 9, pp. 86–93, 2013.

[15] X. Ge, H. Cheng, M. Guizani, and T. Han, "5g wireless backhaul networks: Challenges and research advances," *IEEE Network*, vol. 28, no. 6, pp. 6–11, 2014.

[16] Qualcomm, "Extending lte advanced to unlicensed spectrum," *white paper*, Dec 2013.

[17] H. Zhang, X. Chu, W. Guo, and S. Wang, "Coexistence of wi-fi and heterogeneous small cell networks sharing unlicensed spectrum," *IEEE Communications Magazine*, vol. 53, no. 3, pp. 158–164, 2015.

[18] R. Zhang, M. Wang, L. X. Cai, Z. Zheng, X. Shen, and L.-L. Xie, "Lte-unlicensed: the future of spectrum aggregation for cellular networks," *IEEE Wireless Communications*, vol. 22, no. 3, pp. 150–159, 2015.

[19] Y. S. Soh, T. Q. Quek, M. Kountouris, and H. Shin, "Energy efficient heterogeneous cellular networks," *IEEE Journal on Selected Areas in Communications*, vol. 31, no. 5, pp. 840–850, 2013.

[20] L. Li, M. Peng, C. Yang, and Y. Wu, "Optimization of base-station density for high energy-efficient cellular networks with sleeping strategies," *IEEE Transactions on Vehicular Technology*, vol. 65, no. 9, pp. 7501–7514, 2016.

[21] C. Liu, B. Natarajan, and H. Xia, "Small cell base station sleep strategies for energy efficiency," *IEEE Transactions on Vehicular Technology*, vol. 65, no. 3, pp. 1652–1661, 2016.

[22] D. Cao, S. Zhou, and Z. Niu, "Optimal combination of base station densities for energy-efficient two-tier heterogeneous cellular networks," *IEEE Transactions on Wireless Communications*, vol. 12, no. 9, pp. 4350–4362, 2013.

[23] E. Mugume and D. K. So, "Sleep mode mechanisms in dense small cell networks," in *Communications (ICC), 2015 IEEE International Conference on*. IEEE, 2015, pp. 192–197.

[24] A. Prasad, A. Maeder, and C. Ng, "Energy efficient small cell activation mechanism for heterogeneous networks," in *Globecom Workshops (GC Wkshps), 2013 IEEE*. IEEE, 2013, pp. 754–759.

[25] P. Dini, M. Miozzo, N. Bui, and N. Baldo, "A model to analyze the energy savings of base station sleep mode in lte hetnets," in *Green computing and communications (GreenCom), 2013 IEEE and internet of things (iThings/CPSCom), IEEE international conference on and IEEE cyber, physical and social computing*. IEEE, 2013, pp. 1375–1380.

[26] S. Zhang, J. Gong, S. Zhou, and Z. Niu, "How many small cells can be turned off via vertical offloading under a separation architecture?" *IEEE Transactions on Wireless Communications*, vol. 14, no. 10, pp. 5440–5453, 2015.

[27] S. Goyal, P. Liu, S. Hua, and S. Panwar, "Analyzing a full-duplex cellular system," in *Information Sciences and Systems (CISS), 2013 47th Annual Conference on*. IEEE, 2013, pp. 1–6.

[28] H. Tabassum, A. H. Sakr, and E. Hossain, "Analysis of massive mimo-enabled downlink wireless backhauling for full-duplex small cells," *IEEE Transactions on Communications*, vol. 64, no. 6, pp. 2354–2369, 2016.

[29] A. Sharma, R. K. Ganti, and J. K. Milleth, "Joint backhaul-access analysis of full duplex self-backhauling heterogeneous networks," *IEEE Transactions on Wireless Communications*, vol. 16, no. 3, pp. 1727–1740, 2017.

[30] Self-configuring, self-optimizing network use cases, and solutions, "3gpp," *Technical Report TR 36.902*.

[31] H. Hu, J. Zhang, X. Zheng, Y. Yang, and P. Wu, "Self-configuration and self-optimization for lte networks," *IEEE Communications Magazine*, vol. 48, no. 2, 2010.

[32] L. Ewe and H. Bakker, "Base station distributed handover optimization in lte self-organizing networks," in *Personal Indoor and Mobile Radio Communications (PIMRC), 2011 IEEE 22nd International Symposium on*. IEEE, 2011, pp. 243–247.

[33] T. Jansen, I. Balan, J. Turk, I. Moerman, and T. Kurner, "Handover parameter optimization in lte self-organizing networks," in *Vehicular Technology Conference Fall (VTC 2010-Fall), 2010 IEEE 72nd*. IEEE, 2010, pp. 1–5.

[34] M. S. I. Khan, M. M. Rahman, K. Raahemifar, J. Misic, and V. B. Misic, "Self-optimizing control parameters for minimizing ping-pong handover in long term evolution (lte)," in *Communications (QBSC), 2014 27th Biennial Symposium on*. IEEE, 2014, pp. 118–122.

[35] M. Behjati, J. P. Cosmas, R. Nilavalan, G. Araniti, and M. Condoluci, "Self-organising comprehensive handover strategy for multi-tier lte-advanced heterogeneous networks," *IET Science, Measurement & Technology*, vol. 8, no. 6, pp. 441–451, 2014.

[36] A. Ulvan, R. Bestak, and M. Ulvan, "The study of handover procedure in lte-based femtocell network," in *Wireless and Mobile Networking Conference (WMNC), 2010 Third Joint IFIP*. IEEE, 2010, pp. 1–6.

[37] D. Han, S. Shin, H. Cho, J.-m. Chung, D. Ok, and I. Hwang, "Measurement and stochastic modeling of handover delay and interruption time of smartphone real-time applications on lte networks," *IEEE Communications Magazine*, vol. 53, no. 3, pp. 173–181, 2015.

[38] H. Elsawy, H. Dahrouj, T. Y. Al-Naffouri, and M.-S. Alouini, "Virtualized cognitive network architecture for 5g cellular networks," *IEEE Communications Magazine*, vol. 53, no. 7, pp. 78–85, 2015.

[39] H. Ishii, Y. Kishiyama, and H. Takahashi, "A novel architecture for lte-b: C-plane/u-plane split and phantom cell concept," in *Globecom Workshops (GC Wkshps), 2012 IEEE*. IEEE, 2012, pp. 624–630.

[40] H. Song, X. Fang, and L. Yan, "Handover scheme for 5g c/u plane split heterogeneous network in high-speed railway," *IEEE Transactions on Vehicular Technology*, vol. 63, no. 9, pp. 4633–4646, 2014.

[41] D. Lopez-Perez, I. Guvenc, G. De la Roche, M. Kountouris, T. Q. Quek, and J. Zhang, "Enhanced intercell interference coordination challenges in heterogeneous networks," *IEEE Wireless Communications*, vol. 18, no. 3, 2011.

[42] B. Li, D. Zhu, and P. Liang, "Small cell in-band wireless backhaul in massive mimo systems: A cooperation of next-generation techniques," *IEEE Transactions on Wireless Communications*, vol. 14, no. 12, pp. 7057–7069, 2015.

[43] A. Sharma, R. K. Ganti, and J. K. Milleth, "Performance analysis of full duplex self-backhauling cellular network," in *Communications (ICC), 2016 IEEE International Conference on*. IEEE, 2016, pp. 1–6.

[44] E. U. T. R. Access, "Base station (bs) radio transmission and reception," *3GPP TS*, vol. 36, p. V9, 2009.

[45] A. Ghosh, N. Mangalvedhe, R. Ratasuk, B. Mondal, M. Cudak, E. Visotsky, T. A. Thomas, J. G. Andrews, P. Xia, H. S. Jo *et al.*, "Heterogeneous cellular networks: From theory to practice," *IEEE communications magazine*, vol. 50, no. 6, 2012.

[46] H. Zhou, Y. Ji, X. Wang, and S. Yamada, "eicic configuration algorithm with service scalability in heterogeneous cellular networks," *IEEE/ACM Transactions on Networking (TON)*, vol. 25, no. 1, pp. 520–535, 2017.

[47] G. Su, L. Li, X. Lin, and H. Wang, "On the optimal small cell deployment for energy-efficient heterogeneous cellular networks," in *Ubiquitous and Future Networks (ICUFN), 2014 Sixth International Conf on*. IEEE, 2014, pp. 172–175.

[48] V. Chandrasekhar and J. G. Andrews, "Uplink capacity and interference avoidance for two-tier femtocell networks," *arXiv preprint cs/0702132*, 2007.

[49] H. S. Dhillon, R. K. Ganti, F. Baccelli, and J. G. Andrews, "Modeling and analysis of k-tier downlink heterogeneous cellular networks," *IEEE Journal on Selected Areas in Communications*, vol. 30, no. 3, pp. 550–560, 2012.

[50] S. Mukherjee, "Distribution of downlink sinr in heterogeneous cellular networks," *IEEE Journal on Selected Areas in Communications*, vol. 30, no. 3, pp. 575–585, 2012.

[51] W. C. Cheung, T. Q. Quek, and M. Kountouris, "Throughput optimization, spectrum allocation, and access control in two-tier femtocell networks," *IEEE Journal on Selected Areas in Communications*, vol. 30, no. 3, pp. 561–574, 2012.

[52] J. G. Andrews, H. Claussen, M. Dohler, S. Rangan, and M. C. Reed, "Femtocells: Past, present, and future," *IEEE Journal on Selected Areas in Communications*, vol. 30, no. 3, pp. 497–508, 2012.

[53] E. Çınlar, *Probability and stochastics*. Springer Science & Business Media, 2011, vol. 261.

[54] S. N. Chiu, D. Stoyan, W. S. Kendall, and J. Mecke, *Stochastic geometry and its applications*. John Wiley & Sons, 2013.

[55] A. Fehske, G. Fettweis, J. Malmodin, and G. Biczok, "The global footprint of mobile communications: The ecological and economic perspective," *IEEE Communications Magazine*, vol. 49, no. 8, 2011.

[56] D. Kimball, M. Kwak, P. Draxler, J. Jeong, C. Hsia, C. Steinbeiser, T. Landon, O. Krutko, L. Larson, and P. Asbeck, "High efficiency wcdma envelope tracking base-station amplifier implemented with gaas hvhbts," in *Compound Semiconductor Integrated Circuits Symposium, 2008. CSIC'08. IEEE*. IEEE, 2008, pp. 1–4.

[57] Y. Wei, J. Staudinger, and M. Miller, "High efficiency linear gaas mmic amplifier for wireless base station and femto cell applications," in *Power Amplifiers for Wireless and Radio Applications (PAWR), 2012 IEEE Topical Conference on*. IEEE, 2012, pp. 49–52.

[58] H. Claussen, L. T. Ho, and F. Pivit, "Effects of joint macrocell and residential picocell deployment on the network energy efficiency," in *Personal, Indoor and Mobile Radio Communications, 2008. PIMRC 2008. IEEE 19th International Symposium on*. IEEE, 2008, pp. 1–6.

[59] T. Han and N. Ansari, "Powering mobile networks with green energy," *IEEE Wireless Communications*, vol. 21, no. 1, pp. 90–96, 2014.

[60] J. Wu, S. Zhou, and Z. Niu, "Traffic-aware base station sleeping control and power matching for energy-delay tradeoffs in green cellular networks," *IEEE Transactions on Wireless Communications*, vol. 12, no. 8, pp. 4196–4209, 2013.

[61] Z. Niu, "Tango: Traffic-aware network planning and green operation," *IEEE Wireless Communications*, vol. 18, no. 5, 2011.

[62] Z. Niu, Y. Wu, J. Gong, and Z. Yang, "Cell zooming for cost-efficient green cellular networks," *IEEE communications magazine*, vol. 48, no. 11, 2010.

[63] I. Ashraf, F. Boccardi, and L. Ho, "Sleep mode techniques for small cell deployments," *IEEE Communications Magazine*, vol. 49, no. 8, 2011.

[64] M. A. Marsan, L. Chiaraviglio, D. Ciullo, and M. Meo, "On the effectiveness of single and multiple base station sleep modes in cellular networks," *Computer Networks*, vol. 57, no. 17, pp. 3276–3290, 2013.

[65] H. Tabassum, U. Siddique, E. Hossain, and M. J. Hossain, "Downlink performance of cellular systems with base station sleeping, user association, and scheduling," *IEEE Transactions on Wireless Communications*, vol. 13, no. 10, pp. 5752–5767, 2014.

[66] F. Han, Z. Safar, and K. R. Liu, "Energy-efficient base-station cooperative operation with guaranteed qos," *IEEE Transactions on Communications*, vol. 61, no. 8, pp. 3505–3517, 2013.

[67] C. Han, T. Harrold, S. Armour, I. Krikidis, S. Videv, P. M. Grant, H. Haas, J. S. Thompson, I. Ku, C.-X. Wang *et al.*, "Green radio: radio techniques to enable energy-efficient wireless networks," *IEEE communications magazine*, vol. 49, no. 6, 2011.

[68] Z. Shelby, C. Pomalaza-Raez, H. Karvonen, and J. Haapola, "Energy optimization in multihop wireless embedded and sensor networks," *International journal of wireless information networks*, vol. 12, no. 1, pp. 11–21, 2005.

[69] M. Z. Shakir, K. A. Qaraqe, H. Tabassum, M.-S. Alouini, E. Serpedin, and M. A. Imran, "Green heterogeneous small-cell networks: Toward reducing the co 2 emissions of mobile communications industry using uplink power adaptation," *IEEE Communications Magazine*, vol. 51, no. 6, pp. 52–61, 2013.

[70] G. Auer, O. Blume, V. Giannini, I. G. ETH, M. A. Imran, Y. J. EAB, E. Katranaras, M. O. EAB, D. S. TI, P. S. EAB *et al.*, "Infso-ict-247733 earth."

[71] D. Willkomm, S. Machiraju, J. Bolot, and A. Wolisz, "Primary user behavior in cellular networks and implications for dynamic spectrum access," *IEEE Communications Magazine*, vol. 47, no. 3, 2009.

[72] M. Laner, P. Svoboda, S. Schwarz, and M. Rupp, "Users in cells: A data traffic analysis," in *Wireless Communications and Networking Conference (WCNC), 2012 IEEE*. IEEE, 2012, pp. 3063–3068.

[73] E. Oh, K. Son, and B. Krishnamachari, "Dynamic base station switching-on/off strategies for green cellular networks," *IEEE transactions on wireless communications*, vol. 12, no. 5, pp. 2126–2136, 2013.

[74] S. Wang and W. Guo, "Energy and cost implications of a traffic aware and quality-of-service constrained sleep mode mechanism," *IET Communications*, vol. 7, no. 18, pp. 2092–2101, 2013.

[75] E. Oh, B. Krishnamachari, X. Liu, and Z. Niu, "Toward dynamic energy-efficient operation of cellular network infrastructure," *IEEE Communications Magazine*, vol. 49, no. 6, 2011.

[76] W. Guo and T. O'Farrell, "Dynamic cell expansion with self-organizing cooperation," *IEEE Journal on Selected Areas in Communications*, vol. 31, no. 5, pp. 851–860, 2013.

[77] A. Bousia, A. Antonopoulos, L. Alonso, and C. Verikoukis, "" green" distance-aware base station sleeping algorithm in lte-advanced," in *Communications (ICC), 2012 IEEE International Conference on*. IEEE, 2012, pp. 1347–1351.

[78] W. Guo and T. O'Farrell, "Green cellular network: Deployment solutions, sensitivity and tradeoffs," in *Wireless Advanced (WiAd), 2011*. IEEE, 2011, pp. 42–47.

[79] D. Tsilimantos, J.-M. Gorce, and E. Altman, "Stochastic analysis of energy savings with sleep mode in ofdma wireless networks," in *INFOCOM, 2013 Proceedings IEEE*. IEEE, 2013, pp. 1097–1105.

[80] Y. Li, H. Celebi, M. Daneshmand, C. Wang, and W. Zhao, "Energy-efficient femtocell networks: Challenges and opportunities," *IEEE Wireless Communications*, vol. 20, no. 6, pp. 99–105, 2013.

[81] E. Mugume and D. K. So, "Spectral and energy efficiency analysis of dense small cell networks," in *Vehicular Technology Conference (VTC Spring), 2015 IEEE 81st*. IEEE, 2015, pp. 1–5.

[82] L. Saker, S.-E. Elayoubi, R. Combes, and T. Chahed, "Optimal control of wake up mechanisms of femtocells in heterogeneous networks," *IEEE Journal on Selected Areas in Communications*, vol. 30, no. 3, pp. 664–672, 2012.

[83] S.-r. Cho and W. Choi, "Energy-efficient repulsive cell activation for heterogeneous cellular networks," *IEEE Journal on Selected Areas in Communications*, vol. 31, no. 5, pp. 870–882, 2013.

[84] J. Peng, H. Tang, P. Hong, and K. Xue, "Stochastic geometry analysis of energy efficiency in heterogeneous network with sleep control," *IEEE Wireless Communications Letters*, vol. 2, no. 6, pp. 615–618, 2013.

[85] J. Kim, W. S. Jeon, and D. G. Jeong, "Effect of base station-sleeping ratio on energy efficiency in densely deployed femtocell networks," *IEEE Communications Letters*, vol. 19, no. 4, pp. 641–644, 2015.

[86] N. Wang, E. Hossain, and V. K. Bhargava, "Backhauling 5g small cells: A radio resource management perspective," *IEEE Wireless Communications*, vol. 22, no. 5, pp. 41–49, 2015.

[87] M. Duarte, C. Dick, and A. Sabharwal, "Experiment-driven characterization of full-duplex wireless systems," *IEEE Transactions on Wireless Communications*, vol. 11, no. 12, pp. 4296–4307, 2012.

[88] M. Heino, D. Korpi, T. Huusari, E. Antonio-Rodriguez, S. Venkatasubramanian, T. Riihonen, L. Anttila, C. Icheln, K. Haneda, R. Wichman *et al.*, "Recent advances in antenna design and interference cancellation algorithms for in-band full duplex relays," *IEEE Communications Magazine*, vol. 53, no. 5, pp. 91–101, 2015.

[89] D. Korpi, Y.-S. Choi, T. Huusari, L. Anttila, S. Talwar, and M. Valkama, "Adaptive nonlinear digital self-interference cancellation for mobile inband full-duplex radio: Algorithms and rf measurements," in *Global Communications Conference (GLOBECOM), 2015 IEEE*. IEEE, 2015, pp. 1–7.

[90] J. Hoydis, K. Hosseini, S. t. Brink, and M. Debbah, "Making smart use of excess antennas: Massive mimo, small cells, and tdd," *Bell Labs Technical Journal*, vol. 18, no. 2, pp. 5–21, 2013.

[91] D. Nguyen, L.-N. Tran, P. Pirinen, and M. Latva-aho, "On the spectral efficiency of full-duplex small cell wireless systems," *IEEE Transactions on wireless communications*, vol. 13, no. 9, pp. 4896–4910, 2014.

[92] R. Taori and A. Sridharan, "Point-to-multipoint in-band mmwave backhaul for 5g networks," *IEEE Communications Magazine*, vol. 53, no. 1, pp. 195–201, 2015.

[93] Z. Pi and F. Khan, "An introduction to millimeter-wave mobile broadband systems," *IEEE communications magazine*, vol. 49, no. 6, 2011.

[94] U. Siddique, H. Tabassum, E. Hossain, and D. I. Kim, "Wireless backhauling of 5g small cells: challenges and solution approaches," *IEEE Wireless Communications*, vol. 22, no. 5, pp. 22–31, 2015.

[95] J. G. Andrews, S. Singh, Q. Ye, X. Lin, and H. S. Dhillon, "An overview of load balancing in hetnets: Old myths and open problems," *IEEE Wireless Communications*, vol. 21, no. 2, pp. 18–25, 2014.

[96] N. Wang, E. Hossain, and V. K. Bhargava, "Joint downlink cell association and bandwidth allocation for wireless backhauling in two-tier hetnets with large-scale antenna arrays," *IEEE Transactions on Wireless Communications*, vol. 15, no. 5, pp. 3251–3268, 2016.

[97] L. Chen, F. R. Yu, H. Ji, G. Liu, and V. C. Leung, "Distributed virtual resource allocation in small-cell networks with full-duplex self-backhauls and virtualization," *IEEE Transactions on Vehicular Technology*, vol. 65, no. 7, pp. 5410–5423, 2016.

[98] D. Korpi, T. Riihonen, A. Sabharwal, and M. Valkama, "Transmit power optimization and feasibility analysis of self-backhauling full-duplex radio access systems," *IEEE Transactions on Wireless Communications*, vol. 17, no. 6, pp. 4219–4236, 2018.

[99] W. Hao and S. Yang, "Small cell cluster-based resource allocation for wireless backhaul in two-tier heterogeneous networks with massive mimo," *IEEE Transactions on Vehicular Technology*, vol. 67, no. 1, pp. 509–523, 2018.

[100] Y. Niu, C. Gao, Y. Li, L. Su, D. Jin, Y. Zhu, and D. O. Wu, "Energy-efficient scheduling for mmwave backhauling of small cells in heterogeneous cellular networks," *IEEE Transactions on Vehicular Technology*, vol. 66, no. 3, pp. 2674–2687, 2017.

[101] S. Singh, M. N. Kulkarni, A. Ghosh, and J. G. Andrews, "Tractable model for rate in self-backhauled millimeter wave cellular networks," *IEEE Journal on Selected Areas in Communications*, vol. 33, no. 10, pp. 2196–2211, 2015.

[102] D. C. Chen, T. Q. Quek, and M. Kountouris, "Backhauling in heterogeneous cellular networks: Modeling and tradeoffs," *IEEE Transactions on Wireless Communications*, vol. 14, no. 6, pp. 3194–3206, 2015.

[103] E-UTRA and E.-U. O. Description, "3gpp," *TS 36.300 V10.7.0*, Mar. 2012.

[104] P. layer Measurements, "3gpp," *TS 36.214 V10.1.0*, Mar. 2011.

[105] D. Xenakis, N. Passas, L. Merakos, and C. Verikoukis, "Mobility management for femtocells in lte-advanced: key aspects and survey of handover decision algorithms," *IEEE Communications Surveys & Tutorials*, vol. 16, no. 1, pp. 64–91, 2014.

[106] X. Chu, D. López-Pérez, Y. Yang, and F. Gunnarsson, *Heterogeneous Cellular Networks: Theory, Simulation and Deployment*. Cambridge University Press, 2013.

[107] E. U. T. R. Access, "Mobility enhancements in heterogeneous networks," 3GPP TR 36.839, Tech. Rep., 2012.

[108] D. López-Pérez, I. Guvenc, and X. Chu, "Theoretical analysis of handover failure and ping-pong rates for heterogeneous networks," in *Communications (ICC), 2012 IEEE International Conference on*. IEEE, 2012, pp. 6774–6779.

[109] X. Xu, Z. Sun, X. Dai, T. Svensson, and X. Tao, "Modeling and analyzing the cross-tier handover in heterogeneous networks," *IEEE Transactions on Wireless Communications*, vol. 16, no. 12, pp. 7859–7869, 2017.

[110] B. Fang and W. Zhou, "Handover reduction via joint bandwidth allocation and cac in randomly distributed hcns," *IEEE Communications Letters*, vol. 19, no. 7, pp. 1209–1212, 2015.

[111] R. Arshad, H. ElSawy, S. Sorour, T. Y. Al-Naffouri, and M.-S. Alouini, "Handover management in dense cellular networks: A stochastic geometry approach," in *Communications (ICC), 2016 IEEE International Conference on*. IEEE, 2016, pp. 1–7.

[112] C. H. de Lima, M. Bennis, and M. Latva-aho, "Modeling and analysis of handover failure probability in small cell networks," in *Computer Communications Workshops (INFOCOM WKSHPS), 2014 IEEE Conference on*. IEEE, 2014, pp. 736–741.

[113] H. Wang, S. Chen, M. Ai, and H. Xu, "Localized mobility management for 5g ultra dense network," *IEEE Transactions on Vehicular Technology*, vol. 66, no. 9, pp. 8535–8552, 2017.

[114] D.-W. Lee, G.-T. Gil, and D.-H. Kim, "A cost-based adaptive handover hysteresis scheme to minimize the handover failure rate in 3gpp lte system," *EURASIP Journal on Wireless Communications and Networking*, vol. 2010, p. 6, 2010.

[115] G. Venkatesh and P. Rao, "Optimizing handover in lte using son system by handling mobility robustness," in *Recent Trends in Electronics, Information & Communication Technology (RTEICT), 2017 2nd IEEE International Conference on*. IEEE, 2017, pp. 2231–2235.

[116] S. Wu, X. Zhang, R. Zheng, Z. Yin, Y. Fang, and D. Yang, "Handover study concerning mobility in the two-hierarchy network," in *Vehicular Technology Conference, 2009. VTC Spring 2009. IEEE 69th*. IEEE, 2009, pp. 1–5.

[117] P. Xu, X. Fang, J. Yang, and Y. Cui, "A user's state and sinr-based handoff algorithm in hierarchical cell networks," in *Wireless Communications Networking and Mobile Computing (WiCOM), 2010 6th International Conference on*. IEEE, 2010, pp. 1–4.

[118] G. Yang, X. Wang, and X. Chen, "Handover control for lte femtocell networks," in *Electronics, Communications and Control (ICECC), 2011 International Conference on*. IEEE, 2011, pp. 2670–2673.

[119] M. Z. Chowdhury, W. Ryu, E. Rhee, and Y. M. Jang, "Handover between macrocell and femtocell for umts based networks," in *Advanced Communication Technology, 2009. ICACT 2009. 11th International Conference on*, vol. 1. IEEE, 2009, pp. 237–241.

[120] Z. Becvar and P. Mach, "Adaptive hysteresis margin for handover in femtocell networks," in *Wireless and Mobile Communications (ICWMC), 2010 6th International Conference on*. IEEE, 2010, pp. 256–261.

[121] K. Ghanem, H. Alradwan, A. Motermawy, and A. Ahmad, "Reducing ping-pong handover effects in intra eutra networks," in *Communication Systems, Networks & Digital Signal Processing (CSNDSP), 2012 8th International Symposium on*. IEEE, 2012, pp. 1–5.

[122] K.-L. Tsai, H.-Y. Liu, and Y.-W. Liu, "Using fuzzy logic to reduce ping-pong handover effects in lte networks," *Soft Computing*, vol. 20, no. 5, pp. 1683–1694, 2016.

[123] J. Gu, S. J. Bae, M. Y. Chung, K.-y. Cheon, and A.-S. Park, "Mobility-based handover decision mechanism to relieve ping-pong effect in cellular networks," in *Communications (APCC), 2010 16th Asia-Pacific Conference on*. IEEE, 2010, pp. 487–491.

[124] H.-D. Bae, B. Ryu, and N.-H. Park, "Analysis of handover failures in lte femtocell systems," in *Telecommunication Networks and Applications Conference (ATNAC), 2011 Australasian*. IEEE, 2011, pp. 1–5.

[125] Y. Lee, B. Shin, J. Lim, and D. Hong, "Effects of time-to-trigger parameter on handover performance in son-based lte systems," in *Communications (APCC), 2010 16th Asia-Pacific Conference on*. IEEE, 2010, pp. 492–496.

[126] M. Ismail, A. Abdrabou, and W. Zhuang, "Cooperative decentralized resource allocation in heterogeneous wireless access medium," *IEEE Transactions on Wireless Communications*, vol. 12, no. 2, pp. 714–724, 2013.

[127] B. Chen, J. Chen, Y. Gao, and J. Zhang, "Coexistence of lte-laa and wi-fi on 5 ghz with corresponding deployment scenarios: A survey," *IEEE Communications Surveys & Tutorials*, vol. 19, no. 1, pp. 7–32, 2017.

[128] A. Babaei, J. Andreoli-Fang, Y. Pang, and B. Hamzeh, "On the impact of lte-u on wi-fi performance," *International Journal of Wireless Information Networks*, vol. 22, no. 4, pp. 336–344, 2015.

[129] F. Liu, E. Bala, E. Erkip, M. C. Beluri, and R. Yang, "Small-cell traffic balancing over licensed and unlicensed bands," *IEEE transactions on vehicular technology*, vol. 64, no. 12, pp. 5850–5865, 2015.

[130] M. Kuhnert and C. Wietfeld, "Performance evaluation of an advanced energy-aware client-based handover solution in heterogeneous lte and wifi networks," in *Vehicular Technology Conference (VTC Spring), 2014 IEEE 79th*. IEEE, 2014, pp. 1–5.

[131] S. Lee, K. Sriram, K. Kim, Y. H. Kim, and N. Golmie, "Vertical handoff decision algorithms for providing optimized performance in heterogeneous wireless networks," *IEEE transactions on vehicular technology*, vol. 58, no. 2, pp. 865–881, 2009.

[132] T. Chakraborty, M. S. Hossain, and M. Atiquzzaman, "A testbed implementation of hybrid decision model based seamless lightweight vertical handover," in *Communications (ICC), 2017 IEEE International Conference on*. IEEE, 2017, pp. 1–6.

[133] A. Roy, P. Chaporkar, and A. Karandikar, "Optimal radio access technology selection algorithm for lte-wifi network," *IEEE Transactions on Vehicular Technology*, 2018.

[134] W. Yoon and B. Jang, "Enhanced non-seamless offload for lte and wlan networks," *IEEE Communications Letters*, vol. 17, no. 10, pp. 1960–1963, 2013.

[135] Q. Chen, G. Yu, A. Maaref, G. Y. Li, and A. Huang, "Rethinking mobile data offloading for lte in unlicensed spectrum," *IEEE Transactions on Wireless Communications*, vol. 15, no. 7, pp. 4987–5000, 2016.

[136] J. Xu, S. Wu, L. Xu, N. Zhang, and Q. Zhang, "Green-oriented user-satisfaction aware wifi offloading in hetnets," *IET Communications*, vol. 12, no. 5, pp. 501–508, 2017.

[137] J. Lee, H. Ko, and S. Pack, "Performance evaluation of lte-unlicensed in handover scenarios," in *Information and Communication Technology Convergence (ICTC), 2015 International Conference on*. IEEE, 2015, pp. 1043–1045.

[138] D. Solomitckii, M. Gapeyenko, S. S. Szyszkowicz, S. Andreev, H. Yanikomeroglu, and Y. Koucheryavy, "Toward massive ray-based simulations of mmwave small cells on open urban maps," *IEEE Antennas and Wireless Propagation Letters*, vol. 16, pp. 1435–1438, 2017.

[139] Y. Gao, G. Wang, and S. A. Jafar, "Topological interference management for hexagonal cellular networks," *IEEE Transactions on Wireless Communications*, vol. 14, no. 5, pp. 2368–2376, 2015.

[140] P. P. Hasselbach and A. Klein, "An analytic model for outage probability and bandwidth demand of the downlink in packet switched cellular mobile radio networks," in *Communications, 2008. ICC'08. IEEE International Conference on*. IEEE, 2008, pp. 252–256.

[141] D. Lopez-Perez, X. Chu, and İ. Guvenc, "On the expanded region of picocells in heterogeneous networks," *IEEE Journal of Selected Topics in Signal Processing*, vol. 6, no. 3, pp. 281–294, 2012.

[142] F. Adelantado, J. Perez-Romero, and O. Sallent, "Nonuniform traffic distribution model in reverse link of multirate/multiservice wcdma-based systems," *IEEE Transactions on Vehicular Technology*, vol. 56, no. 5, pp. 2902–2914, 2007.

[143] J. G. Proakis and M. Salehi, *Digital Communications*. McGraw-Hill Higher Education, 2007.

[144] S. M. Ross, *Introduction to probability models*. Academic press, 2014.

[145] X. Kang, Y.-C. Liang, A. Nallanathan, H. K. Garg, and R. Zhang, "Optimal power allocation for fading channels in cognitive radio networks: Ergodic capacity and outage capacity," *IEEE Trans. Wireless Commun.*, vol. 8, no. 2, pp. 940–950, Feb 2009.

[146] R. P. Brent, *Algorithms for minimization without derivatives*, ser. Prentice-Hall series in automatic computation. Englewood Cliffs, N.J. Prentice-Hall, 1973.

[147] H.-S. Jo, Y. J. Sang, P. Xia, and J. G. Andrews, "Heterogeneous cellular networks with flexible cell association: A comprehensive downlink sinr analysis," *IEEE Transactions on Wireless Communications*, vol. 11, no. 10, pp. 3484–3495, 2012.

[148] G. TSG-RAN, "Evolved universal terrestrial radio access (e-utra) and evolved universal terrestrial radio access network (e-utran); overall description;," 3GPP Technical Report, 3G TR 36.300, 2011.

[149] Z. Becvar, M. Vondra, and P. Mach, "Dynamic optimization of neighbor cell list for femtocells," in *Vehicular Technology Conference (VTC Spring), 2013 IEEE 77th*. IEEE, 2013, pp. 1–6.

[150] D. Lopez-Perez, I. Guvenc, and X. Chu, "Mobility management challenges in 3gpp heterogeneous networks," *IEEE Communications Magazine*, vol. 50, no. 12, 2012.

[151] T. Hida, "Brownian motion," in *Brownian Motion*. Springer, 1980, pp. 44–113.

[152] Y. Li, B. Cao, and C. Wang, "Handover schemes in heterogeneous lte networks: challenges and opportunities," *IEEE Wireless Communications*, vol. 23, no. 2, pp. 112–117, 2016.

[153] F. M. Abinader, E. P. Almeida, F. S. Chaves, A. M. Cavalcante, R. D. Vieira, R. C. Paiva, A. M. Sobrinho, S. Choudhury, E. Tuomaala, K. Doppler *et al.*, "Enabling the coexistence of lte and wi-fi in unlicensed bands," *Communications Magazine, IEEE*, vol. 52, no. 11, pp. 54–61, 2014.

[154] G. Bianchi, "Performance analysis of the ieee 802.11 distributed coordination function," *Selected Areas in Communications, IEEE Journal on*, vol. 18, no. 3, pp. 535–547, 2000.

[155] 3GPP TR 36.839 V11.1.0, "3rd Generation Partnership Project; Technical Specification Group Radio Access Network; Evolved Universal Terrestrial Radio Access (E-UTRA); Mobility enhancements in heterogeneous networks(Release 11)."

[156] Z. Yazdanshenasan, H. S. Dhillon, M. Afshang, and P. H. Chong, "Poisson hole process: Theory and applications to wireless networks," *IEEE Transactions on Wireless Communications*, vol. 15, no. 11, pp. 7531–7546, 2016.

[157] S. Singh and J. G. Andrews, "Joint resource partitioning and offloading in heterogeneous cellular networks," *IEEE Transactions on Wireless Communications*, vol. 13, no. 2, pp. 888–901, 2014.